Transport and Surface Phenomena for Silicon Epitaxial Growth

HITOSHI HABUKA

Isobe R&D Center, Shin-Etsu Handotai Co., Ltd.

A Thesis Presented to
the Faculty of Engineering
Hiroshima University

July, 1996

ABSTRACT

Transport phenomena, surface chemical processes, dopant concentration profiles and surface roughness of substrate for silicon epitaxial growth are discussed theoretically and experimentally. The objective of this thesis is to develop the models to predict various phenomena relating to the silicon epitaxial wafer. The major part of discussion is based on the calculations of the transport phenomena and the chemical reactions at the surface. At first, the transport phenomena in a pancake reactor and in a single-wafer horizontal reactor are discussed. Secondary, the substrate rotation and the chemical reactions for the epitaxial growth are discussed to describe the growth rate and the film thickness. For further studies, the epitaxial wafer's qualities, the dopant distribution and the surface roughness of silicon substrate, are investigated.

The transport phenomena in a pancake reactor are discussed based on a gas flow visualization technique using a high-sensitivity analogue camera and numerical calculations. At room temperature and the epitaxial growth temperature of 1423 K, a large recirculation exists in the reactor chamber, in which the gases near the susceptor flow from the outside toward the center of the susceptor. The profile of the epitaxial film growth rate observed agrees qualitatively with that predicted by visualization and calculations.

An evaluation of silicon epitaxial thin-film growth using the $SiHCl_3$-H_2 system in a single-wafer horizontal reactor is discussed by solving the transport equations for gas velocity, temperature and concentration of chemical species taking into account of the dependence of gas properties on temperature and composition, assuming a simple Arrhenius-type expression for the chemical reaction of $SiHCl_3$ and H_2 on a substrate. Non-Linear increase in the growth rate due to changes in thermal diffusion and diffusion is found to become significant as the $SiHCl_3$ concentration in the reactor increases.

For an enhancement of studies, the effect of substrate rotation on transport of

reactive gases and epitaxial growth rate is investigated for a single-wafer horizontal reactor using a model and experiments. The rotating substrate causes a circulating gas flow region above itself, in which an asymmetric and nonuniform $SiHCl_3$ distribution is formed by thermal diffusion and species consumption due to the surface chemical reaction, even when the growth rate profile on the substrate surface is nearly uniform. The good uniformity in the film thickness observed in calculation and measurement is mainly attributed to the averaging effect by integrating the local growth rate along a concentric circle on the substrate surface, and partially by the species concentration distribution change, both of which are caused by the rotating motion of the substrate.

For the discussion of the dependence of the epitaxial growth rate on the source species concentrations, a transport and epitaxy model following Eley-Rideal to describe silicon epitaxial film growth in an $SiHCl_3$-H_2 system is developed by numerical calculations and comparison with experiments. The state of the surface during the epitaxial growth is also discussed considering the intermediate species, elementary reactions and rate limiting processes.

The boron concentration profile in silicon epitaxial films grown on a p-type substrate under atmospheric pressure is investigated in two types of epitaxial reactors, a single-wafer horizontal reactor and a pancake reactor. It is concluded thst large amounts of recirculation of gas in an epitaxial reactor should be avoided to obtain an abrupt boron concentration profile.

Since silicon surface after the epitaxial growth must be very smooth and flat, surface roughness of a silicon wafer heated at 800–1100 °C under atmospheric pressure in hydrogen ambient is studied. AFM images show that the surface heated at 900 °C has many small pits which are formed due to the difference in the chemical reaction rates between hydrogen-silicon and hydrogen-silicon dioxide. The behavior of surface roughness with pressure and heating time agrees well with that predicted by the pit formation model in this study.

ACKNOWLEDGEMENT

First of all, I wish to express my gratitude to Professor Kikuo Okuyama and Professor Manabu Shimada of Department of Chemical Engineering, Hiroshima University for their continueing guidance and encouragement throughout this study. I wish to thank Professor Yoshihiro Kikuchi and Professor Takayuki Takahagi for their helpful suggestion and advice.

I am very much grateful to all the members of Isobe R&D Center and Epi Production Division of Shin-Etsu Handotai Co., Ltd. In particular, I am deeply indebted to Mr. Hidemi Matsuzawa, Dr. Akira Yoshinaka, Dr. Takao Takenaka and Dr. Masatake Katayama for their continueing support in all phases of this work. I must appreciate Mr. Takatoshi Nagoya and Mr. Masanori Mayusumi for supplying key data of epitaxial growth rates. I am very happy to work with Mr. Hitoshi Tsunoda having fresh idea to progress this work. I also appreciate Mr. Naoto Tate for his many suggestions based on his wide and many experience on silicon epitaxial growth and charaterization.

Finally, my special thanks are due to my family. Satoko, my wife, encouraged to proceed this work. I wish to note here that she is a skillful engineer of computer system. Satoru and Rie, my son and daughter, always made me refresh and made me very happy throughout this work.

CONTENTS

Chapter 1

Introduction

1.1 Background

1.1.1 *Silicon crystal*

Crystalline materials are used in many fields of science and technology. Especially, artificial crystals, such as germanium, silicon, gallium phosphide, gallium arsenide, are fascinating materials for modern and future microelectronics. Silicon is one of the most popular element on earth, being included in earth's crust as silicon oxides. Since silicon dioxide is quite stable in air, silicon crystal must be obtained artificially using crystal growth technique. A silicon crystal ingot is grown using the Czochralsky (CZ) method or the Floating Zone (FZ) method.[1] The ingot is sliced to obtain thin wafers, which are polished to have mirror surface for the fabrication of microelectronics devices. For microelectronic device fabrication, regions, layers or films with various conductivity type and resistivity must be formed in a wafer using the technique of epitaxial growth, diffusion and ion-implantation. The epitaxial growth of silicon has been studied and widely accepted as a key technology since the first report in 1957.[2] Currently, a silicon epitaxial wafer having a very thin epitaxial film is suitable especially for the fabricaton of metal-oxide-semiconductor (MOS) devices[3-6] for latch-up prevention and soft-error reduction. In the near future, the diameter of silicon wafers become larger than 200 mm to achieve high cost performance in the fabrication of microprocessor and computer memories or other devices. Significantly enhanced silicon microelectronic devices require the improvement of the quality of silicon crystal films. Fundamental researches on epitaxial growth are required for future design of silicon crystal and devices.

1.1.2 *Epitaxial growth*

Chemical vapor deposition (CVD) is a key technology to produce thin and uniform films of semiconductor crystals or amorphous materials. Silicon epitaxial growth is

one kind of the CVD, where the film obtained is a single crystal over the substrate.

For epitaxial growth, an epitaxial reactor, source materials and substrates are necessary. Figure 1-1 depicts various phenomena in the epitaxial reactor using gases. The gases including the source species are introduced from the inlet of the reactor and flow to the substrate following the transport phenomena in the reactor. In the preparation of silicon epitaxial thin-films, SiH_4, SiH_2Cl_2, $SiHCl_3$, $SiCl_4$ are generally used with H_2 as the carrier gas. Although $SiHCl_3$ is widely used for epitaxial growth of thin-films in industrial applications, theoretical analysis of film preparation in this system has been discussed in only a few papers,[52-55] in contrast to the SiH_4 [11, 15, 16, 26, 47, 48] and SiH_2Cl_2[17, 18, 56-58] systems which have been studied extensively. In addition, a model for the chemical reaction between $SiHCl_3$ and H_2 has not yet been fully established.

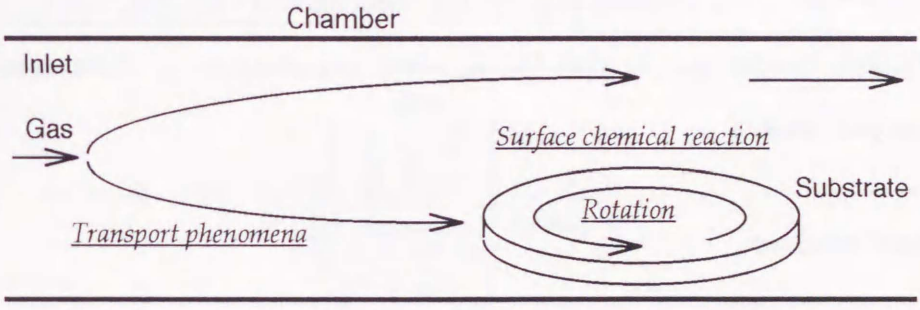

Fig.1-1 Phenomena in an epitaxial reactor.

For many cases in the industrial applications, the substrate usually rotates on its axis or revolves to achieve a flat epitaxial film thickness profile. The substrate has appropriately controlled temperature, which induces the chemical reaction to supply silicon atoms to the substrate surface. The chamber wall of the reactor is usually cooled with air to suppress the chemical reaction at the inside of chamber wall. This temperature environment is called *cold wall*, which is used in many reactors for silicon epitaxial growth.

Since the analyses of film growth in the existing studies for the $SiHCl_3$ system were based on boundary layers and equilibrium theory,[52-55] they are limited to regions in the vicinity of the growth surfaces and must make assumptions about the

concentration of the reactant gas near the surfaces. For an analysis of heterogeneous chemical reaction, such as epitaxial growth, the species concentrations are usually quite different from those at the reactor inlet. Therefore, the transport phenomena in a reactor have recognized as an important subject to be studied.[19] In other words, the transport phenomena in an epitaxial reactor must be solved for the analysis of chemical reactions for the epitaxial growth.

The transport phenomena and the chemical reactions must be clarified for development of new technology in epitaxial growth, since a correct model on the these phenomena can predict an actual epitaxial growth and examine the experimental conditions to reduce the cost of experiments. Issues or subjects to be discussed for the development of the silicon epitaxial growth technology are so many, such as type of an epitaxial reactor, transport phenomena in a reactor including a substrate rotation, surface chemical process, dopant concentration profile, process temperature and surface roughness. In this thesis, these are studied by theoretical and experimental methods.

1.1.3 *Epitaxial reactors*

Here, types of the epitaxial reactors are reviewed briefly, since the characteristics of the films prepared depend on the type of reactor used, for example, (a) pancake, (b) cylinder, (c) barrel, (d) horizontal, (e) single-wafer horizontal and (f) single-wafer vertical type as shown in Fig. 1-2.

A number of pancake reactors (Fig. 1-2 (a)) are commonly used worldwide to prepare silicon epitaxial thin-films. Pancake reactors have a large volume and a tall cold-wall chamber in which significant natural convection is likely to occur. Gases are introduced from the inlet nozzle at the center of the reactor and are exhausted through the outlets at the bottom of the reactor.

Figures 1-2 (b) and (c) schematically show the cylinder[20] and the barrel type reactors. These reactors can perform the epitaxial growth on many substrates at

the same time ascribed to their large volume and tall cold-wall chamber as well as the pancake reactor. Gases are introduced from the top of the reactor and go out through the outlets at the bottom of the reactor.

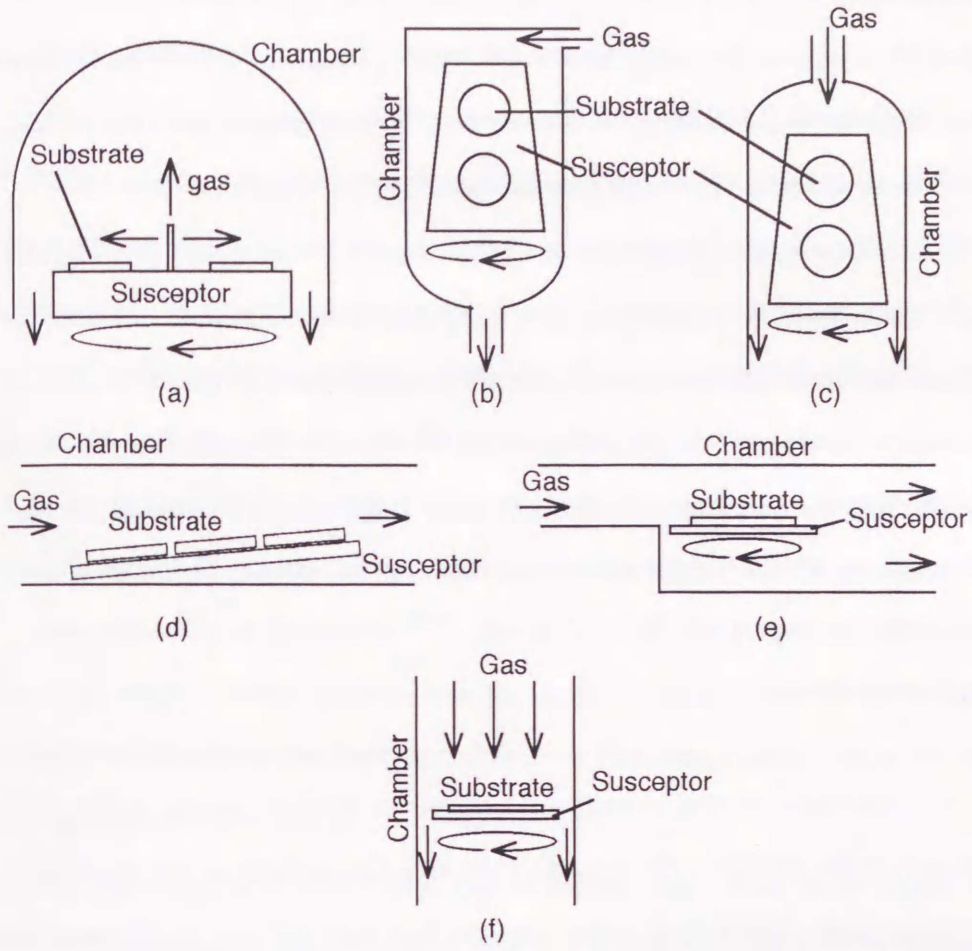

Fig.1-2 Reactor types for silicon epitaxial growth. (a) pancake reactor, (b) cylinder reactor, (c) barrel reactor, (d) horizontal reactor, (e) single-wafer horizontal reactor and (f) single-wafer vertical reactor.

The horizontal reactor shown in Fig. 1-2 (d) is one of the oldest reactor which has substrates along the gas stream. Gases flow horizontally from the inlet to the outlet over the substrates which are arranged in the gas flow direction. Since the substrates cannot be rotated or revolved in this reactor due to its mechanical configuration, the thickness profile is adjusted by tilting the susceptor[7,8] to obtain the uniform thicknesses

A single-wafer horizontal reactor (Fig.1-2 (e)) has only one substrate, which rotates in the reactor chamber. Currently, this type of reactor is widely used in both research and industry; some demonstrate excellent capabilities for preparing large-diameter films on substrates.

Figure. 1-2 (f) depicts a single-wafer vertical type reactor in which gases flow vertically from the top to the bottom of the reactor. The substrate can rotate with high rotation rate to achieve very high growth rate.[9]

All reactors for silicon epitaxial growth use the temperature environment of *cold-wall*, in which the transport phenomena are very complicated because of the co-existence of high and low temperatures, which affect gas density, physical constants of gases, species transport and chemical reactions. To describe the relation between the epitaxial film quality and the reactor type, both the transport phenomena and the chemical reactions should be solved simultaneously and should be made clear.

1.1.4 *Transport phenomena*

Transport of mass, momentum, energy and chemical species occurs in the epitaxial reactor and strongly affect the growth rate and the quality of epitaxial film. Generally, the transport phenomena, especially gas flow motions, are studied mainly by two methods, the gas flow visualization and the numerical simulation. The gas flow visualization is an experiment by which the motions of gases are observed as those of tracer particles or as photo images by the schlieren method. Since the gas flow visualization clearly provides the key information on the transport phenomena in the reactor, this technique has been commonly used for studying gas motions in various fields.[10] However, there exist some problems with respect to the experimental technique of the tracer method, for example, tracer material and equipment for observation. The reliability of the tracer method must be examined since the tracer motions sometimes disagree with the actual gas motions due to a quite higher density of tracer particles than that of gases. For avoiding an errorneous results,

it is quite necessary to compare the gas motions by the gas flow visualization with those by numerical calculations of transport phenomena, which are performed based on the equations of the transport phenomena using a computer.

Numerical simulations of transport phenomena related to film growth by CVD have been reported in many papers for various types of reactors. Although most of them adopted an analysis based on a two-dimensional grid, three-dimensional models [11-16] have become possible recently because of marked improvement in the computing environment. The transport phenomena in pancake[17, 18] and cylinder[20, 21] reactors having jet nozzles and outlets for gas, however, have not been analyzed by any three-dimensional models considering the relatively complicated geometry of the reactors. Unstable and asymmetric gas flows are likely to occur in such reactor chambers because of their great height and large Rayleigh number. Although several notable studies on the pancake reactors have been reported, such as gas flow visualization [22] and numerical calculations.[23-25], large part of the transport phenomena in the pancake reactor is still unclear due to the diffuculty in the analysis. Chapter 2 of this thesis describes the heat and flow in a pancake reactor based on experiments and numerical calculations.

CVD phenomena in horizontal reactors have been studied by many researchers. [12-16, 26-33] Because of its low height and low Rayleigh number, the gas flow tends to be stable even in a cold-wall environment. Kleijn and Hoogendoorn[13] stated that the analysis obtained by a two-dimensional model had nearly the same accuracy as that by three-dimensional model for horizontal reactors with low Rayleigh number and high aspect ratio. This implies that a two-dimensional analysis can be, in some cases, applied with sufficient accuracy to predict transport phenomena and growth rates in a horizontal reactor. In Chapter 3 of this thesis, the transport phenomena in a single-wafer horizontal reactor are focused on using the two-dimensional calculations.

The substrate rotation should be discussed as well as the reactor type and geometry. The susceptor which holds the substrate usually rotate or revolve in the epitaxial reactors shown in Fig. 1-2 in a basic operation. The rotating substrate

induces various changes in transport of reactive gases and temperature above and around itself. In vertical reactors,[9,34-39] the rotating substrate gives relatively simple laminar gas flow above the substrate which provides high growth rate and flat thickness profile.[9,37-39] The reason why the vertical reactor has simple laminar flow is that the direction of gas introduced from the reactor inlet is the same as that of the rotating axis of the substrate. In a single-wafer horizontal reactor, however, gas flow is very complicated because the substrate rotates around a vertical axis while the mainstream flows horizontally. In this reactor, the effect of substrate rotation cannot be described by a two-dimensional model because of the gas motion induced by the rotation. Although many works to model three-dimensional transport phenomena in a reactor have been reported both experimentally and theoretically,[40-46] the rotation of the substrate in horizontal reactors has not yet been discussed. In Chapter 4 of this thesis, the effect of the substrate rotation in a single-wafer horizontal reactor is discussed for the first time.

To evaluate correctly the transport phenomena in a reactor, the dependence of the physical properties of the gas on the gas composition must be considered as well as the dependence on temperature since reactants are often introduced into reactors at relatively high concentrations in actual processes to achieve high productivity. However, this dependence has been considered[13,17,31,47-49] but not enough. In addition, thermal diffusion[11,13-15,17,18,26,28-30,47-51] is expected to affect growth rates in chlorosilane-H_2 system because the difference in molecular weight of SiH_2Cl_2, $SiHCl_3$ and $SiCl_4$ from H_2 is very large. The dependence of growth rate, temperature and gas velocities on the gas compositions should be taken into account for the prediction of the silicon epitaxial growth. This issue is discussed in Chapter 3 of this thesis.

1.1.5 *Surface process*

An epitaxial growth is a result of chemical processes at a substrate surface. An appropriate model for describing the chemical reactions should be developed to

calculate the epitaxial growth rate under the transport phenomena over wide ranges of the growth conditions of the species concentration and the growth temperature.

In silicon epitaxial growth, the growth rate of silicon film increases nonlinearly with increasing reactant concentration and finally saturates at a certain value depending on the growth temperature. A nonlinear dependence of the growth rate on the concentration of $SiHCl_3$ in a $SiHCl_3$-H_2 system is partly attributed to the changes in the gas flow, temperature fields and the thermal diffusion in the reactor. However, the contribution of the transport phenomena are rather small to describe the entire nonlinear behavior of the film growth rate, because the change in the transport phenomena cannot predict the saturation of the growth rate. The elementary reactions should be therefore investigated for an analysis of the growth rate, but appropriate and practical methods for the theoretical approach have not been established. An analysis of complex phenomena in silicon epitaxial growth is quite difficult and still requires large amounts of computation time. The most important thing is to develop compact model which can predict the actual characteristics of the epitaxial film by the epitaxial reactor within a tolerable calculation time.

At the substrate surface, the initial step of the rate limiting process is considered to be a chemisorption of the reactants on the silicon surface, followed by a decomposition of the chemisorbed species and a desorption of the by-products.[59] Based on the discussion for the saturation of the silicon growth rate,[60,61] it is suggested that the Eley-Rideal mechanism[62] is applicable to describe the epitaxial growth rate. By several researchers,[63-69] some modified Langmuir-type models or CVD model have been discussed to describe the actual rate process for chemical vapor deposition (CVD) or etching process. However, these studies have been focused only on the surface reaction processes neglecting the transport phenomena including momentum, heat and species transport throughout a reactor.

To discuss quantitatively the epitaxial growth rate, both surface chemical reactions and transport phenomena in an entire reactor should be taken into account since the concentrations of chemical species at the substrate surface are usually quite

different from the concentration at the entrance of the reactor. However, this kind of studies are only a few. Hierlemann et al.[70] calculated silicon epitaxial growth rate in a SiH_2Cl_2-H_2 system in a showerhead-type rapid thermal low pressure CVD reactor using kinetic data from data base packages.[72, 73] Narusawa[71] showed that the saturation of the epitaxial growth rate in a $SiCl_4$-H_2 system can be described by the model of the transport phenomena in conjunction with the surface reaction model [66, 67] considering adsorption, surface diffusion and heterogeneous chemical reaction. For a $SiHCl_3$ system, theoretical studies should be performed with determining the rate constants of the surface chemical processes based on the experimental results of the epitaxial growth rates. Experimental and theoretical approaches to these topics are discussed in Chapter 5 of this thesis.

1.1.6 *Dopant concentration profile*

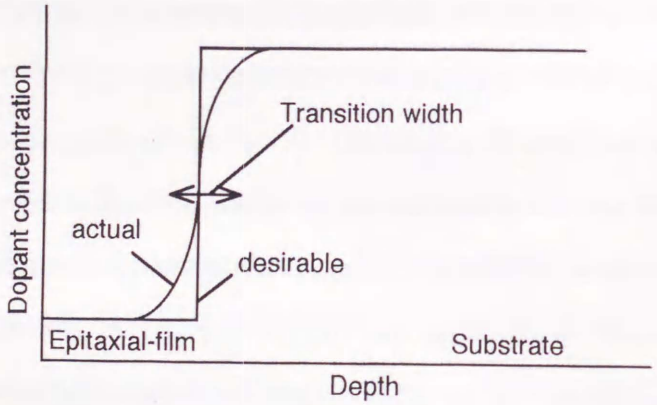

Fig. 1-3 Dopant concentration profile near the interface between substrate and epitaxial film

Quality of an epitaxial wafer should be also discussed as well as the growth rate and the film thickness profile. In an epitaxial wafer, the concentration of dopant atoms changes at the interface between the epitaxial film and the substrate as schematically shown in Fig. 1-3. Although an abrupt profile is desirable, an actual profile inevitably

has some width where the boron conentration changes gradually. The abruptness of the boron concentration profile is evaluated as the transition width.[4] The issue of transition width is very old but has recently become a new problem, since a small transition width is required for the improvement of device integration.[74]

Boron concentration profile in a silicon wafer is formed mainly by two mechanisms: autodoping[75-77] and solid-state diffusion[76,78] as schematically shown in Fig. 1-4. There have been many reports on the autodoping of dopant species incorporated in a substrate, such as boron,[4,79-81] phosphorus,[76,79,82,83] arsenic,[76,79,81,84-88] gallium [76] and antimony.[76,79,83,89] For antimony, phosphorus and arsenic, reduced-pressure epitaxial growth is effective to obtain sharp profiles.[79,82,85,86]

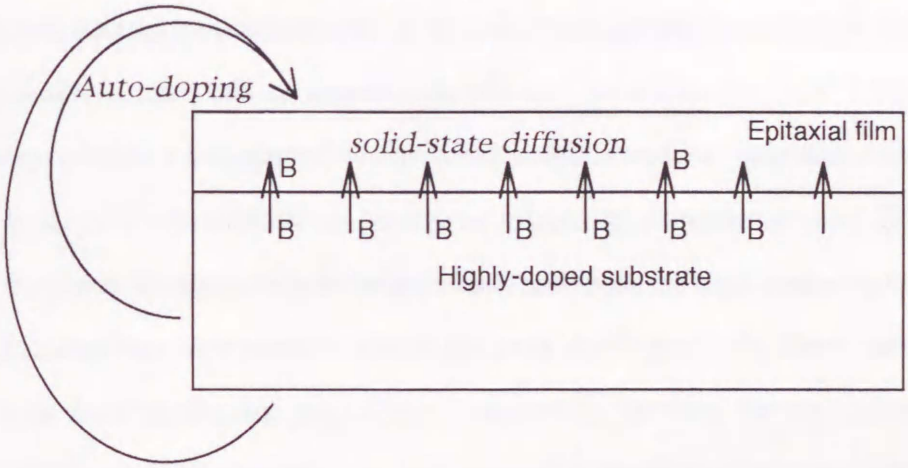

Fig. 1-4 Major mechanism for transport of B atoms from substrate to epitaxial film

The epitaxial wafers for MOS devices generally have a high-resistivity p-type epitaxial film on a low-resistivity p-type substrate, and have boron atoms as dopants in both the epitaxial film and the substrate. Studies have been made on boron autodoping (1) by reduced-pressure epitaxial growth,[4,79,90] (2) by addition of HCl to the ambient during epitaxial growth using silane[80] or (3) by masking the back of the substrate with silicon dioxide.[76,87,88] (1) is reported to enhance autodoping[79] and (2) cannot be applied to the widely used chlorosilane system. (3) is effective and widely used but insufficient.

The boron concentration profile can be sharpened by decreasing the growth temperature, where solid-state diffusion is dominant rather than autodoping. Furthermore, the problem of crystal quality[4] in atmospheric-pressure low-temperature epitaxial growth has been solved by using very high purity gases.[82,91-94] However, the growth rate and the throughput are decreased with decreasing growth temperature. Therefore, atmospheric-pressure epitaxial growth at reasonably high temperatures should be pursued to achieve both an abrupt boron concentration profile and a high cost performance.

From the viewpoint of fluid dynamics, especially under atmospheric pressure, gas recirculation due to natural and forced convection occurs easily to transport the dopant species via the gas phase. These conditions may enhance autodoping and broaden the dopant concentration profile since the convection carries the dopant species to and from the substrate via the gas stream in the reactor. Such a flow field increases the gas residence time, which must be short to obtain an abrupt interface[95,96] in a compound semiconductor hetero-epitaxial wafer.

Natural convection can be suppressed when the height of gas flow region in the reactor is very small. Although such a configuration is currently employed in modern single-wafer horizontal reactors, autodoping and boron concentration profile in the epitaxial wafer grown in such an environment have not been sufficiently discussed. The sharper doping profile was reported[97] to be observed in a single-wafer epitaxial reactor rather than in a batch-type reactor; however, the mechanism has not yet been made clear. Moreover, although autodoping has been discussed for the gas phase in close proximity to the substrate[75-77,80,98-102] or in relation to the growth conditions such as the substrate rotation rate,[9] the difference in the dopant concentration profile between epitaxial reactors having various main gas flow conditions has not been discussed. Therefore, the boron concentration profiles are studied in Chapter 6 of this thesis mainly from the viewpoint of the transport phenomena.

1.1.7 *Process temperature and surface roughness*

For silicon wafers with small diameter, the processes with temperatures up to 1473 K have been often used for the improvement of Czochralski silicon wafers as high-temperature annealing.[103] In the near future, the diameter of silicon wafers is expected to become larger than 200 mm to achieve high cost performance in device fabrication. In processes for wafers larger than 300 mm, thermal stress and slip generation will pose serious problems, because slip generation of a large-diameter wafer is very sensitive to the temperature distribution within the wafer.[104] However, it is very difficult to develop a heating method that has a very uniform temperature profile over the entire wafer. To achieve a slip-free process, the wafer process temperature should be shifted to near or lower than 1000 °C where the mechanical strength, such as the yield stress, is high.[105]

Recently, several researchers[106-110] have discussed surface roughness of a silicon surface heated below 1000 °C in hydrogen ambient. For silicon epitaxial growth process the heat treatment in hydrogen ambient is desirable to remove the native oxide film on the slicon substrate. Ohkura et al.[106] reported that prebaking in hydrogen ambient under 100 torr led to a minimum degree of microroughening, and that the native oxide films acted as a protective film against roughening at the silicon surface. However, Ueda et al.[107] showed that many pits on the silicon surface were formed at 1000 °C through a heating process in hydrogen ambient. They proposed that surface roughening might be due to the behavior of oxygen atoms incorporated in the silicon crystal. Muraoka et al.[108] showed that the low-temperature prebaking process used in epitaxial growth resulted in a rough epitaxial silicon film surface. Yanase et al.[109] studied the silicon surface after hydrogen annealing in detail, and found that the surface annealed at 900 °C had many pits which might be due to the reaction of silicon with small amounts of moisture and oxygen in hydrogen gas in conjunction with the incomplete removal of the native oxide film. Although the chemical reaction between silicon and hydrogen gas was ignored in these studies,

Gallois et al.[110] recently showed that the etch rates of silicon by hydrogen gas at various temperatures were considerably fast.

To realize a desirable heat treatment process, roughening of the silicon surface during the removal of the native oxide film at the temperatures lower than 1000 °C should be studied. Moreover, surface roughening under atmospheric pressure must be investigated because atmospheric-pressure epitaxial growth can be applied to improve cost performance in microelectric device fabrication. The mechanism of surface roughening is investigated in Chapter 7 of this thesis, since it has been unfortunately unknown in spite of the importance of such research.

1.2 Scope of this thesis

After this chapter of introduction, silicon epitaxial growth and epitaxial wafer are discussed from the viewpoints of transport phenomena and surface chemical reactions.

In Chap. 2, gas flow and heat transfer in a pancake reactor for silicon epitaxial film growth are discussed based on a gas flow visualization technique, numerical calculations and growth rate profile of silicon epitaxial film. In the gas flow visualization, motions of NH_4Cl or SiO_2 particles are observed using a high-sensitivity analogue camera. The observed gas flow motions are compared with those obtained by three-dimensional calculations of the transport equations of the mass, momentum and energy.

In Chap. 3, an evaluation of silicon epitaxial thin-film growth using the $SiHCl_3$-H_2 system in a single-wafer horizontal reactor is discussed. Since $SiHCl_3$ is widely used for the epitaxial growth of silicon thin-films in industrial applications, the transport equations for gas velocity, temperature and concentration of chemical species in $SiHCl_3$-H_2 system are solved, taking into account of the dependence of gas properties on temperature and composition. By comparing the measured and calculated growth rates under atmospheric pressure, the increase in growth rate with temperature and $SiHCl_3$ concentration are discussed by assuming an Arrhenius-type expression for the chemical reaction of $SiHCl_3$ and H_2 on a substrate. Transport phenomena in the single-wafer horizontal reactor are discussed in detail.

In Chap. 4, the effect of substrate rotation on transport of reactive gases and epitaxial growth rate is investigated for a single-wafer horizontal reactor using a model and experiments. The governing equations for gas velocity, temperature and chemical species transport are solved for the $SiHCl_3$-H_2 system for silicon thin-film preparation. The effect of the rotating motion of the substrate is discussed under the conditions giving nearly uniform film thickness profile.

In Chap. 5, a transport and epitaxy model to describe silicon epitaxial film growth in a $SiHCl_3$-H_2 system is developed by numerical calculations and comparison with

experiments. The rate of epitaxial growth is calculated by computing the transport of momentum, heat and chemical species in a reactor incorporating chemical reactions at a substrate surface described by the Eley-Rideal model. The reaction processes determining the growth rate consist of chemisorption of $SiHCl_3$ and decomposition by H_2, rate constants of which are evaluated from the model and measured results. The state of the surface during the epitaxial growth is also discussed considering the intermediate species, elementary reactions and rate limiting processes.

In Chap. 6, the boron concentration profile in silicon epitaxial wafers grown under atmospheric pressure is investigated in two types of epitaxial reactors, a single-wafer horizontal reactor and a pancake reactor. Transport phenomena are studied in these reactors by numerical calculations or by a gas flow visualization technique. The difference between the measured boron concentration profile and the calculated one using Fick's law is assumed to be due to autodoping which is mainly due to recirculation of gas in an epitaxial reactor.

In Chap. 7, surface roughness of a silicon wafer heated at 800–1100 °C under atmospheric pressure in hydrogen ambient is studied. Haze of the surface is discussed from the viewpoint of the competitive etching reactions of silicon and silicon dioxide with hydrogen gas. The behavior of surface roughness with pressure and heating time agrees well with that predicted by the pit formation model in this study.

References

[1] F. Shimura, *Semiconductor Silicon Crystal Technology* (Academic Press, San Diego, 1989) Chap.5.

[2] R. C. Sangster, E. F. Maverick and M. L. Croutch, *J. Electrochem. Soc.*, **104**, 317 (1957).

[3] J. G. Posa, *Electronics*, p.93, Feb. 10 (1981).

[4] C. I. Drowley and J. E. Turner, *Proceedings of the Tenth International Conference on Chemical Vapor Deposition 1987*, p.243 (1987).

[5] C. C. Huang, M. D. Hartranft, N. F. Pu, C. Yue, C. Rahn, J. Schrankler, G. D. Kirchner, F. L. Hampton and T. E. Hendrickson, *1982 Int. Electron Devices Meeting Technical Digest*, The Institute of Electrical and Electronics Engineers, Inc., p.454.

[6] D. Takacs, J. Harter, E. P. Jacobs, C. Werner, U. Schwabe, J. Winnerl and E. Lange, *1983 Int. Electron Devices Meeting Technical Digest*, The Institute of Electrical and Electronics Engineers, Inc., p.159.

[7] F. C. Eversteyn, P. J. W. Severin, C. H. J. v. d. Brekel and H. L. Peek, *J. Electrochem. Soc.*, **117**, 925 (1970).

[8] F. C. Eversteyn, *Philips Res. Rep.*, **29**, 45 (1974).

[9] Y. Sato, T. Tamura and T. Ohmine, *Extended Abstracts 1992 Int. Conf. Solid State Devices and Materials*, 20 (1992).

[10] W. J. Yang, Handbook of Flow Visualization (Hemisphere, New York, 1989).

[11] L. Yang, B. Farouk and R. L. Mahajan, *J. Electrochem. Soc.*, **139**, 2666 (1992).

[12] F. S. Lee and G. J. Hwang, *Trans. ASME, J. Heat Transfer*, **113**, 363 (1991).

[13] C. R. Kleijn and C. J. Hoogendoorn, *Chem. Eng. Sci.*, **46**, 321 (1991).

[14] K.F.Jensen, D.I.Fotiadis and T.J.Mountziaris, *J.Cryst.Growth*, **107**, 1 (1991).

[15] H. K. Moffat and K. F. Jensen, *J. Electrochem. Soc.*, **135**, 459 (1988).

[16] S. A. Gokoglu, M. Kuczmarski, P. Tsui and A. Chait, *J. Phys.(Paris)*, **C-5**, 17 (1989).

[17] I.H.Oh, C.G.Takoudis and G.W.Neudeck, *J.Electrochem.Soc.*, **138**, 554 (1991).

[18] I. H. Oh and C. G. Takoudis, *J. Appl. Phys.*, **69**, 8336 (1991).

[19] T. Kagiya, *Kagakuhannou no sokudoronteki kenkyuuhou*(Kagaku Dojin, Kyoto, 1970), Chap.17.

[20] G. W. Cullen, J. F. Corboy and R. Metzl, *RCA Rev.*, **44**, 187 (1983).

[21] X. A. Wang and R. L. Mahajan, *J. Electrochem. Soc.*, **142**, 3123 (1995).

[22] T. Suzuki, Y. Inoue, T. Aoyama and M. Maki, *J. Electrochem. Soc.*, **132**, 1480 (1985).

[23] I.H.Oh, C.G.Takoudis and G.W.Neudeck, *J.Electrochem.Soc.*, **138**, 554 (1991).

[24] I. H. Oh and C. G. Takoudis, *J. Appl. Phys.*, **69**, 8336 (1991).

[25] T. Tsukada, M. Hozawa and N. Imaishi, *J. Chem. Eng. Jpn.*, **25**, 692 (1992).

[26] R. L. Mahajan and C. Wel, *Trans. ASME, J. Heat Transfer*, **113**, 688 (1991).

[27] P. B. Chinoy and S. K. Ghandhi, *J. Cryst. Growth*, **108**, 105 (1991).

[28] P. B. Chinoy, D. A. Kaminski and S. K. Ghandhi, *Numer. Heat Transfer, Part A*, **19**, 85 (1991).

[29] P. B. Chinoy, D. A. Kaminski and S. K. Ghandhi, *J. Electrochem. Soc.*, **138**, 1452 (1991).

[30] A. N. Jansen, M. E. Orazem, B. A. Fox and W. A. Jesser, *J. Cryst. Growth*, **112**, 316 (1991).

[31] L. R. Black, I. O. Clark, B. A. Fox and W. A. Jesser, *J. Cryst. Growth*, **109**, 241 (1991).

[32] M. H. J. M. de Croon and L. J. Giling, *J. Electrochem. Soc.*, **137**, 3606 (1990).

[33] V. S. Ban and S. L. Gilbert, *J. Cryst. Growth* **31**, 284 (1975).

[34] C. R. Kleijn, *J. Electrochem. Soc.*, **138**, 2190 (1991).

[35] C. R. Kleijn, C. J. Hoogendoorn, A. Hasper, J. Holleman and J. Middlehoek, *J. Electrochem. Soc.*, **138**, 509 (1991).

[36] D.I.Fotiadis, A.M.Kremer, D.R.McKenna and K.F.Jensen, *J. Cryst. Growth*, **85**, 154 (1987).

[37] W. G. Breiland and G. H. Evans, *J. Electrochem. Soc.*, **138**, 1806 (1991).

[38] R. Pollard and J. Newman, *J. Electrochem. Soc.*, **127**, 744 (1980).

[39] S. Murakami, Y. Sakachi, H. Nishino, T. Saito, K. Shinohara and H. Takigawa, *J. Cryst. Growth*, **117**, 33 (1992).

[40] C. R. Kleijn and C. J. Hoogendoorn, *Chem. Eng. Sci.*, **46**, 321 (1991).

[41] R.Takahashi, Y.Koga and K.Sugawara, *J.Electrochem.Soc.*, **119**, 1406 (1972).

[42] H. K. Moffat and K. F. Jensen, *J. Cryst. Growth*, **77**, 108 (1986).

[43] H. K. Moffat and K. F. Jensen, *J. Electrochem. Soc.*, **135**, 459 (1988).

[44] F. S. Lee and G. J. Hwang, *J. Heat. Trans.*, **113**, 363 (1991).

[45] S. A. Gokogulu, M. Kuczmarski, P. Tsui and A. Chait, *J. Phys.*(Paris), **C-5**, 17 (1989).

[46] U. Narusawa, *J. Electrochem. Soc.*, **140**, 1509 (1993).

[47] M.E.Coltrin, R.J.Kee and J.A.Miller, *J.Electrochem.Soc.*, **133**, 1206 (1986).

[48] C. R. Kleijn, *J. Electrochem. Soc.*, **138**, 2190 (1991).

[49] C. R. Kleijn, C. J. Hoogendoorn, A. Hasper, J. Holleman and J. Middlehoek, *J. Electrochem. Soc.*, **138**, 509 (1991).

[50] A. H. Dilawari and J. Szekely, *J. Cryst. Growth*, **108**, 491 (1991).

[51] J. P. Jenkinson and R. Pollard, *J. Electrochem. Soc.*, **131**, 2911 (1984).

[52] P. C. Rundle, *Int. J. Electron.*, **24**, 405 (1968).

[53] P. C. Rundle, *J. Cryst. Growth*, **11**, 6 (1971).

[54] D. Laskafeld and T. Roznoy, *Int. Chem. Eng.*, **9**, 440 (1969).

[55] S. E. Bradshaw, *Int. J. Electron.*, **21**, 205 (1966).

[56] F. Langlais, C. Prebende and J. P. Couderc, *J. Cryst. Growth*, **113**, 606 (1991).

[57] Y. Ohshita, A. Ishitani and T. Takada, *J. Cryst. Growth*, **108**, 499 (1991).

[58] C. E. Morosanu, D. Iosif and E. Segal, *J. Cryst. Growth*, **61**, 102 (1983).

[59] S. E. Bradshaw, *Int. J. Electronics*, **21**, 205 (1966).

[60] J. M. Charig and B. A. Joyce, *J. Electrochem. Soc.*, **109**, 957 (1962).

[61] Y. Ohshita, A. Ishitani and T. Takada, *J. Crystal Growth*, **108**, 499 (1991).

[62] D. D. Eley and E. K. Rideal, *Proc. Roy. Soc. (London)*, **A178**, 429 (1941).

[63] M. Kato, J. Murota and S. Ono, *J. Crystal Growth*, **115**, 117 (1991).

[64] J. J. Hsieh, *J. Vac. Sci. Tech.*, **A11**, 304I (1993).

[65] P. A. Coon, M. L. Wise and S. M. George, *J. Crystal Growth*, **130**, 162 (1993).

[66] J. Korec and M. Heyen, *J. Crystal Growth*, **60**, 286 (1982).

[67] J. Korec, *J. Crystal Growth*, **61**, 32 (1983).

[68] R. C. Bracken, *Chemical Vapor Deposition, 2nd Int. Conf.* (Eds.:J. M. Blocher, Jr. and J. C. Withers) The Electrochemical Society (1970), p. 731.

[69] Y. F. Wang and R. Pollard, *J. Electrochem. Soc.*, **142**, 1712 (1995).

[70] M.Hierlemann, A.Kersch, C.Werner and H.Schäfer, *J.Electrochem.Soc.*, **142**, 259 (1994).

[71] U. Narusawa, *J. Electrochem. Soc.*, **141**, 2072 (1994).

[72] R.J.Kee, F.M.Ruply and J.A.Miller, *Chemkin–II: A Fortran Chemical Kinetic Package for the analysis of Gas-Phase Chemical Kinetics*, Sandia National Laboratories, Livermore, CA (1989).

[73] M.E.Coltrin, R.J.Kee and F.M.Ruply, *Surface Chemkin: A Fortran Package for Analyzing Heterogeneous Chemical Kinetics at a Solid-Surface - Gas-Phase Interface*, Sandia National Laboratories, Livermore, CA (1990).

[74] H. M. Liaw, J. Jose and P. L. Fejes, *Solid State Technology*, p.135, May 1984.

[75] J. J. Grossman, *J. Electrochem. Soc.*, **110**, 1065 (1963).

[76] B.A.Joyce, J.C.Weaver and D.J.Maule, *J.Electrochem.Soc.*, **112**, 1100 (1965).

[77] P. H. Langer and J. I. Goldstein, *J. Electrochem. Soc.*, **121**, 563 (1974).

[78] A. S. Grove, A. Roder and T. Sah, *J. Appl. Phys.*, **36**, 802 (1965).

[79] M. W. M. Graef, B. J. M. Leunissen and H. H. C. de Moor, *J. Electrochem. Soc.*, **132**, 1942 (1985).

[80] P. H. Langer and J. I. Goldstein, *J. Electrochem. Soc.*, **124**, 592 (1977).

[81] F. Wong, C. Y. Chen and Y. H. Ku, *Mat. Res. Soc. Symp. Proc.*, **146**, 27 (1989).

[82] T. O. Sedgwick, P. D. Agnello, D. N. Ngoc, T. S. Kuan and G. Scilla, *Appl. Phys. Lett.*, **58**, 1896 (1991).

[83] D. Wong, J. O. Borland and S. Hahn, *Emerging Semiconductor Technology, ASTM Technical Publication 960, Fourth Int. Sym. on Semiconductor*

Processing, p.51, 1987.

[84] J. Halaj, *Cryst. Res. Technol.*, **29**, 33 (1994).

[85] E. Krullmann and W. L. Engl, *IEEE Trans. Electron Devices*, **ED-29**, 491 (1982).

[86] G. R. Srinivasan, *J. Electrochem. Soc.*, **127** 1334 (1980).

[87] G. Skelley and A. C. Adams, *J. Electrochem. Soc.*, **120**, 116 (1973).

[88] W. H. Shepherd, *J. Electrochem. Soc.*, **115**, 652 (1968).

[89] J. Halaj, *Cryst. Res. Technol.*, **28**, 1071 (1993).

[90] C. Galewski and W. G. Oldham, *J. Electrochem. Soc.*, **139**, 543 (1992).

[91] T.O.Sedgwick, M.Berkenblit and T.S.Kuan, *Appl.Phys.Lett.*, **54**, 2689 (1989).

[92] P. D. Agnello and T. O. Sedgwick, *J. Electrochem. Soc.*, **138**, 2785 (1991).

[93] T. O. Sedgwick, P. D. Agnello, M. Berkenblit and T. S. Kuan, *J. Electrochem. Soc.*, **138**, 3042 (1991).

[94] S. K. Kim and H. H. Lee, *J. Electrochem. Soc.*, **141**, 2470 (1994).

[95] C. A. Wang, S. H. Groves, S. C. Palmateer, D. W. Weyburne and R. A. Brown, *J. Crystal Growth*, **77**, 136 (1986).

[96] D.I.Fotiadis, A.M.Kremer, D.R.McKenna and K.F.Jensen, *J.Crystal Growth*, **85**, 154 (1987).

[97] T. Koike, *Proceedings of 19th Workshop on ULSI Ultra Clean Technology*, Tokyo, p.123, 1992.

[98] R. Reif and R. W. Dutton, *J. Electrochem. Soc.*, **128**, 909 (1981).

[99] R. Reif and M. Vanzi, *J. Electrochem. Soc.*, **128**, 2187 (1981).

[100] M. Wong and R. Reif, *IEEE Trans. Electron Devices*, **ED-32**, 83 (1985).

[101] M.Wong, R.Reif and G.R.Srinivasan, *IEEE Trans.Electron Devices*, **ED-32**, 89 (1985).

[102] H. B. Pogge, D. W. Boss and E. Ebert, *Chemical Vapor Deposition, 2nd Int. Conf.* The Electrochemical Society, (Ed: J. M. Blocher, Jr. and J. C. Withers) (1970), p. 768.

[103] D. Gräf, U. Lambert, M. Brohl, A. Ehlert, R. Wahlich and P. Wagner, *J.*

Electrochem. Soc., **142**, 3189 (1995).

[104] F. Shimura, *Semiconductor Silicon Crystal Technology* (Academic Press, San Diego, 1989) Chap.7 , p.285.

[105] K. Yasutake, J. Murakami, M. Umeno and H. Kawabe, *Jpn. J. Appl. Phys.*, **21**, L288 (1982).

[106] A. Ohkura, H. Oku, K. Matsumoto and T. Ohmi, *Extended Abstracts of the 1991 Int. Conf. Solid State Devices and Materials*, Yokohama, 1991, p.559.

[107] K. Ueda, A. Miyauchi, Y. Inoue and T. Suzuki, *Extended Abstracts (The 55th Autumn Meeting, 1994); The Japan Society of Applied Physics*, 19p-ZB-7 ,p. 602 (1994).

[108] T. Muraoka, T. Yasue, T. Nishioka, S Hire and S. Kawazu, *Extended Abstracs (The 41st Spring Meeting, 1994); The Japan Society of Applied Physics and Related Societies*, 29a-ZB-1, p. 250 (1994).

[109] Y. Yanase, H. Horie, Y. Oka, M. Sano, S. Sumita and T. Shigematsu, *J. Electrochem. Soc.*, **141**,3259 (1994).

[110] B. M. Gallois, T. M. Besmann and M. W. Stott, *J. Am. Ceram. Soc.*, **77**, 2949 (1994).

Chapter 2

Gas Flow and Heat Transfer in a Pancake Reactor

2.1 Introduction

In this chapter, the transport phenomena in a pancake reactor, especially gas flow motions, are visualized and calculated using a three-dimensional model including the inlet, the outlets, the susceptor and the bell jar as the crucial parts. The silicon epitaxial thin film is actually prepared in the pancake reactor under the same conditions as those in the gas flow visualization and the numerical calculations since the growth rate profile also provides information on the gas flow direction especially in a single-wafer horizontal reactor[1].

The aim of this investigation is to study correctly the gas flow and heat transfer in a pancake reactor in a steady state. The results from gas flow visualization, numerical calculations and growth rate profile observed in the pancake reactor under atmospheric pressure are compared with each other for the first time. Additionally, the gas flow motions in a pancake reactor are discussed in comparison with those in a single-wafer horizontal reactor.

2.2 Gas flow visualization

2.2.1 *Reactor configuration and experimental conditions*

Figure 2-1 shows the pancake reactor used for this study. Substrates from 3- to 6-inches in diameter are held on a 0.42 m diameter susceptor. This reactor has one inlet nozzle at the center of the susceptor from which the gases flow to the top of the quartz chamber. The reactor also has two outlets connected to the base plate, through which the gases flow out of the reactor chamber. Gas motions are visualized and observed under atmospheric pressure at room temperature and 1423K when the susceptor was not rotated. The gas velocity and the pressure at the inlet were $1.0\,\mathrm{m\,s^{-1}}$ and $1.0133 \times 10^5\,\mathrm{Pa}$, respectively.

Small tracer particles of SiO_2 and NH_4Cl were generated in the reactor to observe

their motions in the gas stream. At room temperature, NH_4Cl particles were produced from the chemical reaction of NH_4OH and HCl. A small plate containing NH_4OH aqueous solution was placed on the susceptor, then HCl gas flowing at 0.5–2 l/min was introduced from the inlet nozzle. As HCl gas approached the susceptor, tracer particles of NH_4Cl were generated. The motions of the transported tracer particles were observed under the hydrogen flow rate of 40 l/min from the inlet nozzle. The temperature of the susceptor was raised to the epitaxial growth temperature of 1423 K, under a hydrogen gas environment with a flow rate of 40 l/min. The gases of $SiHCl_3$ and CO_2 were introduced through the inlet nozzle at the flow rate of 1 l/min. Small tracer particles of SiO_2 were generated from the chemical reaction between $SiHCl_3$ and CO_2 in the gas phase.

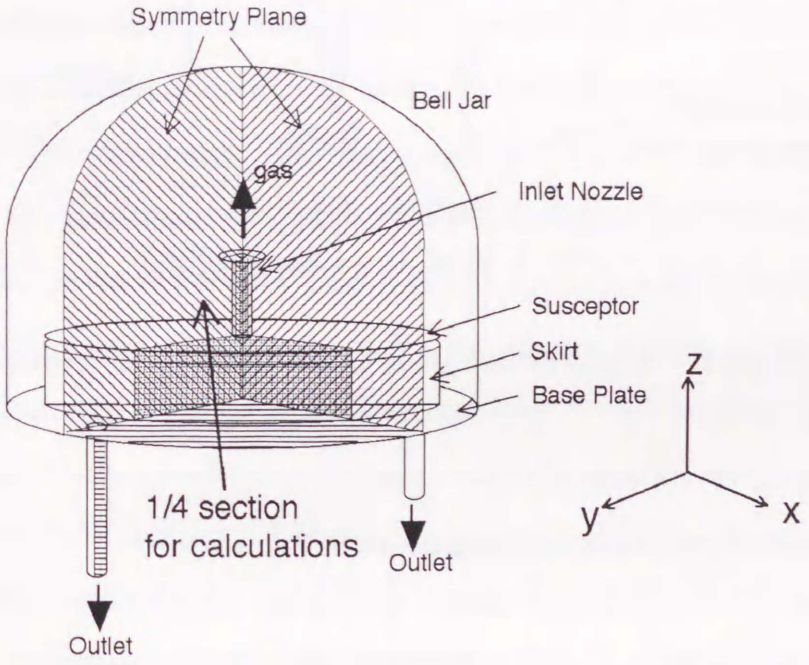

Fig.2-1 Schematic diagram of a pancake reactor for gas flow observation. One-fourth of the reactor is used for the calculation.

As shown in Fig. 2-2, the motions of SiO_2 or NH_4Cl small particles were observed under a two-dimensional sheet of Ar^+ laser (4W) light and were recorded on video by a high-performance analogue camera and an image processing system composed of

SUPER EYE C2847 and DVS-3000 (Hamamatsu Photonics Co., Ltd., Hamamatsu). The SUPER EYE system has been used for optical observation in various fields, such as air flow analysis in a clean room[2] and cell biology[3]. The sheet of Ar^+ laser light enabled visualization of the tracer motions at an angle of about 45 degrees from the front of the reactor chamber. Because the video image of this system included weak noises from the radio induction heating system of the reactor, the video image was taken immediately after cutting off the heat induction current.

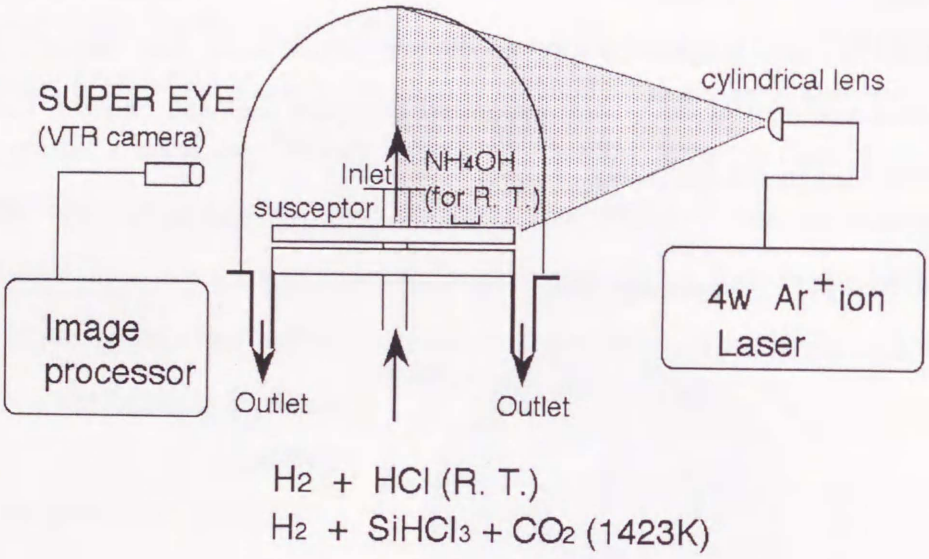

Fig.2-2 The observation system for the smoke tracer method.

2.2.2 *Solution of problems underlying the tracer method*

Gas flow visualization at high temperature in such a large reactor is very difficult because of problems such as the influences of temperature, gas composition, observation period and thermophoresis of the tracer particles in nonisothermal flow. Under inappropriate conditions, tracer motions may show a completely different behavior from that of the actual gas motions. These problems must be solved prior to performing the gas flow observations.

Observations of gas motions at a temperature higher than 1273 K are often dan-

gerous because equipment located near the susceptor as well as the operators are exposed to intense heat radiation from the heated susceptor through the large window designed for the observations. To avoid this, some parts of the reactor and the equipment are modified to assure safe operation when the susceptor is heated to the epitaxial growth temperature. The upper half of the chamber window made of transparent quartz glass is concealed by a door equipped with water cooling pipes, hence the observation is concentrated on the region near the susceptor where the epitaxial film growth occurs.

The gas composition for observations cannot be exactly the same as that for the actual epitaxial growth. The gas flow visualization requires the SiO_2 or NH_4Cl tracers in the present method; however, these particles do not exist during epitaxial growth. Since tracer particles weigh several orders of magnitude more than a carrier gas such as hydrogen, they occasionally show quite different motions from those of carrier gases, for example, tracers travel to the bottom due to gravity even in a horizontal stream. Thermophoresis[4] also causes a problem; the different motions of the particles from the gas stream are due to a temperature gradient[5]. Thermophoretic force transports the tracer particles away from the hot surface of the susceptor and leads to a layer near the surface having a very small amount of tracer particles, which is sometimes incorrectly assumed to be a stagnant layer[4,6]. Very small SiO_2 particles in hydrogen gas at atmospheric pressure have nearly the same thermophoretic coefficient as that of TiO_2 particles[4] which are usually used for gas flow visualization[4,7]. Additionally SiO_2 desirably has much lower density than TiO_2. For these reasons, SiO_2 particles are chosen as tracers for the observations at high temperature. At room temperature, NH_4Cl particles are used for the visualization, because NH_4Cl has lower density than SiO_2 and SiO_2 cannot be produced at room temperature from $SiHCl_3$ and CO_2. NH_4Cl particles are used only at room temperature because they decompose at high temperature. Another reason for using SiO_2 and NH_4Cl instead of TiO_2 is that the source gases, such as NH_4OH, HCl, $SiHCl_3$ and CO_2, do not cause any metallic contamination in the reactor, thus allowing an accurate

epitaxial growth rate with excellent film and without unexpected perturbations.

Immediately after introducing and generating the tracer particles, the tracer motions at various regions in the reactor chamber can be observed clearly since the concentration of the tracer particles is still low. However, this situation lasts only for several seconds after the introduction of the tracer particles[8] since the tracer particles increase in concentration and begin to appear as a dense white cloud. Because a high amount of reactant is necessary to produce the tracer particles, the concentration of the generated particles is rather high and it is often difficult to continue the observation for a long period of time. Furthermore, it is quite difficult to adjust the concentration of the tracer particles. Therfore, the steady-state gas motions cannot be observed by any ordinary method, the naked eye or a normal-sensitivity camera. In this study, the high-sensitivity analogue camera makes it possible to perform the observation for more than 20 minutes after stopping the generation of SiO_2 or NH_4Cl particles. This observation reveals a state with a very low concentration of small-diameter tracer particles, which can be assumed to be the motions of hydrogen gas without any tracers.

The tracer motions should be compared with the calculated motions of gases composed of hydrogen. By showing the agreement between the observed tracer motions and the calculated gas motions, the gas flow motions during the epitaxial growth can be clarified.

2.3 Basic equations governing the epitaxial reactor

2.3.1 *Reactor geometry for calculations*

As Fig. 2-1 shows, the pancake reactor has two symmetry planes: one including the outlet and the other rotated 90 degrees from the outlet. The hatched region between the two symmetry planes, which comprises one-quarter of the entire reactor, is used for the numerical calculations as the representative geometry. With this geometry,

the model is simplified to reduce the calculation time. Although the susceptor is usually rotated during the epitaxial growth, this model cannot be applied to calculate the effect of the susceptor rotation. The difference in gas motions between the results with and without rotation was examined prior to a series of experiments of the visualization. There was no significant change for the range of rotation rate between 0 and 10 rpm; therfore, the results in this study are also applicable to the case where the susceptor has small rotation rates.

2.3.2 *Transport equations and boundary conditions*

To examine the results from the visualization method, it is necessary to compare the results of gas motions obtained experimentally with those obtained by the numerical calculations of the transport phenomena in the reactor in a steady state using three-dimensional Cartesian coordinates. The governing equations for the gas velocity are as follows.

Conservation of mass:

$$\frac{\partial \rho u}{\partial x} + \frac{\partial \rho v}{\partial y} + \frac{\partial \rho w}{\partial z} = 0. \tag{2-1}$$

Conservation of momentum:

$$\frac{\partial \rho uu}{\partial x} + \frac{\partial \rho vu}{\partial y} + \frac{\partial \rho wu}{\partial z} = -\frac{\partial p}{\partial x} - \frac{\partial \tau_{xx}}{\partial x} - \frac{\partial \tau_{yx}}{\partial y} - \frac{\partial \tau_{zx}}{\partial z}, \tag{2-2}$$

$$\frac{\partial \rho uv}{\partial x} + \frac{\partial \rho vv}{\partial y} + \frac{\partial \rho wv}{\partial z} = -\frac{\partial p}{\partial y} - \frac{\partial \tau_{xy}}{\partial x} - \frac{\partial \tau_{yy}}{\partial y} - \frac{\partial \tau_{zy}}{\partial z}, \tag{2-3}$$

$$\frac{\partial \rho uw}{\partial x} + \frac{\partial \rho vw}{\partial y} + \frac{\partial \rho ww}{\partial z} = -\frac{\partial p}{\partial z} + \rho g - \frac{\partial \tau_{xz}}{\partial x} - \frac{\partial \tau_{yz}}{\partial y} - \frac{\partial \tau_{zz}}{\partial z}, \tag{2-4}$$

where

$$\tau_{xx} = -\mu \left[2\frac{\partial u}{\partial x} - \frac{2}{3}\left(\frac{\partial u}{\partial x} + \frac{\partial v}{\partial y} + \frac{\partial w}{\partial z} \right) \right], \tag{2-5}$$

$$\tau_{yy} = -\mu \left[2\frac{\partial v}{\partial y} - \frac{2}{3}\left(\frac{\partial u}{\partial x} + \frac{\partial v}{\partial y} + \frac{\partial w}{\partial z} \right) \right], \tag{2-6}$$

$$\tau_{zz} = -\mu \left[2\frac{\partial w}{\partial z} - \frac{2}{3}\left(\frac{\partial u}{\partial x} + \frac{\partial v}{\partial y} + \frac{\partial w}{\partial z} \right) \right], \tag{2-7}$$

$$\tau_{xy} = \tau_{yx} = -\mu \left(\frac{\partial u}{\partial y} + \frac{\partial v}{\partial x} \right), \tag{2-8}$$

$$\tau_{yz} = \tau_{zy} = -\mu\left(\frac{\partial v}{\partial z} + \frac{\partial w}{\partial y}\right), \tag{2-9}$$

$$\tau_{zx} = \tau_{xz} = -\mu\left(\frac{\partial w}{\partial x} + \frac{\partial u}{\partial z}\right). \tag{2-10}$$

In equations (2-1)–(2-10), ρ, p and μ are the density, pressure and viscosity of the gas and u, v and w are velocities in the x-, y- and z-directions, respectively. The gas velocities, u, v and w, are set to be zero on all surfaces of the solid walls as boundary conditions. The gas velocity and pressure at the inlet are $1.0\,\mathrm{m\,s^{-1}}$ and $1.0133 \times 10^5\,\mathrm{Pa}$, respectively, which are consistent with the actual observation.

The temperature, T, in the reactor is expressed by the following energy equation. Conservation of energy:

$$\frac{\partial \rho u C_\mathrm{p} T}{\partial x} + \frac{\partial \rho v C_\mathrm{p} T}{\partial y} + \frac{\partial \rho w C_\mathrm{p} T}{\partial z} = \frac{\partial}{\partial x}\left(\lambda \frac{\partial T}{\partial x}\right) + \frac{\partial}{\partial y}\left(\lambda \frac{\partial T}{\partial y}\right) + \frac{\partial}{\partial z}\left(\lambda \frac{\partial T}{\partial z}\right). \tag{2-11}$$

In this equation, C_p is the heat capacity of the gas at constant pressure, and λ is the thermal conductivity of the gas.

The effect of radiation in the gas phase is of minor significance, because monoatomic and diatomic gases, such as hydrogen, helium and nitrogen, radiate weakly, even at high temperature. Radiation from the susceptor surface affects only the temperature of the quartz chamber wall[9]. According to the assumptions mentioned above, the heat transfer by radiation is ignored in this study and the following boundary conditions are imposed on equation (2-11). The temperature of the susceptor surface, T_s, is 1423 K. The temperature of the quartz wall surrounding the entire gas stream is assumed to be 300 K. In fact, the temperature at the outside surface of the quartz chamber wall did not exceed 500 K even when the susceptor was heated to 1473 K. Therefore the difference in the wall temperature between the calculations and actual value should be within 200 K, and this difference is assumed to be allowable in such an environment having a very large temperature difference.

The gas density obeys the ideal gas law

$$\rho = \frac{pM}{RT}, \tag{2-12}$$

where M is the molecular weight of the gas and R is the gas constant.

To solve the transport equations described above, the calculation domain is divided into a nonuniform mesh with 31 × 34 × 49 grid points (total 51646) in the x-, y- and z-directions. Although the use of so-called boundary fitted coordinates (BFC) has been very common for several years to model flows in complex geometries, the rectangular gridding on Cartesian coordinates are used in this study because the results from these coordinates in various geometries are qualitatively correct[10] and the calculatation time is shorter than that on BFC. To estimate the influence due to rectangular gridding on Cartesian coordinates and the number of grid points, it was found that the results from about half the grid points were essentially the same as those in this paper. The gas is assumed to be composed of 100% hydrogen. The gas properties of H_2, such as viscosity, heat capacity and thermal conductivity, are taken from the literature[11-13]. Each physical constant is expressed as a function of temperature.

Equations (2-1)–(2-12) for gas velocity and temperature are discretized into finite difference formulae and solved based on the SIMPLER algorithm[10]. The calculations are performed on an Apple Macintosh IIcx personal computer with a Tektronix RP88 coprocessor board. The calculations in this work took over six months.

2.4 Results and discussion

2.4.1 *Gas motions at room temperature*

As a preliminary step, the gas flow visualizations and the calculations are performed at room temperature in order to evaluate the capability of the visualization system used, especially its ability to allow observations for long periods of time.

Figure 2-3 shows the observed particle streamlines at room temperature. Observations could be made from the start of the introduction of the tracer particles to the end of their generation, and even up to the state where they were present at

very low concentrations. The entire process was carried out for more than 20 minutes without any trouble. Gases including the small tracer particles of NH_4Cl are transported to the top of the quartz chamber. After reaching the top, the gases flow downward along the sidewall and approach to the center of the susceptor.

Fig.2-3 Gas motions observed in the pancake reactor at room temperature. Hydrogen flow rate is 40 l/min.

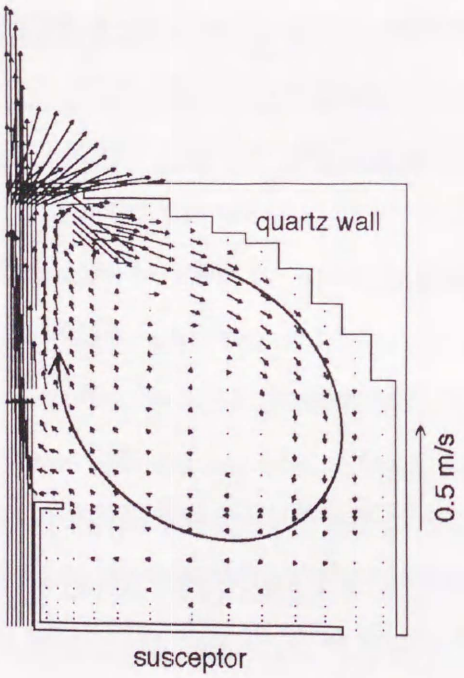

Fig.2-4 Vector diagrams of gas flow velocity at room temperature in the pancake reactor. Hydrogen flow rate is 40 l/min.

These observed recirculating gas streams are compared with the calculated ones. The calculated gas streams are shown in Fig. 2-4, which are obtained in the steady state. The calculated gas motions also show large recirculation. Since the gases spread throughout the entire quartz chamber, the gas velocity along the susceptor is much lower than that near the top of the chamber. The gas motions in Figs. 2-3 and 2-4 show good qualitative agreement. It is therefore concluded that the gases in the pancake reactor recirculate in the chamber.

2.4.2 *Gas flow and heat transfer at epitaxial growth temperature*

In this section, the gas motions in the pancake reactor at the temperature for epitaxial growth are discussed. As mentioned above, the observation is limited to the vicinity of the susceptor. Although the diameter of the SiO_2 particles during the observation could not be measured, the diameter measured after the observation was found to be less than 20 μm under an optical microscope. This value indicates the maximum diameter because it was measured after many processes such as aggregation in the gas phase, sedimentation on the susceptor and sticking on the chamber wall. The diameter of particles observed in this study is assumed to be much less than 20 μm and to be close to 1 μm which is easily recognized by the SUPER EYE. In the reactor, near-steady-state motions of the gas flow are observed, as shown in Fig. 2-5. The gases flow from the outside toward the center of the susceptor, then these flow upward from the inlet nozzle and downward along the sidewall of the reactor chamber.

For a more precise discussion, numerical calculations are performed for this gas flow system. The calculated gas motions are shown in Fig. 2-6, which are the same as the tracer motions observed in Fig. 2-5. At the epitaxial growth temperature, the gases near the susceptor flow parallel to the susceptor. Figure 2-6 shows that the gases along the susceptor have high velocity because of the expansion of gas volume near the heated susceptor. These gases flow upward at the center of the susceptor

and are accelerated by the gases introduced from the inlet nozzle.

Fig.2-5 Gas motions observed around the susceptor in the pancake reactor. The temperature of susceptor is 1423 K and hydrogen flow rate is 40 l/min.

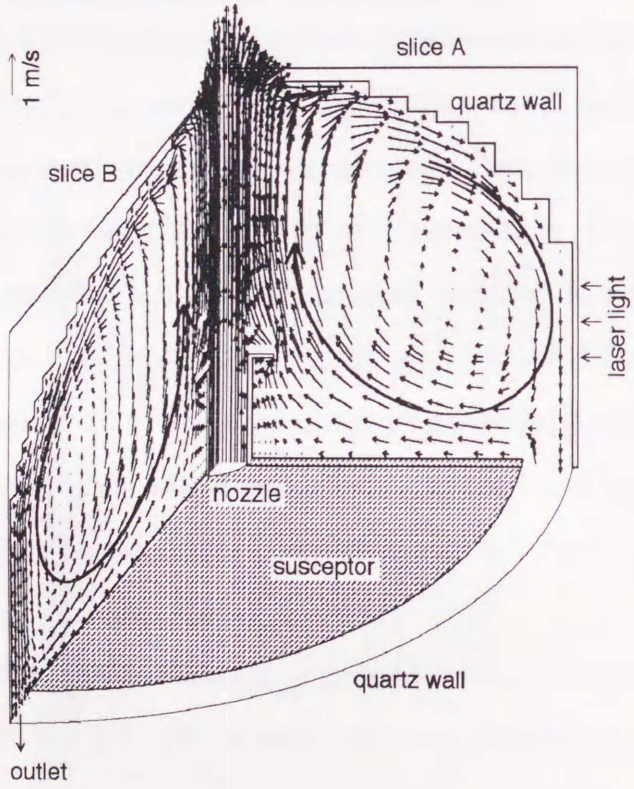

Fig.2-6 Calculated gas flow motions in two vertical slices of the pancake reactor. Slice A is the plane enlightened by the laser light and slice B is that including the outlet. The temperature of susceptor is 1423 K and hydrogen flow rate is 40 l/min.

Although the gas motions at the top of the reactor chamber cannot be observed in the visualization because of safety problems, the results of calculations show that the gas motions are essentially similar to those at room temperature in the entire reactor chamber.

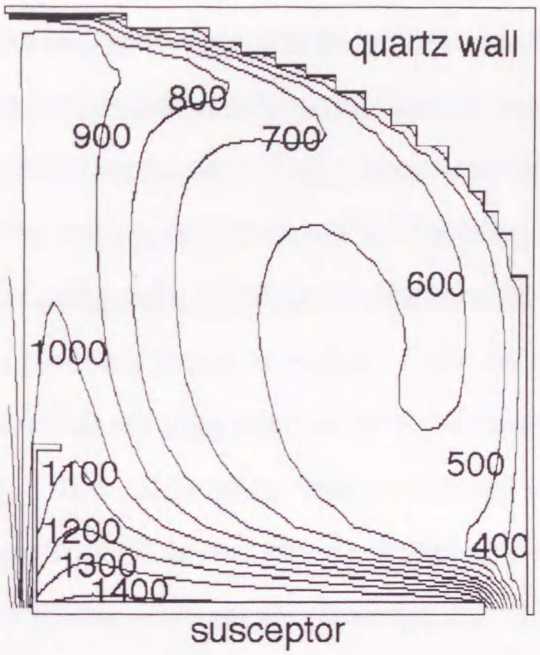

Fig.2-7 Contour diagram of temperature in the pancake reactor. The temperature of susceptor is 1423 K and hydrogen flow rate is 40 l/min.

During these gas motions in the gas phase, the temperature near the center of the susceptor is higher than that at the outer edge of the susceptor and near the chamber wall, as shown in Fig. 2-7. The temperature profile in Fig. 2-7 tends to induce natural convection because the temperature near the susceptor is higher than that near the top of the chamber. However, the gas motions are found to maintain a horizontal flow. The downstreaming of gases along the chamber wall forces the gases on the susceptor to flow horizontally toward the center of the susceptor. The forced horizontal gas flow is considered to suppress the generation of natural convection. The maximum gas velocity in the horizontal direction appears at a position about 0.03–0.05 m above the susceptor, as shown in Fig. 2-6. When this distance is assumed

as the typical length, the Grashof and Rayleigh numbers near the susceptor are estimated as about 300, which is much smaller than the critical Rayleigh number[14]. The gas motions can hence be considered to be in a near-steady state, as observed in this study.

The pancake reactor is sometimes called the vertical reactor because it has been speculated that this reactor provides uniform and vertical gas flow toward the susceptor[15]. However, the gases near the susceptor in this study behave like those in a single-wafer horizontal reactor according to the discussion above, and coincides with the results of Oh and co-workers[9,16]. To confirm the gas motions obtained from the observations and numerical calculations, epitaxial silicon film is prepared using the $SiHCl_3$-H_2 system under the same conditions of gas flow rate and temperature as discussed above. When gases flow over the substrate, the chemical reaction by which silicon film growth occurs results in consumption of the $SiHCl_3$ molecules, thus the depletion of $SiHCl_3$ leads to a higher growth rate at the upstream side and a lower one at the downstream side. This growth rate profile is usually observed in a single-wafer horizontal reactor[1]. From the viewpoint of the gas flow direction, the actual growth rate profile in Fig. 2-8 clearly shows that the upstream side corresponds to the outer edge of the susceptor and the downstream side corresponds to the center of the susceptor. The trend of the observed epitaxial growth rate profile is in good agreement with those predicted by observations and numerical calculations of gas motions.

In this study, the three-dimensional calculations can also estimate the effect of the location of gas outlets because these calculations take into consideration the position of the outlets in the reactor chamber. Figure 2-6 shows that the gas flow motions above the susceptor are almost symmetrical around the inlet nozzle located at the center of the reactor chamber. The influence of the position of the outlets on epitaxial growth is negligible in the pancake reactor.

In industrial applications, silicon epitaxial thin films with a very uniform thickness profile are produced on the substrates. The results obtained in this study do not

show the conditions required to obtain good uniformity. Thus modifying the gas flow rate, the temperature profile on the susceptor and the design of the nozzle jet[8] is a suitable way to achieve good thickness uniformity. Increasing the diameter or height of the reactor chamber may generate several vortices in addition to the large recirculation stream discussed in this study. In the pancake reactors discussed by Oh and co-workers[9,16], the height of which was twice that in this study, the existence of two recirculating flows in opposite direction was shown at higher flow rates. In this situation, gas streams in the pancake reactor become very complicated and unstable and the variation of the growth rate on the substrate due to such gas streams may be averaged to obtain a flat profile of the thin film by rotating the susceptor or by unstably changing gas streams.

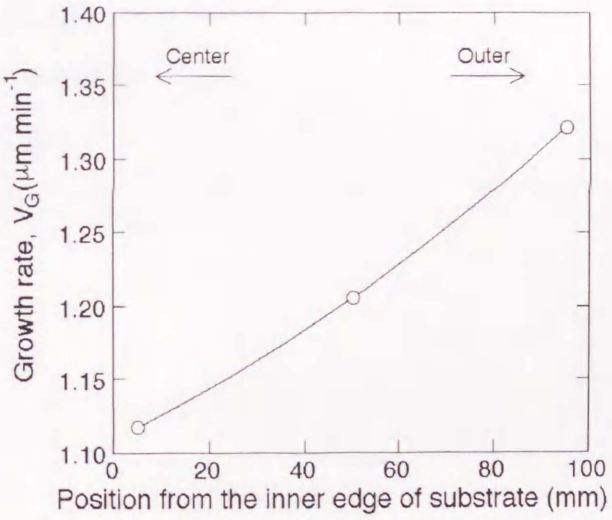

Fig.2-8 Observed growth rate profile of silicon epitaxial film in the pancake reactor. The temperature of susceptor is 1423 K and hydrogen flow rate is 40 l/min including 0.7 mol% of $SiHCl_3$.

2.5 Conclusions

The transport phenomena in a pancake reactor for preparation of silicon epitaxial

thin films have been discussed experimentally and numerically. The motions of tracers composed of low-density materials, such as NH_4Cl or SiO_2, can be observed for a very long period using a high-sensitivity analogue camera. The gas motions are numerically calculated from the viewpoint of transport phenomena. These results are consistent with those indicated by the growth rate profile. A large recirculating flow in the reactor chamber exists at both room temperature and the epitaxial growth temperature. It is concluded that the gases near the susceptor flow horizontally in the pancake reactor under atmospheric pressure for epitaxial silicon film growth.

Nomenclature

C_p : heat capacity at constant pressure	$(J\,kg^{-1}\,K^{-1})$
g : acceleration due to gravity	$(m\,s^{-2})$
M: molecular weight of gas	$(kg\,mol^{-1})$
p : pressure	(Pa)
R : gas constant	$(J\,mol^{-1}\,K^{-1})$
T : temperature	(K)
u : fluid velocity in x-direction	$(m\,s^{-1})$
v : fluid velocity in y-direction	$(m\,s^{-1})$
w : fluid velocity in z-direction	$(m\,s^{-1})$
x : coordinate in horizontal direction	(m)
y : coordinate in horizontal direction	(m)
z : coordinate in vertical direction	(m)
λ : thermal conductivity of gas	$(W\,m^{-1}\,K^{-1})$
μ : viscosity of gas	(Pa·s)
ρ : density of gas	$(kg\,m^{-3})$

References

[1] Chapter 3 in this thesis.

[2] M. Inoue, T. Shirai, T. Yoshida and T. Okada, *J. Visualization Soc. Jpn.*, **14**, 34 (1994).

[3] E. Kamitsubo, Y. Ohashi and M. Kikuyama, *Protoplasma*, **152,** 148 (1989).

[4] D. I. Fotiadis and K. F. Jensen, *J. Crystal Growth*, **102**, 743 (1990).

[5] L. Talbot, R. K. Cheng, R. W. Schaefer and D. R. Willis, *J. Fluid Mech.*, **101**, 737 (1980).

[6] F.C.Eversteyn, P.J.W.Severin, C.H.J.v.d.Brekel and H.L.Peek, *J.Electrochem. Soc.*, **117**, 925 (1970).

[7] E. P. Visser, C. R. Kleijn, C. A. M. Govers, C. J. Hoogendoorn and L. J. Giling, *J. Crystal Growth*, **94**, 929 (1989).

[8] T. Suzuki, Y. Inoue, T. Aoyama and M. Maki, *J. Electrochem. Soc.*, **132**, 1480 (1985).

[9] I.H.Oh, C.G.Takoudis and G.W.Neudeck, *J.Electrochem.Soc.*, **138**, 554 (1991).

[10] S. V. Patankar,*Numerical Heat Transfer and Fluid Flow* (McGraw-Hill, New York, 1990).

[11] *Kagaku Binran* (Handbook of Chemistry) (Iwanami, Tokyo, 1984) 3rd ed., Chap. 6, p. II-39 [in Japanese].

[12] *Kagaku Binran* (Handbook of Chemistry) (Iwanami, Tokyo, 1984) 3rd ed., Chap. 6, p. II-71 [in Japanese].

[13] *Kagaku Binran* (Handbook of Chemistry) (Iwanami, Tokyo, 1984) 3rd ed., Chap. 9, p. II-239 [in Japanese].

[14] C. P. Jackson and K. H. Winters, *Int. J. Num. Methods Fluids*, **4**, 127 (1984).

[15] F. Shimura, *Semiconductor Silicon Crystal Technology* (Academic Press, San Diego, 1989) Chap.5, p.204.

[16] I. H. Oh and C. G. Takoudis, *J. Appl. Phys.*, **69**, 8336 (1991).

Chapter 3

Numerical Evaluation of Silicon Thin Film Growth from $SiHCl_3$-H_2 Gas Mixture in a Single-Wafer Horizontal Reactor

3.1 Introduction

The primary purpose of this Chapter is to develop a numerical model which can practically describe silicon epitaxial film growth from a $SiHCl_3$ and H_2 gas mixture in a single-wafer horizontal reactor. To accurately analyze the transport of reactant gases in a reactor with highly nonisothermal flow, a computational model to predict gas flow, temperature and concentration fields is presented taking into account the change in gas properties due to gas composition and temperature. The rate of a simplified surface reaction scheme is evaluated to describe film preparation processes since the elementary reaction schemes have not been fully clarified yet. The reaction rate is estimated using measured and predicted growth rates. The effects of $SiHCl_3$ concentration and thermal diffusion on the growth rate are also discussed.

3.2 Preparation of epitaxial silicon thin film

3.2.1 *Reactor configuration and chemical reaction*

Figure 3-1 shows the geometry of the reactor studied in this work. For our analysis of thin-film preparation on a heated substrate, we consider the preparation of silicon epitaxial thin films by the thermal decomposition of $SiHCl_3$ with H_2 gas. The gas mixture is introduced into the reactor and reacts at the surface of a substrate held horizontally in the reactor (1 in Fig. 3-1). The susceptor is designed to prepare an epitaxial layer on an 8-inch-diameter wafer. The substrate is heated to 1450 K using infrared furnaces through the reactor walls consisting of quartz glass.

In order to evaluate the film growth rate in the case of the reactor with nonuniformly distributed temperature and gas flow fields, the mass, momentum and energy transport equations must be solved. The present model consists of transport equations and a chemical reaction at the surface of the substrate. Substrate rotation and heat of reaction are ignored in this Chapter. Crystalline defects due probably to

fine particles formed by gas-phase reaction were not observed for the present reactor. Consequently, effects of thermal non-equilibrium states induced by radiation by the infrared furnaces, such as enhancement of gas-phase reaction, are considered to be very small, thus these effects are also ignored in the analysis. We focus mainly on the growth rate of a Si-thin film at the center of the substrate and investigate the dependence of the growth rate on temperature and the concentration of $SiHCl_3$.

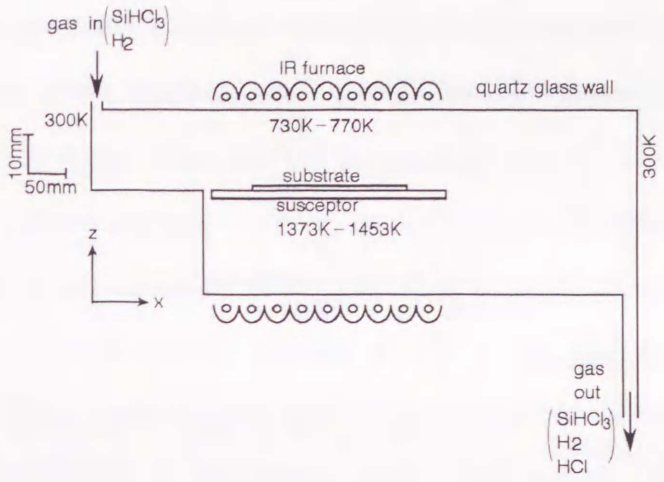

Fig. 3-1 Single-wafer horizontal reactor for preparation of silicon film.

In many previous theoretical analyses of the film preparation processes, surface reactions are described using a physical mechanism such as the mass flux by diffusion[1-9] or a collision model.[10-12] These models may be appropriate when all elementary reactions for film formation are understood. However, neither the elementary reactions nor the rate-limiting process in the reactions have been determined for the $SiHCl_3$-H_2 system. In this case, using an Arrhenius-type expression for the chemical reactions and considering a simplified reaction scheme is a practical method to model all the reaction phenomena. We therefore consider the preparation of a silicon film on the basis of the following overall reaction:

$$SiHCl_3 + H_2 \rightarrow Si + 3HCl. \tag{3-1}$$

In this Chapter, we determine the rate of chemical reaction of equation (3-1) by the numerical model described later. The activation energy, E, is assumed to be

that proposed by Eversteyn[13] ($E = 1.38 \times 10^5\,\mathrm{J\,mol^{-1}}$) for the reaction-limited regime since the path of the chemical reaction is assumed to be the same over a wide temperature range. The pre-exponential factor, which has not been reported to date, is estimated in this Chapter.

3.2.2 *Basic equations governing the epitaxial reactor*

The transport phenomena in the reactor in a steady state are solved using two-dimensional Cartesian coordinates. The governing equations for the gas velocity are as follows:

Conservation of mass:

$$\frac{\partial}{\partial x}(\rho u) + \frac{\partial}{\partial y}(\rho v) = 0. \tag{3-2}$$

Conservation of momentum:

$$\frac{\partial}{\partial x}(\rho u u) + \frac{\partial}{\partial y}(\rho v u) = \frac{\partial}{\partial x}\left(2\mu\frac{\partial u}{\partial x}\right) + \frac{\partial}{\partial y}\left(\mu\frac{\partial u}{\partial y}\right) + \frac{\partial}{\partial y}\left(\mu\frac{\partial v}{\partial x}\right) - \frac{\partial p}{\partial x}. \tag{3-3}$$

$$\frac{\partial}{\partial x}(\rho u v) + \frac{\partial}{\partial y}(\rho v v) = \frac{\partial}{\partial y}\left(2\mu\frac{\partial v}{\partial y}\right) + \frac{\partial}{\partial x}\left(\mu\frac{\partial v}{\partial x}\right) + \frac{\partial}{\partial x}\left(\mu\frac{\partial u}{\partial y}\right) - \frac{\partial p}{\partial y} + \rho g. \tag{3-4}$$

In eqs. (3-2)–(3-4), u and v are horizontal and vertical velocities, ρ, p and μ are the density, pressure and viscosity, respectively, of the mixture of $SiHCl_3$, H_2 and HCl gas.

The gas density obeys the ideal gas law

$$\rho = \frac{pM_{\mathrm{av}}}{RT}, \tag{3-5}$$

where M_{av} is the local average molecular weight of the gas and R is the gas constant.

The gas velocities, u and v, are set to be zero on all the surfaces of the solid walls as boundary conditions. The gas velocity and pressure at the inlet are $0.67\,\mathrm{m\,s^{-1}}$ and $1.0133 \times 10^5\,\mathrm{Pa}$, respectively.

The temperature distribution, T, in the reactor is expressed by the following energy equation:

Conservation of energy:

$$\frac{\partial}{\partial x}(\rho C_{\mathrm{p}} T u) + \frac{\partial}{\partial y}(\rho C_{\mathrm{p}} T v) = \frac{\partial}{\partial x}\left(\lambda \frac{\partial T}{\partial x}\right) + \frac{\partial}{\partial y}\left(\lambda \frac{\partial T}{\partial y}\right). \tag{3-6}$$

In this equation, C_{p} is the heat capacity of the gas at constant pressure, and λ the thermal conductivity of the gas.

The temperature of the substrate surface, T_{s}, is varied between 1393 K and 1453 K. This temperature is maintained constant by continuously monitoring the temperature and controlling the input power of the infrared furnaces. The temperature at the inner surface of the walls immediately above and below the substrate (region 2 in Fig. 3-1) is higher than the temperature of the other walls. The outer surfaces of these quartz walls are, however, cooled with a sufficiently large amount of cold air, so that it is reasonable to neglect absorption of radiation heat by the transparent walls. Since the concentrations of $SiHCl_3$ and HCl are low, effects of radiation heat on these gases are assumed to be negligible. According to the assumptions mentioned above, we ignore heat transfer by radiation in equation (3-6) and impose the following boundary conditions on the equation. Since accurate measurement of the temperature in region 2 is extremely difficult, the temperature is estimated empirically and assumed to vary linearly with the substrate temperature in the range between 730 K and 770 K. The reactor wall illustrated by the hatched region in Fig. 3-1 is treated as a conducting wall with the thermal conductivity of quartz glass. The outer surface of this region (dotted lines in Fig. 3-1) is taken to be surrounded by adiabatic walls. The temperature of the other reactor walls is regarded as 300 K since the walls are continuously cooled with water.

Conservation of chemical species i (i = $SiHCl_3$, H_2 and HCl) is described by the following equation:

Conservation of species:

$$\frac{\partial}{\partial x}(\rho u \omega_i) + \frac{\partial}{\partial y}(\rho v \omega_i) = \frac{\partial}{\partial x}\left(\rho D_i \frac{\partial \omega_i}{\partial x} + D_i^{\mathrm{T}} \frac{\partial \ln T}{\partial x}\right) + \frac{\partial}{\partial y}\left(\rho D_i \frac{\partial \omega_i}{\partial y} + D_i^{\mathrm{T}} \frac{\partial \ln T}{\partial y}\right). \tag{3-7}$$

In this equation, ω_i is the mass fraction of species i. The diffusion coefficient, D_i, is

assumed to be the binary diffusion coefficient of species i in H_2 gas since the mole fraction (not mass fraction) of species other than H_2 is small. The mass transport phenomena driven by the temperature gradient (thermal diffusion) are described by the terms relating to D_i^T, the thermal diffusion coefficient. D_i^T is expressed as

$$D_i^T = \alpha_i \rho D_i \omega_i \omega_{H_2}, \tag{3-8}$$

where α_i is the thermal diffusion factor of species i.

At the inlet of the reactor the composition of the $SiHCl_3$ and H_2 gas mixture is expressed in terms of the average molecular weight MW given by

$$MW = \sum_i x_i M_i \quad (i = SiHCl_3 \text{ and } H_2), \tag{3-9}$$

where x_i and M_i are the mole fraction and molecular weight of species i. The average molecular weight at the inlet, MW, is varied between 2×10^{-3} and 55×10^{-3} kg mol^{-1}, which corresponds to pure H_2 and 39.7 mol% (or 97.8 wt%) $SiHCl_3$ in H_2, respectively.

At the surface of the substrate, mass changes due to chemical reaction on the surface are considered in the boundary conditions. Assuming that the reaction of equation (3-1) is a second-order reaction, the mass rate of consumption or generation of species i at the surface is expressed as

$$R_i = \nu_i M_i k [SiHCl_3][H_2], \tag{3-10}$$

where k is the rate constant for the reaction expressed as $k = A \exp(-E/RT)$, and the values of the molar stoichiometry coefficient, ν_i, are - 1 for $i = SiHCl_3$ and H_2, and 3 for $i = HCl$. The concentration of each species at the surface is governed by a balance between the rate of chemical reaction and the diffusion processes driven by the concentration and temperature gradients. The boundary conditions on the substrate surface are therefore

$$R_i = j_C + j_T = -\rho D_i \frac{\partial \omega_i}{\partial y} - D_i^T \frac{\partial \ln T}{\partial y}, \tag{3-11}$$

where j_C and j_T denote the diffusion fluxes driven by the concentration and temperature gradients.

The accumulation of silicon per unit time and area of the surface

$$R_{\mathrm{Si}} = M_{\mathrm{Si}} k[\mathrm{SiHCl_3}][\mathrm{H_2}] \tag{3-12}$$

gives the growth rate of silicon film as

$$V_{\mathrm{G}} = 6 \times 10^7 R_{\mathrm{Si}}/\rho_{\mathrm{Si}} \quad (\mu\mathrm{m\,min^{-1}}), \tag{3-13}$$

where ρ_{Si} is the density of Si, and the factor 6×10^7 is used for the unit conversion of $\mathrm{m\,s^{-1}}$ to $\mu\mathrm{m\,min^{-1}}$.

To solve the transport equations described above, the calculation domain is divided into a nonuniform mesh with 78×52 grid points in the x- and y-directions. Then the equations for gas velocity, temperature and mass of chemical species are discretized into finite difference formulae. In this Chapter, the computational fluid dynamics code FLUENT (ver. 3.03)[14] is used as the solver.

The gas properties of H_2 such as viscosity, heat capacity and thermal conductivity are taken from the literature.[15-17] The properties of $SiHCl_3$ and HCl are given by Pollard and Newman.[18] Each physical constant is expressed as a function of temperature using a polynomial fit. The properties of the mixed gas are estimated theoretically.[14]

The binary diffusion coefficients of $SiHCl_3$ and HCl in H_2 are estimated with the method described in the literature.[19] Following Holstein,[20] the thermal diffusion coefficients of $SiHCl_3$ and HCl are obtained. Although the thermal diffusion coefficients also vary with the local species concentration, the values of the coefficients in this simulation are expressed only as a function of temperature at a representative concentration because of a limitation on the format of physical constants in the FLUENT code. The concentration at the center of the substrate surface is used as the representative concentration.

3.3 Results and discussion

3.3.1 *Estimation of the rate of chemical reaction from the growth rate*

The solid line in Fig. 3-2 shows the calculated growth rate, V_G, as a function of the temperature at the substrate surface, T_s, for an average molecular weight at the inlet of MW=6.7 $\times$ 10^{-3} kg mol^{-1}. This figure shows that the growth rate increases with T_s. In this calculation, the pre-exponential factor, A, in the rate of chemical reaction, k, was fixed so that V_G calculated for T_s = 1423 K agrees with the growth rate measured at that temperature when the substrate did not rotate (the solid circle at the center). The rate of reaction is therefore estimated to be

$$k = 2.65 \times 10^3 \exp(-1.38 \times 10^5/RT) \quad (\mathrm{m^4\,mol^{-1}\,s^{-1}}). \tag{3-14}$$

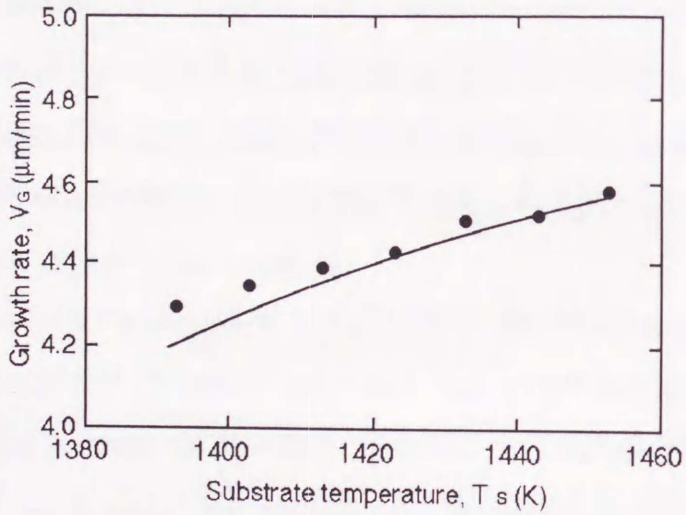

Fig. 3-2 Comparison of calculated (solid line) and measured (solid circles) growth rates. The average molecular weight at the inlet, MW, is 6.7 $\times$ 10^{-3} kg mol^{-1}.

Figure 3-2 illustrates that the values of V_G obtained by the present model with equation (3.1) agree well with those obtained experimentally in the temperature range from 1393 K to 1453 K. Although the rate-limiting step for preparing silicon film in the $SiHCl_3$-H_2 system is generally recognized to be mass transport, the

dependence of growth rate on temperature in the temperature region considered here is successfully described by the activation energy obtained under reaction-limited conditions. It is also considered that the simplified reaction scheme, equation (3-1), in which only the concentrations of the source gases are taken into account, can describe the film growth process. The mechanisms of chemical reaction contributing to the film growth are hence considered to be unchanged irrespective of the rate-limiting step.

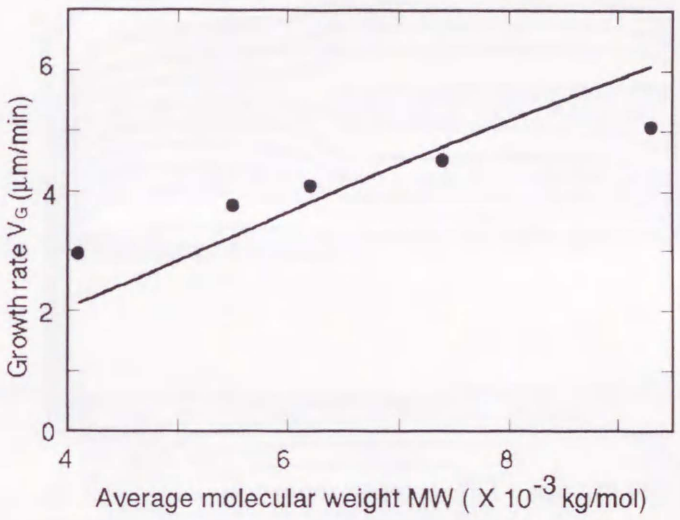

Fig. 3-3 Comparison of calculated (solid line) and measured (solid circles) growth rates. The substrate temperature, T_s, is 1398 K.

Figure 3-3 shows the dependence of experimental and calculated growth rate upon the average molecular weight of gas at the inlet, MW, for a substrate temperature of T=1398 K. The calculated growth rates increase with the average molecular weight, which corresponds to an increase in the concentration of $SiHCl_3$ at the inlet. The slight deviation between the calculated and measured values is considered to be due to surface chemical processes which will be discussed in Chapter 5. Although the slope of the calculated line is somewhat higher than that of the measured values, the present calculations describe the experimental trends satisfactorily.

3.3.2 *Transport phenomena in the reactor*

As described in §3.2, the amount of reactant gas actually consumed on the substrate is affected by distributions in the gas velocity, temperature and concentration of each reactant gas. In this section, we present typical calculated gas velocity, temperature and concentration fields in the reactor for the case of an average molecular weight $MW = 6.7 \times 10^{-3}\,\mathrm{kg\,mol^{-1}}$ and a substrate temperature $T_s = 1423\,\mathrm{K}$.

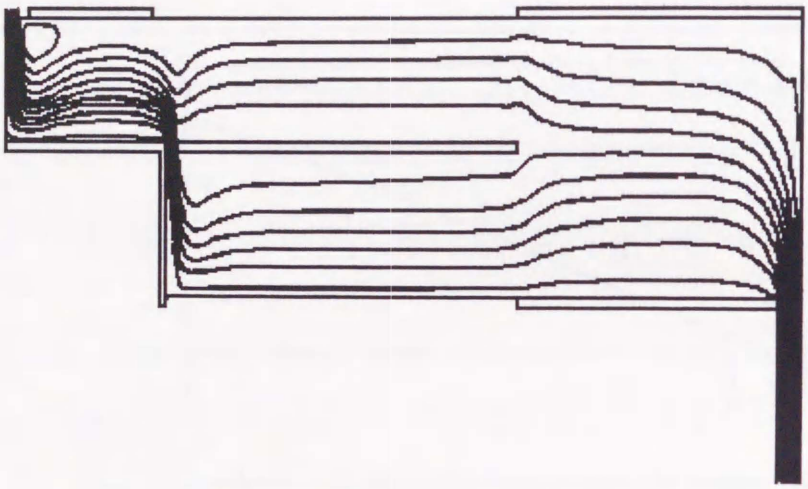

Fig. 3-4 Streamlines in the reactor. The average molecular weight at the inlet, MW, is $6.7 \times 10^{-3}\,\mathrm{kg\,mol^{-1}}$ and the substrate temperature, T_s, is 1423 K.

Figure 3-4 shows the streamlines for the gas flow in the reactor, while Fig. 3-5 is a contour plot of the gas velocity in the horizontal direction, u. Figure 3-4 shows that the streamlines above the substrate are almost parallel to the surface except the region near the leading edge of the substrate, where the gas stream from the inlet divides into the streams above and below the substrate. Flow induced by natural convection was not observed in the reactor. The gas flow above the center of the substrate is, as described in Fig. 3-5, found to have a parabolic profile, so that the flow is regarded to be nearly developed.

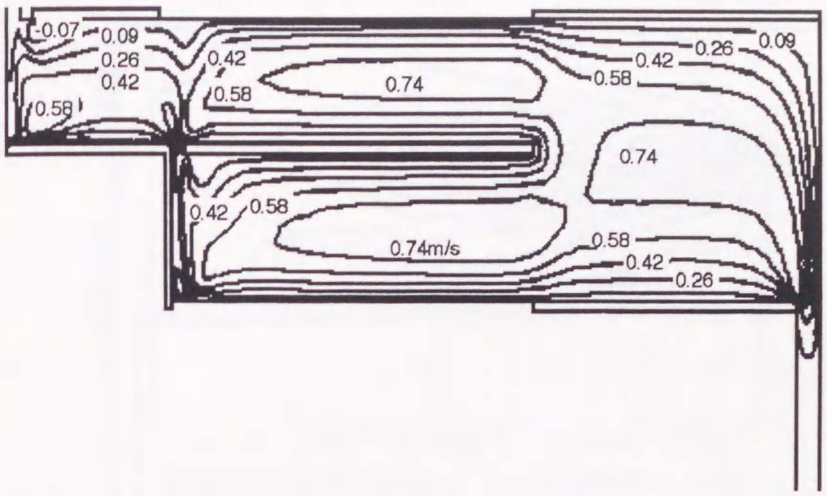

Fig. 3-5 Contour lines of gas velocity component in the x direction, u, in the reactor. The average molecular weight at the inlet, MW, is 6.7 $\times$ 10^{-3} kg mol^{-1} and the substrate temperature, T_s, is 1423 K.

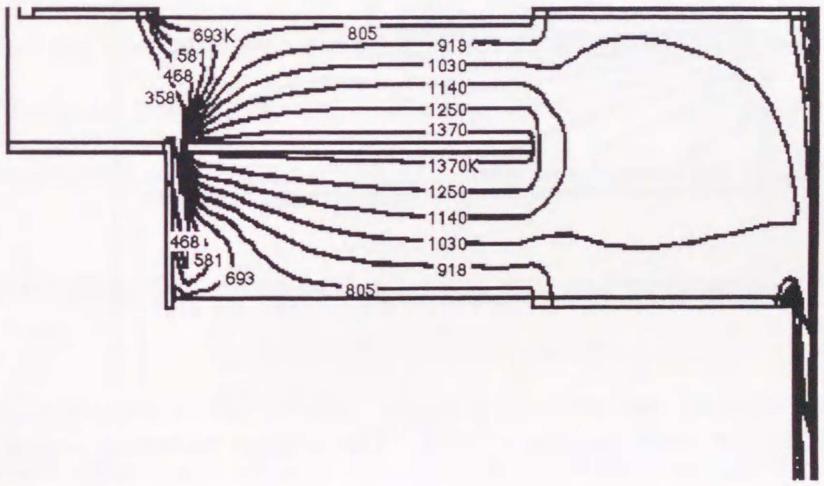

Fig. 3-6 Contour lines of temperature, T, in the reactor. The average molecular weight at the inlet, MW, is 6.7 $\times$ 10^{-3} kg mol^{-1} and the substrate temperature, T_s, is 1423 K.

The contour plot for the gas temperature, Fig. 3-6, reveals that the gas temperature increases rapidly at the leading edge of the substrate. However, the contour lines near the center of the substrate are almost parallel, similar to those of the gas

velocity.

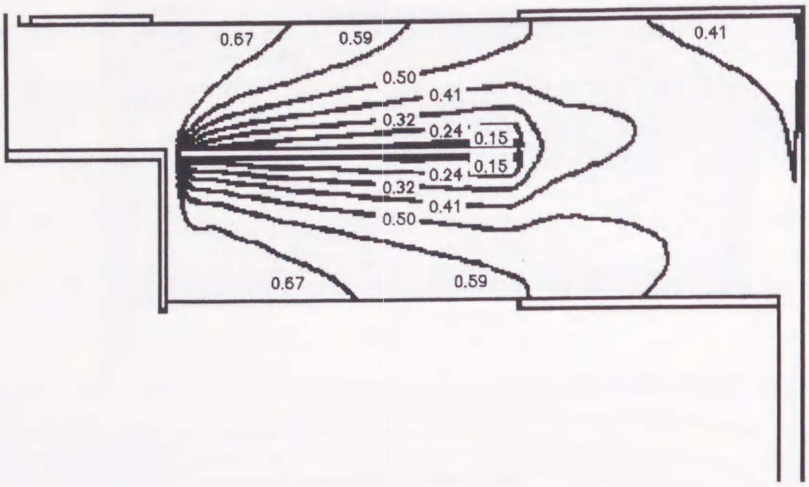

Fig. 3-7 Contour lines of mass fraction of $SiHCl_3$. The average molecular weight at the inlet, MW, is 6.7 $\times$ 10^{-3} kg mol^{-1} and the substrate temperature, T_s, is 1423 K.

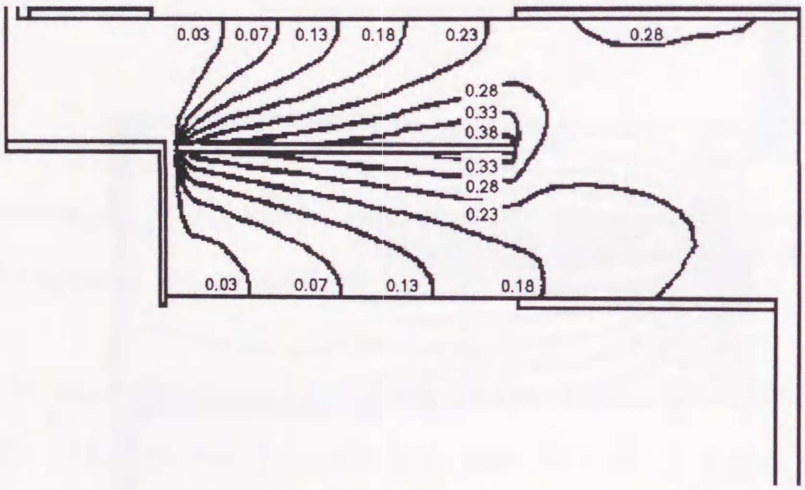

Fig. 3-8 Contour lines of mass fraction of HCl. The average molecular weight at the inlet, MW, is 6.7 $\times$ 10^{-3} kg mol^{-1} and the substrate temperature, T_s, is 1423 K.

The transport of reactant gas takes place in the environment described above. Figures 3-7 and 3-8 show the contour diagrams for the concentrations of $SiHCl_3$ and HCl, respectively. The concentration of $SiHCl_3$ decreases as the substrate surface is approached because of consumption by the chemical reaction contributing to silicon film formation, while HCl concentration increases due to generation on the substrate

simultaneously.

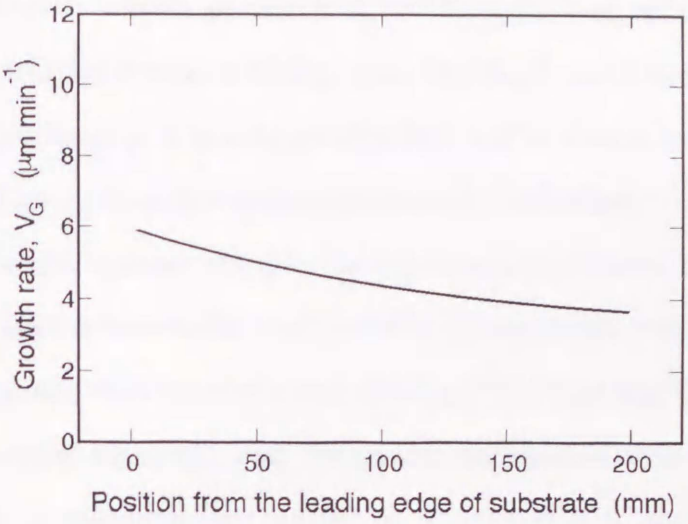

Fig. 3-9 Profile of calculated growth rate on substrate surface along x direction. The average molecular weight at the inlet, MW, is 6.7×10^{-3} kg mol^{-1} and the substrate temperature, T_s, is 1423 K.

These figures also indicate that the concentrations of $SiHCl_3$ and HCl are not uniform along the substrate surface. This results in a non-uniform growth rate profile along the gas flow direction as shown in Fig. 3-9. The growth rate is largest at the leading edge of the substrate and decreases toward the trailing edge.

3.3.3 *Effect of $SiHCl_3$ concentration on gas flow and temperature*

Since the present model, which considers simultaneous transport phenomena and a chemical reaction, can explain the measured growth rates well, the effects of varying the $SiHCl_3$ concentration on gas velocity and temperature field is investigated further.

Figure 3-10 shows the gas velocity profile in the x-direction, u, above the center of the substrate for $T_s = 1423$ K and MW between 6.7×10^{-3} and 55×10^{-3} kg mol^{-1}. At a low average molecular weight, the gas velocity attains its maximum near the central position between the substrate ($h_s = 0$ mm) and the upper wall of the sub-

strate ($h_s = 20\,\mathrm{mm}$). When the MW increases, i.e., the $SiHCl_3$ concentration at the inlet becomes larger, the position at which the velocity becomes maximum shifts toward the substrate surface. Equation (3-1) indicates that the volume of gas increases by a volume of 1 mole of gas during formation of 1 mole of solid Si and 3 moles of HCl gas. The gas volume increasing in a unit time was estimated from the calculated growth rate of the silicon film. By comparing this volume with the volumetric flow rate above the substrate where there was no chemical reaction ($MW = 2 \times 10^{-3}\,\mathrm{kg\,mol^{-1}}$ in Fig. 3-10, the increase in the gas velocity with MW, shown in Fig. 3-10, was almost explained. Since HCl gas is generated only at the substrate surface, it is reasonable to ascribe the significant increase in gas velocity near the substrate surface to production of HCl by the chemical reaction.

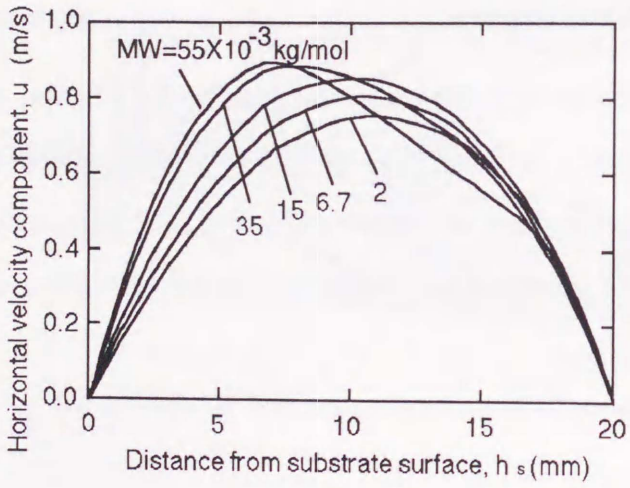

Fig. 3-10 Calculated profile of velocity in the x direction, u, above the center of the substrate. The substrate temperature, T_s, is 1423 K.

The decrease in gas velocity near the reactor wall with increasing MW is thought to be caused by the change in the temperature field near the wall. Figure 3-11 shows the change in temperature profile above the center of the substrate as MW increases. At low average molecular weight, the temperature decreases almost linearly with the distance from the substrate, h_s. With increasing average molecular weight,

however, the temperature between the substrate and reactor wall tends to decrease more rapidly. One reason for this trend is considered to be that increase in gas temperature by heat transported from the hot substrate is suppressed because of the large heat capacity of gas of a large MW. The temperature on the surfaces of the walls facing the substrate might decrease accordingly. The temperature of the wall surface is, however, fixed in the simulation because of the reason described in §3.2.2. Figures 3-10 and 3-11 indicate that an increase in the average molecular weight changes the flow and temperature fields and that the gas flow is not fully developed over the substrate when the concentration of $SiHCl_3$ is large.

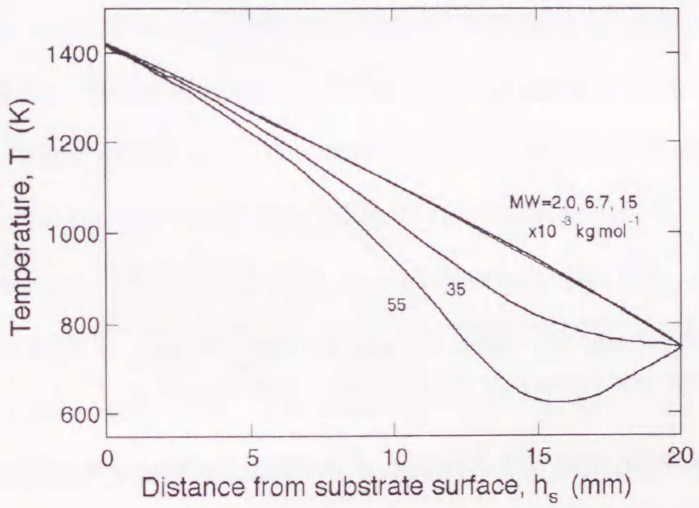

Fig. 3-11 Calculated profile of temperature, T, above the center of the substrate. The substrate temperature, T_s, is 1423 K.

If the average molecular weight is extremely low, and thus the gas velocity and temperature fields in the reactor are sufficiently close to those for pure H_2 system, a model that does not consider the effect of gas composition may be adequate for predicting transport phenomena in the reactor. However, as demonstrated here, such a model will fail to predict the growth rate for large MW because the composition of gas has a considerable effect on the flow and temperature fields.

3.3.4 *Effect of $SiHCl_3$ concentration and thermal diffusion on growth rate*

Relatively high concentrations of reactant gas are often used in industrial processes in order to achieve large growth rates. We therefore investigated the effect of $SiHCl_3$ concentration on the growth rate further. The solid line in Fig. 3-12 shows the change in growth rate with the average molecular weight for MW up to $55 \times 10^{-3}\,\mathrm{kg\,mol^{-1}}$. At low values of MW the slope of the graph is relatively large, but the slope becomes flatter as MW increases.

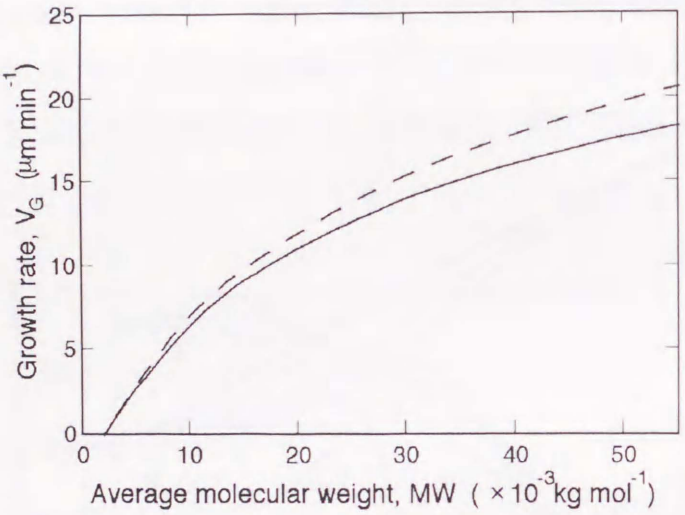

Fig. 3-12 Calculated growth rate as a function of average molecular weight, MW. Solid line indicates the result obtained by considering thermal diffusion; the dashed line is that without considering thermal diffusion.

It is recognized empirically that growth rate does not increase in proportion to the concentration of reactant gas. One possible reason for the non-proportionality often encountered in the actual film preparation process is thought to be etching of the silicon film by HCl synthesized at the surface. As previously discussed, silicon film preparation is governed by transport of the reactant gases and chemical reaction to form the silicon film. Beside these mechanisms, the reaction

$$\mathrm{Si} + 2\mathrm{HCl} \rightarrow \mathrm{SiCl_2} + \mathrm{H_2} \qquad (3\text{-}15)$$

is likely to occur and reduce the growth rate of silicon films. The contribution of this reaction will be significant especially when the concentration of HCl above the silicon film is high, that is, the consumption of reactant gas, $SiHCl_3$ is high. Nevertheless, we have demonstrated the non-proportionality of the growth rate by the present calculation without accounting for the etching reaction by HCl. Consequently, the dependence of the growth rate on MW may be attributed to changes in the transport of reactant gases which are caused by the changes in gas flow and temperature distributions with MW as shown in the previous section.

The relationship between the growth rate of the silicon film and the flux of reactant molecules is expressed by equation (3-11). This equation states that the growth of the film is governed by the balance between reactant consumption due to reaction at the surface of the substrate and diffusion of the reactants driven by concentration and temperature gradients. The concentration gradient in the reactant gas flux, j_C, depends on the flow and temperature distributions which vary with the average molecular weight, MW. The flux due to thermal diffusion, j_T, depends on MW because the flux is proportional to the temperature gradient above the substrate which also varies with MW. For these reasons, it is expected that the growth rate will not increase linearly with the concentration of $SiHCl_3$.

The effect of thermal diffusion is investigated further by using the present numerical model. The flux driven by the temperature gradient, j_T, depends on the thermal diffusion coefficient, D_i^T. The value of D_i^T for $SiHCl_3$ in H_2 increases with the average molecular weight of gas mixture, M_{av}, as shown in Fig. 3-13. Although the value of α_{SiHCl_3} decreases slightly with increase in the $SiHCl_3$ concentration, the increase in the value of $\rho\omega_{SiHCl_3}\omega_{H_2}$ causes D_i^T to become large as shown in the figure. The dashed line in Fig. 3-12 shows the growth rate predicted by neglecting thermal diffusion, i.e., D_i^T being set to zero. Figure 3-14 shows the relative difference between the dashed and solid lines in Fig. 3-12, demonstrating the effect of thermal diffusion on the growth rate. These figures illustrate that thermal diffusion of the reactant gas suppresses the growth rate as the average molecular weight increases.

The effect of a difference between the molecular weight of the carrier and reactant gas has been discussed by Kleijn.[21] To demonstrate the effect of thermal diffusion on the concentration of $SiHCl_3$ above the substrate, additional calculations were carried out in which no surface reaction was assumed. Figure 3-15 shows that the $SiHCl_3$ concentration in the absence of thermal diffusion (dashed line) is almost uniform between the substrate and wall surfaces. In contrast to the dashed line, the $SiHCl_3$ concentration including the effect of D_i^T (solid line) becomes smaller as the substrate surface is approached although no consumption at the surface is assumed. Because the molecular weight of $SiHCl_3$ is much larger than that of H_2, $SiHCl_3$ molecules are transported away from the hotter region near the substrate toward the colder mainstream and the growth rate is reduced. The present calculations indicate that the effect of thermal diffusion is not negligible in predicting the growth rate. A calculation model that does not consider the effect of thermal diffusion will overestimate the growth rate especially when the $SiHCl_3$ concentration, and thus the growth rate, is high.

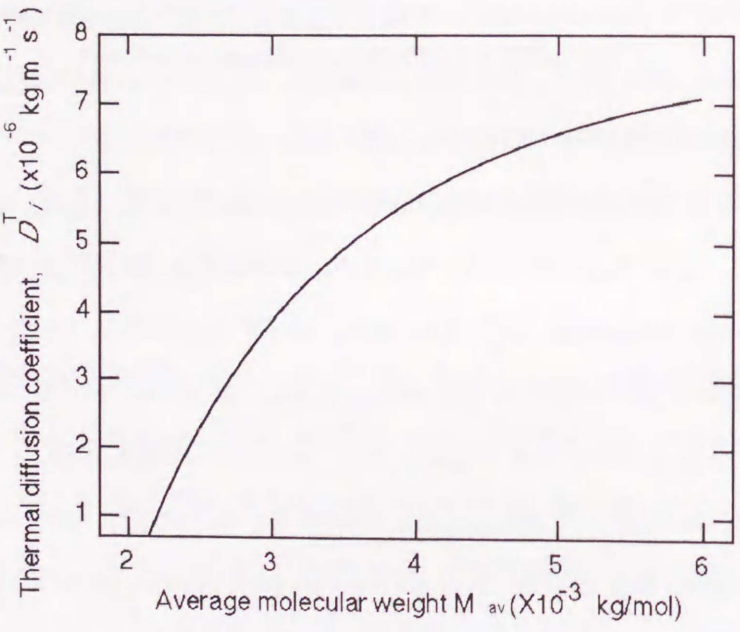

Fig. 3-13 Thermal diffusion coefficient, D_i^T, for $SiHCl_3$ in H_2 as a function of the average molecular weight of gas mixture, M_{av}.

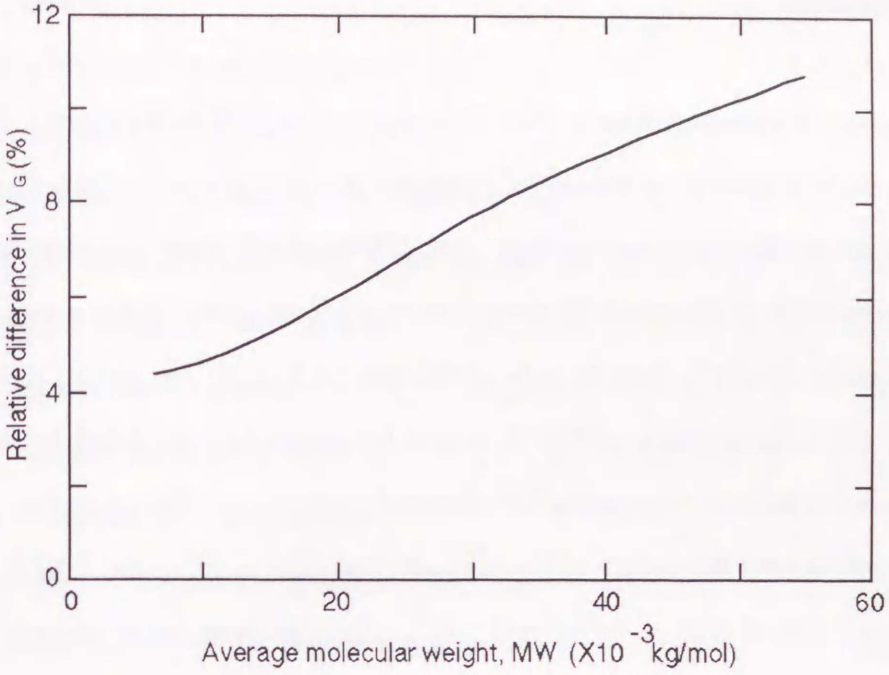

Fig. 3-14 Calculated change in growth rate due to the thermal diffusion as a function of average molecular weight, MW. The ordinate is the relative difference between the predicted values of growth rates, solid and dashed lines in Fig. 3-12.

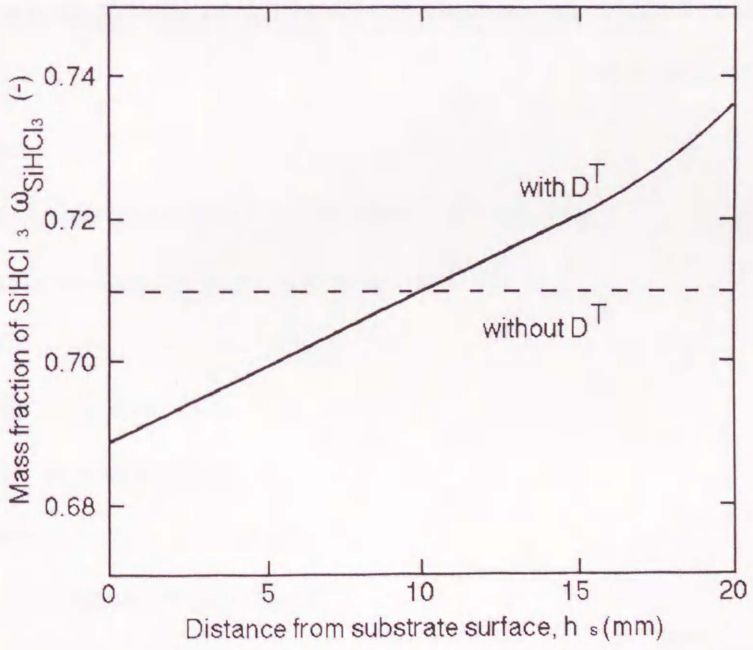

Fig. 3-15 Mass fraction profiles of $SiHCl_3$ calculated for the condition of no surface reaction. The solid line indicates the result obtained by considering thermal diffusion; the dashed line is that without considering thermal diffusion.

3.4 Conclusions

Preparation of epitaxial silicon thin films using the $SiHCl_3$-H_2 system has been discussed using a numerical model. The model predicts gas velocity, temperature, concentration of the gases and growth rate. Thermal diffusion and changes in the physical properties of the gas with temperature and composition are accounted for.

The dependence of the growth rate of the silicon film on the substrate temperature and the concentration of $SiHCl_3$ could be adequately modeled by assuming an Arrhenius-type rate expression for chemical reaction on the substrate surface. The apparent activation energy of the reaction was $1.38 \times 10^5\,J\,mol^{-1}$ with the pre-exponential factor of $2.65 \times 10^3\,m^4\,mol^{-1}\,s^{-1}$. The nonlinear dependence of growth rate on the concentration of $SiHCl_3$ was attributed to the change in the gas flow and temperature fields in the reactor with the $SiHCl_3$ concentration. The effect of thermal diffusion in the present system was found to result in a reduced growth rate. Thermal diffusion of $SiHCl_3$, which transports $SiHCl_3$ molecules away from the hot substrate surface, had a considerable effect on growth rate especially when the growth rate was high.

Nomenclature

A : pre-exponential factor of rate constant	$(\mathrm{m^4\,mol^{-1}\,s^{-1}})$
C_p : heat capacity at constant pressure	$(\mathrm{J\,kg^{-1}\,K^{-1}})$
D_i : binary diffusion coefficient of species i in H_2	$(\mathrm{m^2\,s^{-1}})$
D_i^T : thermal diffusion coefficient of species i in H_2	$(\mathrm{kg\,m^{-1}\,s^{-1}})$
E : activation energy of rate constant	$(\mathrm{J\,mol^{-1}})$
g : acceleration due to gravity	$(\mathrm{m\,s^{-2}})$
h_s : distance from substrate surface	(m)
$[i]$: mole concentration of species i	$(\mathrm{mol\,m^{-3}})$
j_C : diffusion flux driven by concentration gradient	$(\mathrm{kg\,m^{-2}\,s^{-1}})$
j_T : diffusion flux driven by temperature gradient	$(\mathrm{kg\,m^{-2}\,s^{-1}})$
k : Arrhenius-type rate constant	$(\mathrm{m^4\,mol^{-1}\,s^{-1}})$
M_av: average molecular weight of gas mixture	$(\mathrm{kg\,mol^{-1}})$
M_Si: molecular weight of Si	$(\mathrm{kg\,mol^{-1}})$
M_i: molecular weight of species i	$(\mathrm{kg\,mol^{-1}})$
MW: average molecular weight of gas mixture at reactor inlet	$(\mathrm{kg\,mol^{-1}})$
p : pressure	(Pa)
R : gas constant	$(\mathrm{J\,mol^{-1}\,K^{-1}})$
R_i : mass rate of change in species i by chemical reaction	$(\mathrm{kg\,m^{-2}\,s^{-1}})$
R_Si : mass rate of change in Si by chemical reaction	$(\mathrm{kg\,m^{-2}\,s^{-1}})$
T : temperature	(K)
u : fluid velocity in x direction	$(\mathrm{m\,s^{-1}})$
v : fluid velocity in y direction	$(\mathrm{m\,s^{-1}})$
V_G : growth rate	$(\mu\mathrm{m\,min^{-1}})$
x : coordinate in horizontal direction	(m)
x_i : mole fraction of species i	(-)
y : coordinate in vertical direction	(m)
α_i : thermal diffusion factor of species i	(-)
λ : thermal conductivity of gas mixture	$(\mathrm{W\,m^{-1}\,K^{-1}})$

μ : viscosity of gas mixture (Pa·s)

ν_i : molar stoichiometry coefficient for species i in chemical reaction (-)

ρ : density of gas mixture ($\mathrm{kg\,m^{-3}}$)

ρ_{Si} : density of Si ($\mathrm{kg\,m^{-3}}$)

ω_i : mass fraction of species i (-)

References

[1] C. R. Kleijn and C. J. Hoogendoorn, *Chem. Eng. Sci.* **46**, 321 (1991).

[2] I.H.Oh, C.G.Takoudis and G.W.Neudeck, *J.Electrochem.Soc.***138**, 554 (1991).

[3] I. H. Oh and C. G. Takoudis, *J. Appl. Phys.* **69**, 8336 (1991).

[4] R. L. Mahajan and C. Wel, *Trans. ASME, J. Heat Transfer* **113**, 688 (1991).

[5] P. B. Chinoy, D. A. Kaminski and S. K. Ghandhi, *Numer. Heat Transfer*, Part A **19**, 85 (1991).

[6] P. B. Chinoy, D. A. Kaminski and S. K. Ghandhi, *J. Electrochem. Soc.* **138**, 1452 (1991).

[7] F. Langlais, C. Prebende and J. P. Couderc, *J. Cryst. Growth* **113**, 606 (1991).

[8] C. R. Kleijn, C. J. Hoogendoorn, A. Hasper, J. Holleman and J. Middlehoek, *J. Electrochem. Soc.* **138**, 509 (1991).

[9] A. H. Dilawari and J. Szekely, *J. Cryst. Growth* **108**, 491 (1991).

[10] H. K. Moffat and K. F. Jensen, *J. Electrochem. Soc.* **135**, 459 (1988).

[11] M. E. Coltrin, R. J. Kee and J. A. Miller, *J. Electrochem. Soc.* **133**, 1206 (1986).

[12] M. Frenklach and H. Wang, *Phys. Rev.* B **43**, 1520 (1991).

[13] F. C. Eversteyn, *Philips Res. Rep.* **29**, 45 (1974).

[14] FLUENT User's Manual, Ver. 3.0 (Fluent Inc., Hanover, 1990).

[15] *Kagaku Binran* (Handbook of Chemistry) (Iwanami, Tokyo, 1984) 3rd ed., Chap. 6, p. II-39 [in Japanese].

[16] *Kagaku Binran* (Handbook of Chemistry) (Iwanami, Tokyo, 1984) 3rd ed., Chap. 6, p. II-71 [in Japanese].

[17] *Kagaku Binran* (Handbook of Chemistry) (Iwanami, Tokyo, 1984) 3rd ed., Chap. 9, p. II-239 [in Japanese].

[18] P. Pollard and J. Newman, *J. Electrochem. Soc.* **127**, 744 (1980).

[19] R.C.Reid, J.M.Prausnitz and B.E.Poling, *The Properties of Gases and Liquids* (McGraw-Hill, New York, 1987) 4th ed.

[20] W. L. Holstein, *J. Electrochem. Soc.* **135**, 1788 (1988).

[21] C. R. Kleijn, *J. Electrochem. Soc.* **138**, 2190 (1991).

Chapter 4

Modeling of Epitaxial Silicon Thin-Film Growth on a Rotating Substrate in a Single-Wafer Horizontal Reactor

4.1 Introduction

In Chapter 3, the silicon epitaxial growth rate from a $SiHCl_3$-H_2 gas mixture in a single-wafer horizontal epitaxial reactor under atmospheric pressure was discussed experimentally and theoretically using numerical calculation based on two-dimensional Cartesian coordinates. However, the effect of substrate rotation cannot be described by a two-dimensional model because of the gas motion induced by the rotation.

In this Chapter, calculations based on the three-dimensional coordinates including the substrate rotation are therefore performed to evaluate and discuss the effect of the rotation on the mass, momentum, energy and chemical species transport and silicon epitaxial growth rate in a single-wafer horizontal epitaxial reactor. The effect of the rotating motion of the substrate is discussed under the conditions giving nearly uniform film thickness profile. Since $SiHCl_3$ is widely used for the epitaxial growth of silicon thin-films in industrial applications, the epitaxial growth in the $SiHCl_3$-H_2 system is discussed.

4.2 Silicon epitaxial thin-film growth process

4.2.1 *Reactor configuration for experiments and calculations*

For obtaining epitaxial silicon thin-films experimentally, the single-wafer horizontal reactor having the geometry shown in Fig. 4-1 is used, in which the substrate on the susceptor usually rotates. Gas mixture of $SiHCl_3$ and H_2 gas is introduced into the reactor and reacts at the surface of an 8-inch-diameter substrate held horizontally on the rotating susceptor in the reactor. The substrate is heated to 1398 K using infrared furnaces through the transparent quartz glass walls. The epitaxial thin-films were grown for 60–120 s, which thicknesses were measured using interference fringe in Fourier-transform infra-red spectra. As described above, calculations

including the substrate rotation require the use of three-dimensional coordinates because any symmetric nature cannot be assumed throughout the entire space in the reactor. Such three dimensional calculations need much computer memory and computation time, so that focusing only on the main gas flow region is very effective for the cost of calculation. Following this reason, the simpler geometry shown in Fig. 4-2 is assumed to describe the transport phenomena and epitaxial growth on the substrate by calculation. Since the silicon deposition occurs on the susceptor as well as on the substrate, the susceptor and the substrate are assumed to be one large substrate.

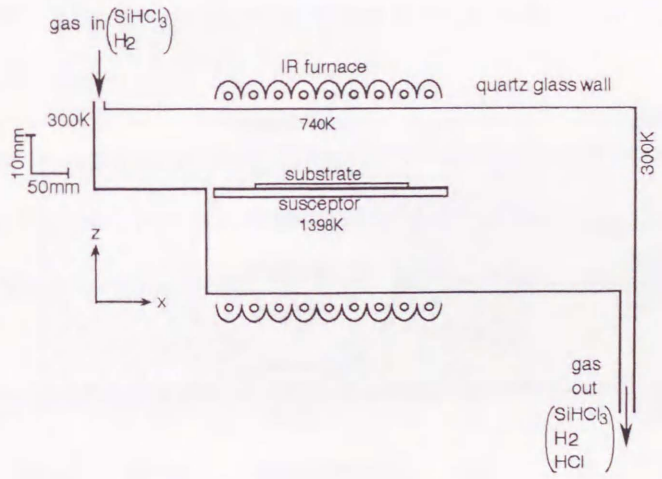

Fig.4-1 Single-wafer horizontal reactor for preparation of epitaxial silicon thin-film.

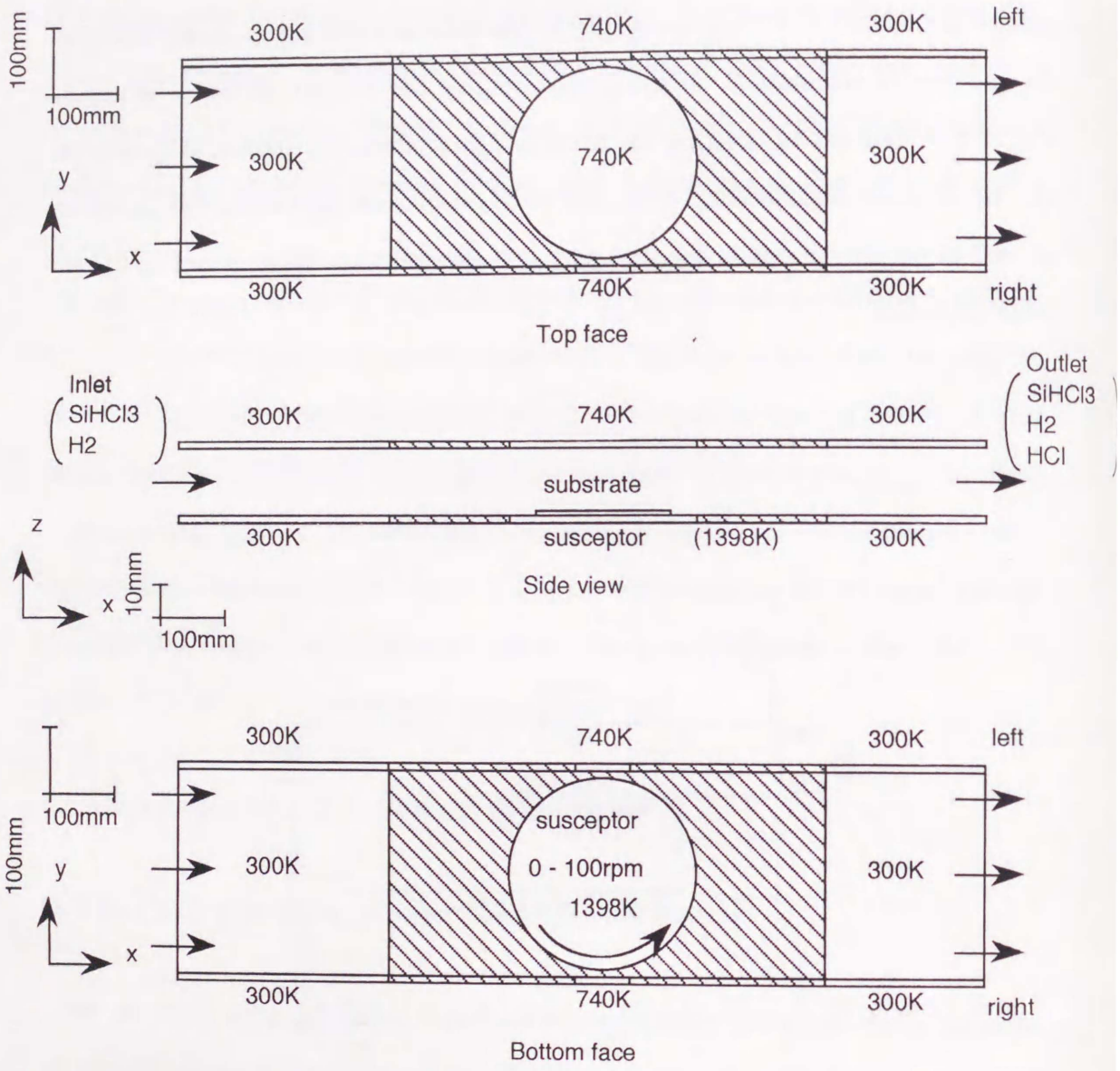

Fig.4-2 Geometry and wall temperature conditions of single-wafer horizontal reactor with rotating substrate for the numerical calculations.

4.2.2 *Basic equations for transport phenomena and chemical reaction*

In order to evaluate the film growth rate in the case of the reactor with nonuniform temperature and gas flow fields, the mass, momentum, energy and chemical species transport equations are solved with a chemical reaction occurring at the surface of the substrate.

Since neither the elementary reactions nor the rate-limiting process in the reactions have been determined for the $SiHCl_3$-H_2 system, an Arrhenius-type expression for the chemical reactions and a simplified reaction scheme were used to model the reaction phenomena. We therefore consider the preparation of a silicon film on the basis of the overall reaction of equation (4-1).

$$SiHCl_3 + H_2 \rightarrow Si + 3HCl. \tag{4-1}$$

The transport phenomena in the reactor at a steady state are solved using Cartesian coordinates. The governing equations for the mass is as follows:

Conservation of mass:

$$\frac{\partial \rho u}{\partial x} + \frac{\partial \rho v}{\partial y} + \frac{\partial \rho w}{\partial z} = 0, \tag{4-2}$$

where u, v and w are velocities in x-, y- and z-directions, respectively. The x-, y- and z-directions are indicated in Figs. 4-1 and 4-2. The equations for the gas velocities are

Conservation of momentum:

$$\frac{\partial \rho uu}{\partial x} + \frac{\partial \rho vu}{\partial y} + \frac{\partial \rho wu}{\partial z} = -\frac{\partial p}{\partial x} - \frac{\partial \tau_{xx}}{\partial x} - \frac{\partial \tau_{yx}}{\partial y} - \frac{\partial \tau_{zx}}{\partial z}, \tag{4-3}$$

$$\frac{\partial \rho uv}{\partial x} + \frac{\partial \rho vv}{\partial y} + \frac{\partial \rho wv}{\partial z} = -\frac{\partial p}{\partial y} - \frac{\partial \tau_{xy}}{\partial x} - \frac{\partial \tau_{yy}}{\partial y} - \frac{\partial \tau_{zy}}{\partial z}, \tag{4-4}$$

$$\frac{\partial \rho uw}{\partial x} + \frac{\partial \rho vw}{\partial y} + \frac{\partial \rho ww}{\partial z} = -\frac{\partial p}{\partial z} + \rho g - \frac{\partial \tau_{xz}}{\partial x} - \frac{\partial \tau_{yz}}{\partial y} - \frac{\partial \tau_{zz}}{\partial z}, \tag{4-5}$$

where

$$\tau_{xx} = -\mu \left[2\frac{\partial u}{\partial x} - \frac{2}{3}\left(\frac{\partial u}{\partial x} + \frac{\partial v}{\partial y} + \frac{\partial w}{\partial z} \right) \right], \tag{4-6}$$

$$\tau_{yy} = -\mu \left[2\frac{\partial v}{\partial y} - \frac{2}{3}\left(\frac{\partial u}{\partial x} + \frac{\partial v}{\partial y} + \frac{\partial w}{\partial z} \right) \right], \tag{4-7}$$

$$\tau_{zz} = -\mu \left[2\frac{\partial w}{\partial z} - \frac{2}{3}\left(\frac{\partial u}{\partial x} + \frac{\partial v}{\partial y} + \frac{\partial w}{\partial z} \right) \right], \tag{4-8}$$

$$\tau_{xy} = \tau_{yx} = -\mu \left(\frac{\partial u}{\partial y} + \frac{\partial v}{\partial x} \right), \tag{4-9}$$

$$\tau_{yz} = \tau_{zy} = -\mu \left(\frac{\partial v}{\partial z} + \frac{\partial w}{\partial y} \right), \tag{4-10}$$

$$\tau_{zx} = \tau_{xz} = -\mu \left(\frac{\partial w}{\partial x} + \frac{\partial u}{\partial z} \right). \tag{4-11}$$

In equations (4-2)–(4-11), ρ, p and μ are the density, pressure and viscosity of the gas mixture. The gas velocities, u, v and w, on the surfaces of the solid walls are set to be the same values as the solid walls have as the boundary conditions. That is, the velocities of u, v and w on the stationary walls are all set to be zero. The method to set the velocity components for the surface of the rotating substrate is described later.

The gas velocity at the inlet section is uniform and $0.1667\,\mathrm{m\,s^{-1}}$ which has been estimated in Chapter 3. where the same reactor was dealt with in calculation. The epitaxial film is grown under the pressure of $1.0133 \times 10^5\,\mathrm{Pa}$, atmospheric pressure.

The gas density obeys the ideal gas law

$$\rho = \frac{pM_{\mathrm{av}}}{RT}, \tag{4-12}$$

where M_{av} is the local average molecular weight of the gas mixture and R is the gas constant.

The distribution of the temperature, T, in the reactor is expressed by the following energy equation:

Conservation of energy:

$$\frac{\partial \rho u C_{\mathrm{p}} T}{\partial x} + \frac{\partial \rho v C_{\mathrm{p}} T}{\partial y} + \frac{\partial \rho w C_{\mathrm{p}} T}{\partial z} = \frac{\partial}{\partial x}\left(\lambda \frac{\partial T}{\partial x} \right) + \frac{\partial}{\partial y}\left(\lambda \frac{\partial T}{\partial y} \right) + \frac{\partial}{\partial z}\left(\lambda \frac{\partial T}{\partial z} \right). \tag{4-13}$$

In this equation, C_{p} is the heat capacity of the gas at constant pressure, and λ the thermal conductivity of the gas.

The temperature of the substrate surface, T_{s}, is 1398 K as shown in Fig. 4-2. The effect of heat transfer by radiation on the substrate temperature is ignored because

the substrate temperature is continuously and precisely controlled by a sensing and heating system of the reactor. Since the concentrations of $SiHCl_3$ and HCl are low, the effects of radiation heat on these gases are also assumed to be negligible. Since accurate measurement of the temperature at the transparent wall of quartz glass is extremely difficult, the side and upper walls near the substrate are empirically assumed to be 740 K, as shown in Fig. 4-2. The quartz walls around the substrate of bottom surface are assumed to be heat conducting walls. Heat of reaction at the growth surface is ignored in the present model.

The transport of chemical species is governed by the following equation:
Conservation of species:

$$\frac{\partial}{\partial x}(\rho u \omega_i) + \frac{\partial}{\partial y}(\rho v \omega_i) + \frac{\partial}{\partial z}(\rho w \omega_i) = -\frac{\partial}{\partial x} j_{\mathrm{x}} - \frac{\partial}{\partial y} j_{\mathrm{y}} - \frac{\partial}{\partial z} j_{\mathrm{z}}, \tag{4-14}$$

where

$$j_{\mathrm{x}} = -\rho D_i \frac{\partial \omega_i}{\partial x} - D_i^{\mathrm{T}} \frac{\partial \ln T}{\partial x}, \tag{4-15}$$

$$j_{\mathrm{y}} = -\rho D_i \frac{\partial \omega_i}{\partial y} - D_i^{\mathrm{T}} \frac{\partial \ln T}{\partial y}, \tag{4-16}$$

$$j_{\mathrm{z}} = -\rho D_i \frac{\partial \omega_i}{\partial z} - D_i^{\mathrm{T}} \frac{\partial \ln T}{\partial z}. \tag{4-17}$$

In these equations, ω_i is the mass fraction of species i. The diffusion coefficient, D_i, is assumed to be the binary diffusion coefficient of species i in H_2 gas since the mole fraction (not mass fraction) of species other than H_2 is much smaller than the case where multi-component diffusion phenomena must be considered.[1] The assumption of the binary coefficient is also considered to be reasonable since the transport of reactants and reaction products by diffusion is less important than that by convection in single-wafer horizontal reactor, and the diffusion coefficients under atmospheric pressure are smaller than those for low-pressure chemical vapor deposition (LPCVD).[1] The mass transport phenomena driven by the temperature gradient (thermal diffusion) are described by the terms relating to D_i^{T}, the thermal diffusion coefficient. D_i^{T} is expressed as

$$D_i^{\mathrm{T}} = \alpha_i \rho D_i \omega_i \omega_{\mathrm{H_2}}, \tag{4-18}$$

where α_i is the thermal diffusion factor of species i.

At the inlet of the reactor the composition of the $SiHCl_3$ and H_2 gas mixture is expressed in terms of the average molecular weight MW given by

$$MW = \sum_i x_i M_i \quad (i = \mathrm{SiHCl_3 \text{ and } H_2}), \tag{4-19}$$

where x_i and M_i are the mole fraction and molecular weight of species i. The average molecular weight at the inlet, MW, is $6.7 \times 10^{-3}\,\mathrm{kg\,mol^{-1}}$, which corresponds to 3.5 mol% of $SiHCl_3$ or the mass fraction of 0.71.

At the surface of substrate, the increase or decrease in the mass of each species by the chemical reaction on the surface is considered in terms of the boundary conditions. Assuming that the reaction of equation (4-1) is a second-order reaction, the mass rate of consumption or generation of species i at the surface is expressed as

$$R_i = \nu_i M_i k[\mathrm{SiHCl_3}][\mathrm{H_2}], \tag{4-20}$$

where k ($\mathrm{m^4\,mol^{-1}\,s^{-1}}$) is the rate constant for the reaction. The values of the molar stoichiometry coefficient, ν_i, are - 1 for $i = SiHCl_3$ and H_2, and 3 for $i = HCl$. The concentration of each species at the surface is governed under a balance between the rate of chemical reaction and the diffusional transport processes driven by the concentration and temperature gradient. The boundary conditions on the substrate surface are therefore

$$R_i = j_\mathrm{C} + j_\mathrm{T} = -\rho D_i \frac{\partial \omega_i}{\partial z} - D_i^\mathrm{T} \frac{\partial \ln T}{\partial z}, \tag{4-21}$$

where j_C and j_T denote the diffusion flux driven by the concentration and temperature gradients, respectively.

The accumulation of silicon per unit time and area of the surface

$$R_\mathrm{Si} = M_\mathrm{Si} k[\mathrm{SiHCl_3}][\mathrm{H_2}] \tag{4-22}$$

gives the growth rate of silicon film as

$$V_\mathrm{G} = 6 \times 10^7 R_\mathrm{Si}/\rho_\mathrm{Si} \quad (\mu\mathrm{m\,min^{-1}}), \tag{4-23}$$

where ρ_{Si} is the density of Si, and the factor 6×10^7 is used for the unit conversion of $\mathrm{m\,s^{-1}}$ to $\mu\mathrm{m\,min^{-1}}$. Since very smooth surface of the epitaxial films without any hillocks are obtained in various growth conditions, only negligible amount of silicon particles are produced by the chemical reaction in the gas phase.

To solve the above equations for the mass, gas velocity, temperature and chemical species, these are discretized into finite difference formulae. The calculation domain, the entire reactor of Fig. 4-2, is divided into a nonuniform computational subdomain. Preliminary calculations using different numbers of grid points showed that a mesh with $43 \times 26 \times 21$ grid points in the x-, y- and z-directions is sufficient to obtain accurate calculation results. The discretized equations are solved based on the SIMPLER algorithm.[2]

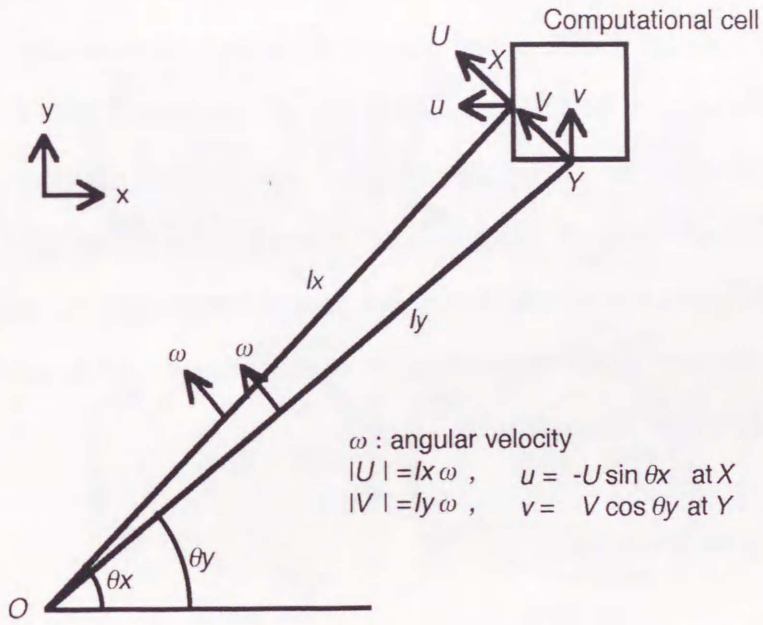

Fig.4-3 Velocity at the substrate surface given by the substrate rotation.

Figure 4-3 illustrates the concept of the method for assigning velocity to the surface of the rotating substrate in the numerical calculation. The rectangular region in the figure corresponds to any computational subdomain (cell) located on the surface of the substrate. The velocities, u and v, for the cell are defined at the positions X

and Y, respectively. The point O in the figure is the center of the substrate, *i.e*, the center of rotation. Defining the distance OX and OY as l_x and l_y, and using the angular velocity of the rotation, ω, the moving velocities, U and V at the positions X and Y in the figure, are expressed as $l_x\omega$ and $l_y\omega$, respectively. Consequently, u and v are derived from the components parallel to the $x-$ and $y-$directions as $u = -U \sin\theta_x$ and $v = V \cos\theta_y$, where θ_x and θ_y are the angles shown in the figure.

To account for the dependence of the distribution of the chemical species, $SiHCl_3$ and HCl, on the gas velocity and temperature, the equations (4-2)–(4-23) are coupled and solved simultaneously.

The gas properties of H_2 such as viscosity, heat capacity and thermal conductivity are taken from the literature.[3-5] The properties of $SiHCl_3$ and HCl are given by Pollard and Newman.[6] Each physical constant is expressed as a function of temperature. The properties of the mixed gas are estimated theoretically.[7,8] The binary diffusion coefficients of $SiHCl_3$ and HCl in H_2 are estimated with the method described in the literature.[9] Following Holstein,[10] the thermal diffusion coefficients of $SiHCl_3$ and HCl are obtained using data of Lennard-Jones potential[9,11,12] and physical properties.[13] In a region with a very low species concentration, such as that near the substrate surface, the thermal diffusion coefficients of $SiHCl_3$ and HCl increase with temperature and concentration.

4.3 Results and discussion

4.3.1 *Silicon thin-film growth rate and thickness on the rotating substrate*

In this section, the growth rate and the thickness of silicon thin-film on the rotating substrate in the single-wafer horizontal reactor is discussed with the results of the measured and calculated epitaxial growth rate.

Figure 4-4 shows the calculated distribution of $SiHCl_3$ mass fraction in the immediate vicinity of the substrate surface. At rotation rate of 0 rpm, the $SiHCl_3$ fraction

is very large at the leading edge of the substrate and decreases as the trailing edge is approached because of the consumption by the surface chemical reaction of equation (4-1). In this case, the contour lines of $SiHCl_3$ on the substrate is symmetrical with respect to the mid-plane of the reactor. At 20 rpm the contour lines of $SiHCl_3$ mass fraction from the inlet to the leading edge of the substrate showed no significant difference from that at 0 rpm, but on the substrate the contour lines are forced to be bent by the rotating motion of the substrate. The rotating substrate transports the $SiHCl_3$ along its path of the rotation of the substrate. With increasing rotation rate, the shape of the contour lines is deformed more and appears to be asymmetric. It can be easily expected that this variation in the concentration will give a nonuniform profile of the film growth rate.

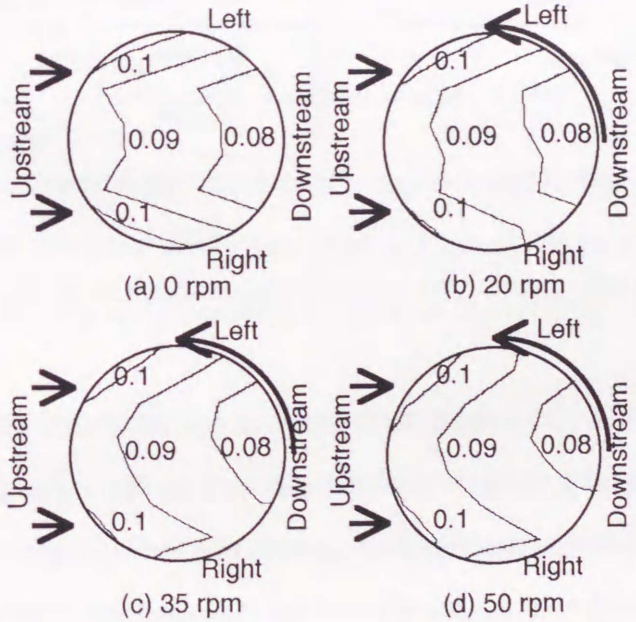

Fig.4-4 Contour lines of mass fraction of $SiHCl_3$ over the substrate in x-y plane 0.0175 mm above the substrate at rotation rate of 0, 20, 50 and 100 rpm. The average molecular weight at the inlet, MW, is 6.7×10^{-3} kg mol^{-1} and the substrate temperature, T_s, is 1398 K.

Figure 4-5 shows the calculated growth rate profiles on the entire surface of the substrate at various rotation rates. With increasing the rotation rate, the calculated

growth rate near the farther side in the figure (left) increases while that at the closer side (right) decreases, but the growth rate profiles do not become flat.

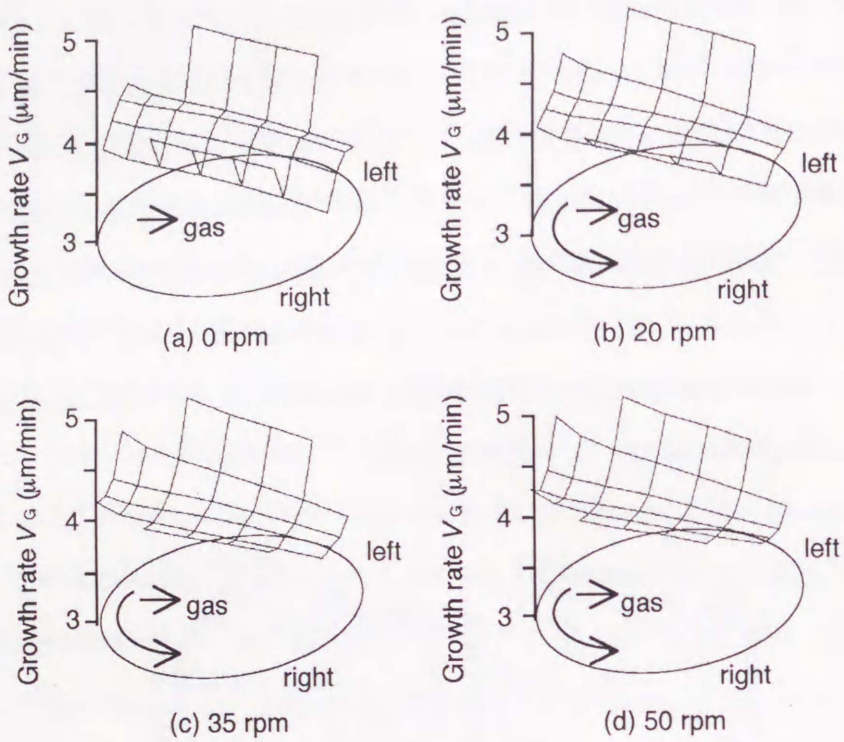

Fig.4-5 Growth rate distribution over substrate surface at 0, 20, 35 and 50 rpm.

Figure 4-6 shows the profiles of the calculated and measured film thickness grown for unit time along the mid-plane of the reactor. At the substrate rotating speed of 35 rpm, the calculated growth rate is largest at the leading edge of the substrate and decreases toward the trailing edge. This is the same tendency as discussed at 0 rpm in Chapter 3. At 35 rpm, however, the measured film thickness profile is very flat on the substrate. To compare the calculated growth rate with the measurement, the continuous change in the position of the substrate due to the substrate rotation must be taken into consideration. The film thickness at a given position on the substrate should be calculated by integrating the growth rate over all the positions which are the same distance away from the substrate center. In other words, the film thickness profile is obtained by integrating the growth rate distribution along many

concentric circles on the substrate. The dashed line in Fig. 4-6 is the integrated one obtained for 35 rpm and agrees well with the measurement.

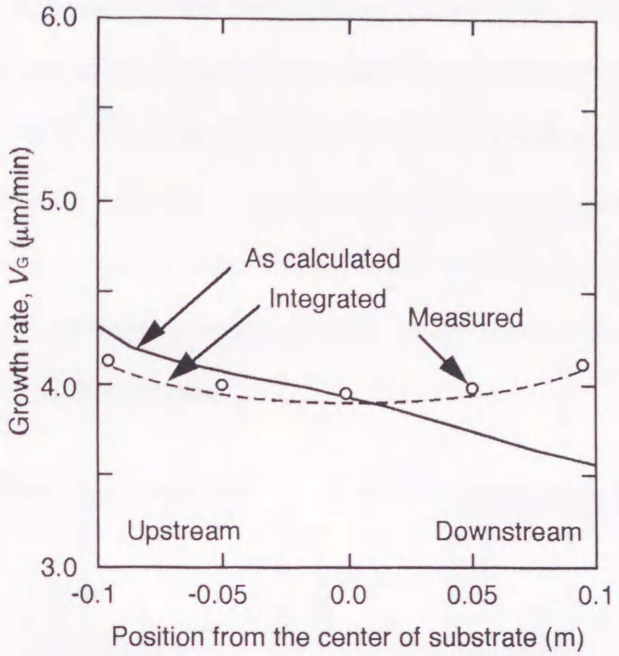

Fig.4-6 Measured (circle) and calculated (solid line) local growth rate at substrate rotation rate of 35 rpm. Dashed line is film thickness grown for unit time obtained by integrating the growth rate along concentric circles on the rotating substrate.

Here, the rate constant, k, for the reaction of equation (4-1) is $0.038\,\mathrm{m^4\,mol^{-1}\,s^{-1}}$ at 1398 K, which is estimated so that the calculated growth rate at the center of the substrate coincides with that of the measured growth rate at 0 rpm. This value differs a little from $0.018\,\mathrm{m^4\,mol^{-1}\,s^{-1}}$ which was obtained in Chapter 3. thus the difference in the growth rates obtained by both rate constants was only about 10 %. It can be concluded that the epitaxial growth is limited by the transport of $SiHCl_3$ molecules.

Figure 4-7 shows the thickness variation of the film as a function of the rotation rate. Here, the thickness variation, t_v (%), is defined as

$$t_v = (t_{max} - t_{min})/(t_{max} + t_{min}) \times 100, \qquad (4\text{-}24)$$

where t_{max} and t_{min} denote the maximum and minimum film thicknesses on the substrate, respectively. The circles show the measured value and the solid line is the calculated results. Although the calculated t_v for 0 rpm is somewhat smaller than the measured one, both the measured and the calculated t_v show the same behavior. The thickness variation is large at 0 rpm, but it drastically decreases even at small rotation rate and shows very small change with the rotation rate as long as the substrate rotates.

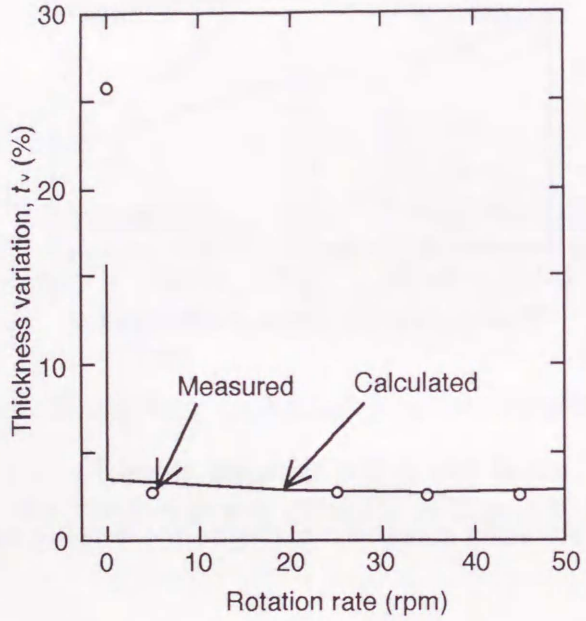

Fig.4-7 Calculated (solid line) and measured (dashed line) film thickness variation t_v at the substrate rotation rate of 0 to 45 rpm.

The results mentioned above clearly indicate that the good uniformity in film thickness is a result of the averaging effect by integrating local growth rate over different positions, which is caused by the rotating motion.

4.3.2 *Transport phenomena induced by rotating substrate*

In this section, the effects of substrate rotation on the distribution in gas velocity,

temperature and chemical species concentration are discussed.

The velocity of gases coming from the inlet changes its profile under an effect of viscosity. Figure 4-8 shows the calculated gas velocity vectors at the x-y plane 0.0175 mm above the substrate for the rotation rate of 0, 20, 50 and 100 rpm. When the substrate does not rotate, the gas in the vicinity of the non-moving wall has very small velocity as shown in Fig. 4-8(a). At 20 rpm, the gas near the substrate has much higher velocity than in the rest of the reactor as shown in Fig. 4-8(b). At 50 and 100 rpm, the gas velocity near the substrate further increases. The gas in the vicinity of the rotating substrate shows large velocity but in the rest the gas motion is hardly affected by the substrate.

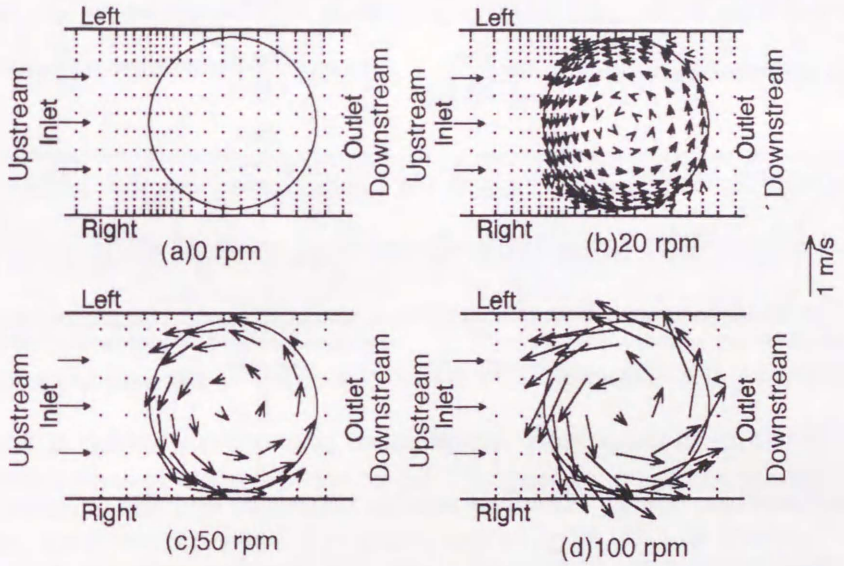

Fig.4-8 Gas flow velocity distribution in x-y plane 0.0175 mm above the substrate at rotation rate of 0, 20, 50 and 100 rpm.

Figure 4-9 shows the contour lines of temperature of the gases in an x-y plane near the substrate. Temperature of the gas introduced from the reactor inlet stays at almost 300 K until the gas comes close to the substrate, and it increases rapidly at its leading edge. The stairway form of the temperature contour lines around the substrate results from the contouring procedure, since rectangular gridding of the domain does not exactly match the round shape of the substrate. In contrast

to the gas velocity distribution, the rotation rate has very small influence on the temperature distribution from 0 through 100 rpm. This is because the thermal conduction from the heated substrate to the gases is very rapid.

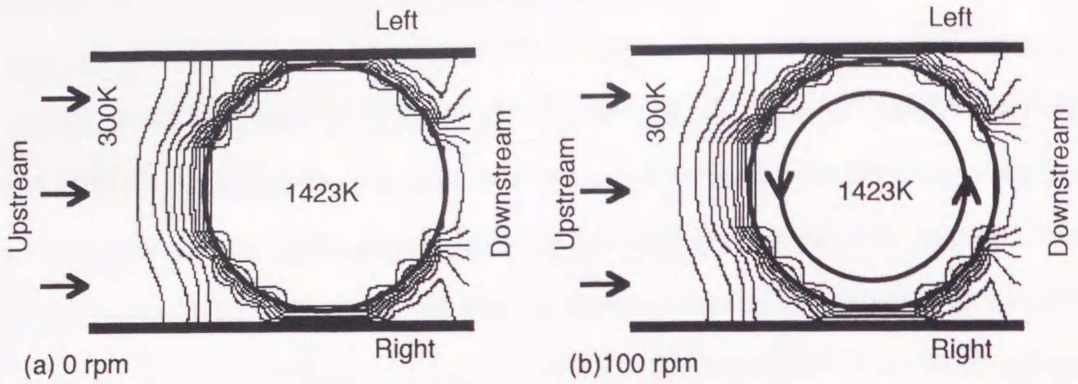

Fig.4-9 Contour lines of temperature in x-y plane of 0.0175 mm above the substrate at rotation rate of 0 and 100 rpm.

During the epitaxial growth, the species consumption by the surface chemical reaction of equation (4-1) causes the concentration gradient of chemical species as well as the thermal diffusion, but the species distribution, at the same time, tend to be homogenized by the diffusion. To extract the effect of the substrate rotation on the species distribution from these complicated phenomena, which is composed of the mass, momentum, energy, chemical species transport and the chemical reaction, additional calculations were performed where the chemical reaction is intentionally ignored. To estimate the effect of the rotation on the species distribution, the composition of the species at the reactor inlet is purposely set to be nonuniform as found in Fig. 4-10 at the reactor inlet. In the calculations, the mass fraction of $SiHCl_3$ is 0.4 near the center of the inlet and those near the right and left side walls are 0.71.

The concentration nonuniformity imposed at the inlet becomes smaller as the gas approaches to the substrate because of the diffusion in the horizontal direction. The temperature gradient is very large at the leading edge of the substrate, where the

thermal diffusion strongly affects on the distribution of the chemical species. The thermal diffusion transports $SiHCl_3$ gas away from the hot substrate surface, and it generates a large region having relatively lower $SiHCl_3$ concentration near the leading edge of the substrate as shown in the figure. With increasing the rotation rate, the shape of the contour lines of mass fraction is deformed more but the variation in the $SiHCl_3$ concentration on the substrate tends to become smaller, as indicated by the increasing area on the substrate with the mass fraction between 0.45 and 0.5.

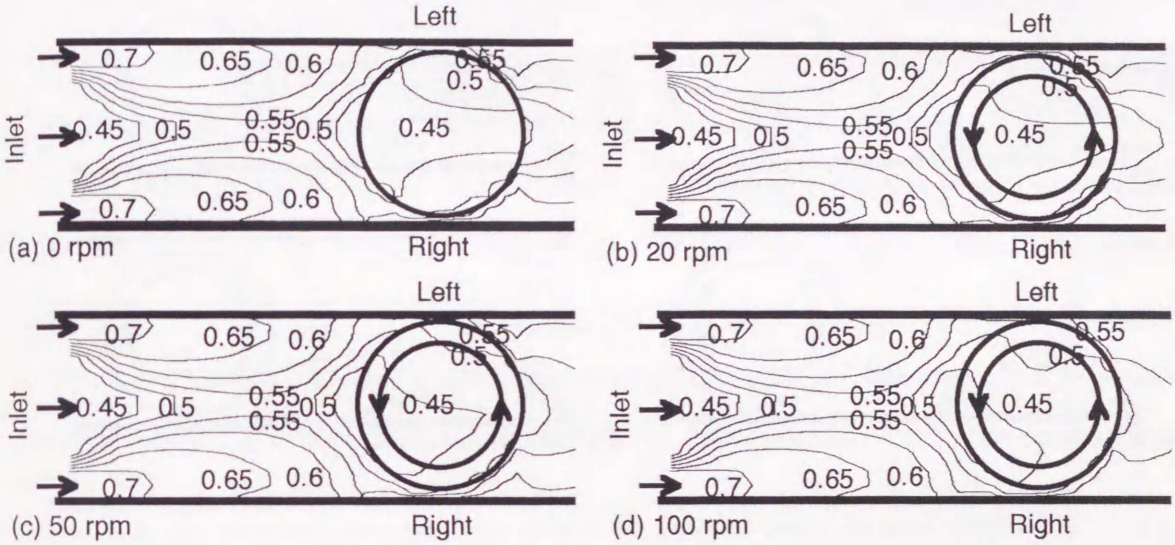

Fig.4-10 Contour lines of mass fraction of $SiHCl_3$ ignoring the chemical reaction in x-y plane 0.25 mm from the substrate at rotation rate of 0, 20, 50 and 100 rpm.

The contribution of thermal diffusion in the silicon thin-film growth has been discussed in Chapter 3. where the calculation neglecting the thermal diffusion overestimated the growth rate. To evaluate the role of thermal diffusion on the reaction with the rotating substrate in detail, calculations are performed additionally ignoring the transport by the thermal diffusion and the chemical reaction.

Figure 4-11 shows the mass fraction distribution of $SiHCl_3$ over an x-y plane 0.25 mm above the substrate, where nonuniform $SiHCl_3$ concentration at the inlet is again assumed. In case the thermal diffusion is ignored, the region having low

concentration do not appear near the leading edge of the substrate. The rotation of substrate distorts the contour lines on the substrate and generates a large region having almost uniform concentration with increasing rotation rate. The difference between the contour lines in Figs. 4-10 and 4-11 indicates that $SiHCl_3$ gas, under the conditions for the epitaxial growth, distributes inhomogeneously due to the thermal diffusion even at high rotation rates.

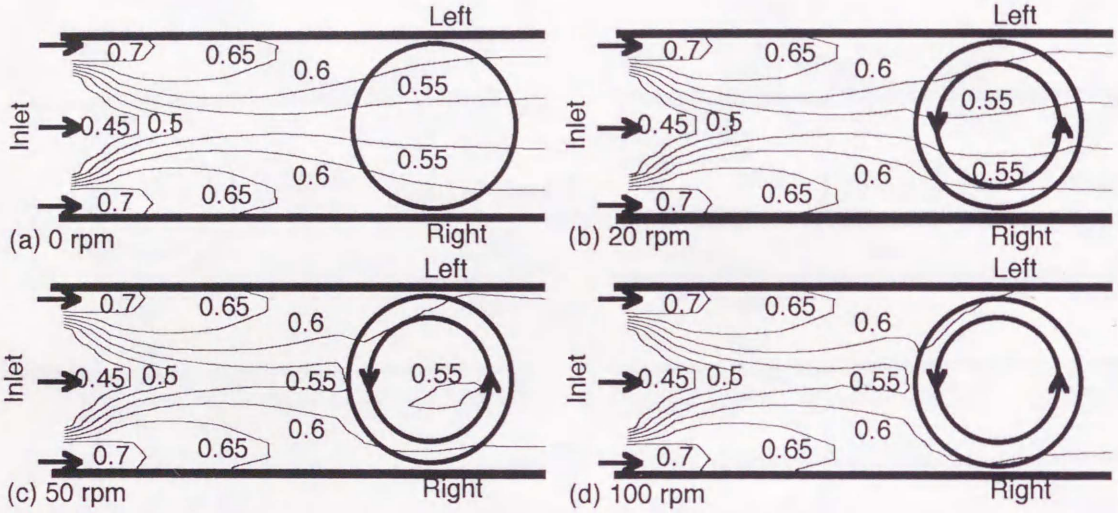

Fig.4-11 Contour lines of mass fraction of $SiHCl_3$ ignoring the chemical reaction and thermal diffusion in $x - y$ plane 0.25 mm from the substrate at rotation rate of 0, 20, 50 and 100 rpm.

According to the discussion above, the thermal diffusion lessens the $SiHCl_3$ concentration at the leading edge of the substrate, whereas the chemical reaction makes the depletion of $SiHCl_3$ toward the trailing edge of the substrate. These two phenomena induce the opposite gradient of $SiHCl_3$ concentration which compensate each other, forming moderate gradient of $SiHCl_3$ concentration and thus assisting the formation of flat profile of the film thickness. However, the distribution in the grown film thickness on the rotating substrate is basically explained as the averaging effect by integrating local growth rate over concentric circles which, at the same time, is aided by the change of the $SiHCl_3$ distribution by the rotating motion. This mechanism

leading to relatively uniform film thickness is fundamentally different from that in a vertical reactor with very high rotation rate of substrate,[14] which is designed to have very simple gas stream and a rather homogeneous species distribution.

4.3.3 *Method to improve film thickness uniformity*

The discussion in this chapter shows that the silicon epitaxial film is formed by integrating the growth rate along concentric circles on the substrate surface. Although the large growth rates at the front side of the substrate and the small ones at the rear side can compensate each other to form uniform thickness profile, the thicknesses at the substrate edges are still larger than that at the center of the substrate. This profile is due to higher growth rates at the substrate edges, especially at the right and the left edges, than those at the inner region of the substrate. Therefore, the growth rates at the right and the left sides cannot compensate each other. This indicates that the uniform temperature at the substrate surface and the uniform source gas concentration at the reactor inlet cannot result in the completely uniform epitaxial film thickness profile. To improve the film thickness uniformity more, two methods are possible from the view point of adjusting the growth rate. One method is to set nonuniform temperature within the substrate; the other is to set nonuniform concentration profile of the source gas, $SiHCl_3$ at the reactor inlet. Since the nonuniform temperature within a substrate often causes the crystal defect of *slip* due to thermal stress, the former method is not appropriate. A large-diameter wafer is very sensitive to the temperature distribution within itself.[15]

The latter method is considered to be effective since Fig. 4-10 shows that the tendency of the nonuniform concentration of $SiHCl_3$ set at the reactor inlet can be kept on the rotating substrate. It should be tried for achieving very high thickness uniformity to set the nonuniform $SiHCl_3$ concentration between the right and left sides of the reactor inlet, which cause the nonuniform growth rate profile to be compemsated between the right and the left edge of the substrate.

4.4 Conclusions

Preparation of silicon thin-film on a large rotating substrate with $SiHCl_3$-H_2 system in a single-wafer horizontal reactor has been discussed using a numerical calculation model. The effect of a substrate rotation in a single-wafer horizontal reactor is quite different from that in a vertical reactor. Although nearly uniform film thickness is achieved by the rotating substrate, the concentration of $SiHCl_3$ itself is not uniform on the substrate even at very high rotation rates. The good uniformity in film thickness is achieved by the continuous change in the substrate surface position due to rotation, which causes averaging effect of the nonuniform growth rate along concentric circles on the substrate surface. The change in the transport phenomena induced by the rotating motion also contributes to the thickness uniformity.

Nomenclature

A : pre-exponential factor of rate constant $(\mathrm{m^4\,mol^{-1}\,s^{-1}})$

C_p : heat capacity at constant pressure $(\mathrm{J\,kg^{-1}\,K^{-1}})$

D_i : binary diffusion coefficient of species i in H_2 $(\mathrm{m^2\,s^{-1}})$

D_i^T : thermal diffusion coefficient of species i in H_2 $(\mathrm{kg\,m^{-1}\,s^{-1}})$

E : activation energy of rate constant $(\mathrm{J\,mol^{-1}})$

g : acceleration due to gravity $(\mathrm{m\,s^{-2}})$

h_s : distance from substrate surface (m)

$[i]$: mole concentration of species i $(\mathrm{mol\,m^{-3}})$

j_C : diffusion flux driven by concentration gradient $(\mathrm{kg\,m^{-2}\,s^{-1}})$

j_T : diffusion flux driven by temperature gradient $(\mathrm{kg\,m^{-2}\,s^{-1}})$

j_x : diffusion flux driven by concentration and temperature gradient in x direction $(\mathrm{kg\,m^{-2}\,s^{-1}})$

j_y : diffusion flux driven by concentration and temperature gradient in y direction $(\mathrm{kg\,m^{-2}\,s^{-1}})$

j_z : diffusion flux driven by concentration and temperature gradient in z direction $(\mathrm{kg\,m^{-2}\,s^{-1}})$

k : Arrhenius-type rate constant $(\mathrm{m^4\,mol^{-1}\,s^{-1}})$

l_x: distance OX (m)

l_y: distance OY (m)

M_av: average molecular weight of gas mixture $(\mathrm{kg\,mol^{-1}})$

M_Si: molecular weight of Si $(\mathrm{kg\,mol^{-1}})$

M_i: molecular weight of species i $(\mathrm{kg\,mol^{-1}})$

MW: average molecular weight of gas mixture at reactor inlet $(\mathrm{kg\,mol^{-1}})$

p : pressure (Pa)

R : gas constant $(\mathrm{J\,mol^{-1}\,K^{-1}})$

R_i : mass rate of change in species i by chemical reaction $(\mathrm{kg\,m^{-2}\,s^{-1}})$

R_Si : mass rate of change in Si by chemical reaction $(\mathrm{kg\,m^{-2}\,s^{-1}})$

T : temperature (K)

T_s : substrate temperature (K)

t_{max} : maximum value of the film thickness (μm)

t_{min} : minimum value of the film thickness (μm)

t_v : thickness variation (%)

u : fluid velocity in x direction ($\mathrm{m\,s^{-1}}$)

v : fluid velocity in y direction ($\mathrm{m\,s^{-1}}$)

V_G : growth rate ($\mu\mathrm{m\,min^{-1}}$)

w : fluid velocity in z direction ($\mathrm{m\,s^{-1}}$)

x : coordinate in horizontal direction (m)

x_i : mole fraction of species i (-)

y : coordinate in horizontal direction (m)

z : coordinate in vertical direction (m)

α_i : thermal diffusion factor of species i (-)

θ_x: angle shown in the Fig.4-3 (rad)

θ_y: angle shown in the Fig.4-3 (rad)

λ : thermal conductivity of gas mixture ($\mathrm{W\,m^{-1}\,K^{-1}}$)

μ : viscosity of gas mixture (Pa·s)

ν_i : molar stoichiometry coefficient for species i in chemical reaction (-)

ρ : density of gas mixture ($\mathrm{kg\,m^{-3}}$)

ρ_{Si} : density of Si ($\mathrm{kg\,m^{-3}}$)

ω : angular velocity of the rotation ($\mathrm{rad\,s^{-1}}$)

ω_i : mass fraction of species i (-)

References

[1] K. J. Kuijlaars, C. R. Keijn and H. E. A. van den Akker, *Chem. Eng. J.*, **57**, 127 (1995).

[2] S.V.Patankar,*Numerical heat transfer and fluid flow* (McGraw-Hill, New York, 1980).

[3] *Kagaku Binran* (Handbook of Chemistry) (Iwanami, Tokyo, 1984) 3rd ed., Chap. 6, p. II-39 [in Japanese].

[4] *Kagaku Binran* (Handbook of Chemistry) (Iwanami, Tokyo, 1984) 3rd ed., Chap. 6, p. II-71 [in Japanese].

[5] *Kagaku Binran* (Handbook of Chemistry) (Iwanami, Tokyo, 1984) 3rd ed., Chap. 9, p. II-239 [in Japanese].

[6] P. Pollard and J. Newman, *J. Electrochem. Soc.*, **127**, 744 (1980).

[7] C. R. Wilke, *J. Chem. Phys.*, **18**, 517 (1950).

[8] I.H.Oh, C.G.Takoudis and G.W.Neudeck, *J.Electrochem.Soc.*, **138**, 554 (1991).

[9] R.C.Reid, J.M.Prausnitz and B.E.Poling, *The Properties of Gases and Liquids* (McGraw-Hill, New York, 1987) 4th ed.

[10] W. L. Holstein, *J. Electrochem. Soc.*, **135**, 1788 (1988).

[11] P. D. Neufeld, A. R. Janzen and R. A. Aziz, *J. Chem. Phys.*, **57**, 1100 (1972).

[12] L. W. Flynn and G. Thodos, *A. I. Ch. E. Journal*, **8**, 362 (1962).

[13] M. A. Drews, W. L. Schenck, Jr., J. D. Smith, J. Walker and C. L. Yaws, *Solid State Technology*, p. 39 (Jan. 1973).

[14] Y. Sato, T. Tamura and T. Ohmine, *Extended Abstracts 1992 Int. Conf. Solid State Devices and Materials*, 20 (1992).

[15] F. Shimura, *Semiconductor Silicon Crystal Technology* (Academic Press, San Diego, 1989) Chap.7 , p.285.

Chapter 5

Model on Transport Phenomena and Silicon Epitaxial Growth of Thin-Film in $SiHCl_3$-H_2 System under Atmospheric Pressure

5.1 Introduction

In this chapter, the elemental surface process in a $SiHCl_3$-H_2 system is discussed quantitatively in conjunction with an entire analysis of the transport phenomena in a single-wafer horizontal reactor for the conditions applicable to industrial epitaxial growth, since the $SiHCl_3$-H_2 system have not yet been discussed sufficiently. The rate processes discussed in this Chapter include chemisorption of $SiHCl_3$ and decomposition of the chemisorbed species. The rate constant of an overall reaction is obtained from the experimental growth rate data and discussed to evaluate the rate constants of the chemisorption and the decomposition. The model developed in this Chapter describes the silicon epitaxial growth over a wide temperature range from the reaction limited region to the transport limited region for various concentrations of $SiHCl_3$.

5.2 Preparation of silicon epitaxial Thin-films

Figure 5-1 shows the geometry of the reactor studied in this study. For the analysis of thin-film preparation on a heated substrate, we prepare silicon epitaxial Thin-films on silicon (100) substrates by $SiHCl_3$ and H_2 gases. The epitaxial thin-film thicknesses were measured using interference fringe in the Fourier-transform infrared spectra. The gas mixture is introduced into the reactor under atmospheric pressure and reacts at the surface of the substrate held horizontally on a susceptor in the reactor. In this Chapter, the susceptor is not rotated. The susceptor is designed to prepare a epitaxial layer on an 8-inch-diameter silicon substrate. The substrate is heated to 1073, 1223 and 1398 K using infrared furnaces through the reactor walls consisting of quartz glass. The temperature is maintained constant by monitoring the temperature and controlling the input power of the infrared furnaces continuously. The outer surfaces of the quartz walls are cooled with a sufficiently large amount of cold air, so that it is reasonable to neglect an absorption of radiation

heat by the transparent walls. Since the concentrations of $SiHCl_3$ and HCl are low, effects of radiation heat on these gases are assumed to be negligible.

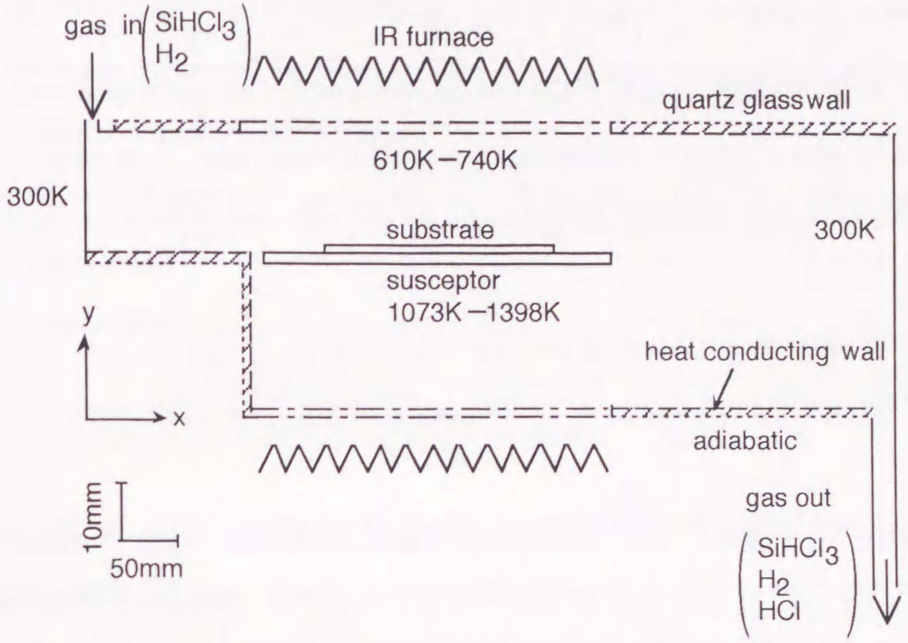

Fig.5-1 Single-wafer horizontal reactor for preparation of silicon epitaxial film.

5.3 Basic equations governing the epitaxial reactor

In order to evaluate the film growth rate in nonuniformly distributed temperature and gas flow fields, the mass, momentum, energy and species transport equations must be solved simultaneously. The present model also includes chemical reactions on the substrate surface.

We focus mainly on the growth rate of a film at the center of the substrate. The transport phenomena in the reactor in a steady state are solved using two-dimensional Cartesian coordinates. The governing equations for the gas velocity are as follows:

Conservation of mass:

$$\frac{\partial}{\partial x}(\rho u) + \frac{\partial}{\partial y}(\rho v) = 0. \tag{5-1}$$

Conservation of momentum:

$$\frac{\partial}{\partial x}(\rho uu) + \frac{\partial}{\partial y}(\rho vu) = \frac{\partial}{\partial x}\left(2\mu\frac{\partial u}{\partial x}\right) + \frac{\partial}{\partial y}\left(\mu\frac{\partial u}{\partial y}\right) + \frac{\partial}{\partial y}\left(\mu\frac{\partial v}{\partial x}\right) - \frac{\partial p}{\partial x}. \quad (5\text{-}2)$$

$$\frac{\partial}{\partial x}(\rho uv) + \frac{\partial}{\partial y}(\rho vv) = \frac{\partial}{\partial y}\left(2\mu\frac{\partial v}{\partial y}\right) + \frac{\partial}{\partial x}\left(\mu\frac{\partial v}{\partial x}\right) + \frac{\partial}{\partial x}\left(\mu\frac{\partial u}{\partial y}\right) - \frac{\partial p}{\partial y} + \rho g. \quad (5\text{-}3)$$

In equations (5-1)–(5-3), x and y are the coordinates in the horizontal and vertical directions, u and v are the velocities in x- and y-directions, ρ, p and μ are the density, pressure and viscosity, respectively, of the mixture of $SiHCl_3$, H_2 and HCl gas.

The gas density obeys the ideal gas law

$$\rho = \frac{pM_{\mathrm{av}}}{RT}, \quad (5\text{-}4)$$

where M_{av} is the local average molecular weight of the gas and R is the gas constant.

The gas velocities, u and v, are set to be zero on all the surfaces of the solid walls as boundary conditions. The gas velocity and pressure at the inlet are $0.67\,\mathrm{m\,s^{-1}}$ and $1.0133 \times 10^5\,\mathrm{Pa}$, respectively.

The temperature distribution, T, in the reactor is expressed by the following energy equation:

Conservation of energy:

$$\frac{\partial}{\partial x}(\rho C_{\mathrm{p}} Tu) + \frac{\partial}{\partial y}(\rho C_{\mathrm{p}} Tv) = \frac{\partial}{\partial x}\left(\lambda\frac{\partial T}{\partial x}\right) + \frac{\partial}{\partial y}\left(\lambda\frac{\partial T}{\partial y}\right). \quad (5\text{-}5)$$

In this equation, C_{p} is the heat capacity of the gas at constant pressure, and λ the thermal conductivity of the gas.

Heat of reaction at the substrate surface is ignored in the present model because the heat capacity of the susceptor, the temperature of which is well controlled, is so much larger than that of the gas mixture that the temperature change by the heat due to the reaction is negligible. We ignore heat transfer by radiation in equation (5-5) as mentioned, and impose the following boundary conditions on the equation. Since accurate measurement of the temperature of the transparent quartz glass walls is extremely difficult, their temperatures are estimated empirically and

assumed to vary linearly with the substrate temperature in the range between 610 K and 740 K. The reactor wall illustrated by the hatched region in Fig. 5-1 is treated as a heat conducting wall with the thermal conductivity of quartz glass. The outer surface of this region (dotted lines in Fig. 5-1) is taken to be surrounded by adiabatic walls. The temperature of the other reactor walls is regarded as 300 K since the walls are continuously cooled with water.

Conservation of chemical species i (i = $SiHCl_3$, H_2 and HCl) is described by the following equation:

Conservation of species:

$$\frac{\partial}{\partial x}(\rho u \omega_i) + \frac{\partial}{\partial y}(\rho v \omega_i) = \frac{\partial}{\partial x}\left(\rho D_i \frac{\partial \omega_i}{\partial x} + D_i^{\mathrm{T}} \frac{\partial \ln T}{\partial x}\right) + \frac{\partial}{\partial y}\left(\rho D_i \frac{\partial \omega_i}{\partial y} + D_i^{\mathrm{T}} \frac{\partial \ln T}{\partial y}\right). \tag{5-6}$$

In this equation, ω_i is the mass fraction of species i. The diffusion coefficient, D_i, is assumed to be the binary diffusion coefficient of species i in H_2 gas since the mole fraction (not mass fraction) of species other than H_2 is small. The mass transport phenomena driven by the temperature gradient (thermal diffusion) are described by the terms relating to D_i^{T}, the thermal diffusion coefficient. D_i^{T} is expressed as

$$D_i^{\mathrm{T}} = \alpha_i \rho D_i \omega_i \omega_{\mathrm{H_2}}, \tag{5-7}$$

where α_i is the thermal diffusion factor of species i.

At the inlet of the reactor the composition of the $SiHCl_3$ and H_2 gas mixture is expressed in terms of the average molecular weight, MW. MW is given by

$$MW = \sum_i x_i M_i \quad (i = \mathrm{SiHCl_3\ and\ H_2}), \tag{5-8}$$

where x_i and M_i are the mole fraction and molecular weight of species i. MW is varied between 2.7×10^{-3} and $11 \times 10^{-3}\,\mathrm{kg\,mol^{-1}}$.

At an initial step, we consider the preparation of a silicon film on the basis of the following overall reaction.

$$\mathrm{SiHCl_3 + H_2 \rightarrow Si + 3HCl} \tag{5-9}$$

Mass changes due to the chemical reaction of equation (5-9) on the surface are considered in the boundary conditions at the surface of the substrate. Assuming that the reaction of equation (5-9) is a second-order reaction, the rate of mass consumption or generation of species i at the surface is expressed as

$$R_i = \nu_i M_i k[\mathrm{SiHCl_3}][\mathrm{H_2}], \tag{5-10}$$

where k is the rate constant for the reaction expressed as $k = A \exp(-E/RT)$, and the values of the molar stoichiometry coefficient, ν_i, are - 1 for $i = \mathrm{SiHCl_3}$ and $\mathrm{H_2}$, and 3 for $i = \mathrm{HCl}$. The concentration of each species at the surface is governed by a balance between the consumption by the chemical reaction and the diffusion fluxes driven by the concentration and temperature gradients. The boundary conditions on the substrate surface are

$$R_i = j_\mathrm{C} + j_\mathrm{T} = -\rho D_i \frac{\partial \omega_i}{\partial y} - D_i^\mathrm{T} \frac{\partial \ln T}{\partial y}, \tag{5-11}$$

where j_C and j_T denote the molecular and thermal diffusion fluxes.

The accumulation of silicon per unit time and area of the surface

$$R_\mathrm{Si} = M_\mathrm{Si} k[\mathrm{SiHCl_3}][\mathrm{H_2}] \tag{5-12}$$

gives the growth rate of silicon film as

$$V_\mathrm{G} = 6 \times 10^7 R_\mathrm{Si}/\rho_\mathrm{Si} \quad (\mu\mathrm{m\,min^{-1}}), \tag{5-13}$$

where ρ_Si is the density of silicon, and the factor 6×10^7 is used for the unit conversion of $\mathrm{m\,s^{-1}}$ to $\mu\mathrm{m\,min^{-1}}$.

To solve the transport equations described above, the calculation domain is divided into a nonuniform mesh with 78×52 grid points in the x- and y-directions. Then the equations for gas velocity, temperature and mass of chemical species are discretized into finite difference formulae. In this Chapter, the computational fluid dynamics code FLUENT (ver. 3.03)[1] is used as the solver.

The gas properties of $\mathrm{H_2}$ such as viscosity, heat capacity and thermal conductivity are taken from the literature.[2-4] The properties of $\mathrm{SiHCl_3}$ and HCl are given by Pollard and Newman.[5] Each physical constant is expressed as a function of temperature

using a polynomial fit. The properties of the mixed gas are estimated theoretically.[1] The binary diffusion coefficients of $SiHCl_3$ and HCl in H_2 are estimated with the method described in the literature.[6] Following Holstein,[7] the thermal diffusion coefficients of $SiHCl_3$ and HCl are obtained.

In this Chapter, the overall rate constant, k, and the concentration of $SiHCl_3$ at the substrate surface are obtained at the initial step so that calculated growth rates agree with the growth rates measured at various temperatures. At the next step, dependence of the overall rate constant on the $SiHCl_3$ surface concentration is discussed to clarify surface processes including the epitaxial growth.

5.4 Mathematical model of the rate process

In this section, epitaxial growth processes in the transport and epitaxy model is discussed after a brief description of the behavior of chemical species in the gas phase and at the silicon surface.

5.4.1 *Chemical species in the gas phase*

The intermediate species in the gas phase for the silicon epitaxy from Si-H-Cl system have been discussed in many papers.[8-13] At a temperature higher than 1400 K, $SiCl_2$ molecules are suggested as a major intermediate gas species for an Si-H-Cl system.[10, 11, 13, 14] The overall reaction of equation (5-9) is discussed by Sirtl et al.,[11] who stated that $SiCl_2$ existed in the gas phase and at the surface. It is also shown by the calculations assuming in an equilibrium state[11-13] that $SiCl_2$ concentration is higher than $SiHCl_3$ above 1300 K under atmospheric pressure. However the entire state in the reactor cannot be in an equilibrium state[8] because the crystal growth cannot be achieved with no free energy change. The entire state in a cold wall reactor with a high growth rate can be in a steady state but should be strictly recognized as a nonequilibrium state.

Among many experimental studies to identify the chemical species in the gas phase,[8,9,15-17] Aoyama et al.[8] demonstrated that chemical species of $SiCl_4$, $SiHCl_3$, SiH_2Cl_2 and $SiCl_2$ existed in the gas phase of $SiCl_4$-H_2 system in a cold wall reactor and that all of them contributed to the epitaxial growth at high growth temperature. However, the concentration of $SiCl_2$ was found to be much lower than that of $SiCl_4$ and $SiHCl_3$ even at 1473 K. This suggest that in the $SiHCl_3$-H_2 system $SiHCl_3$ molecules are transported to the substrate surface to play a major role in the silicon epitaxial growth.

Chemical reactions in the gas phase can also be estimated experimentally from the surface morphology of the epitaxial film. Particle generation in the gas phase sometimes consume much reactant species to decrease the film growth rate.[18] If a large amount of particles are generated near the substrate surface, some portion of the particles will attach to the surface to form hillocks. However, the film grown in this study had a very smooth surface without any hillock. Therefore, it can be assumed that there is no particle generation to reduce the growth rate for the experimental conditions of this study.

Consequently, chemical reactions which cause thermal decomposition of $SiHCl_3$ or particle generation in the gas phase can be assumed to be ignored. Only $SiHCl_3$ is therefore considered to calculate the growth rate.

5.4.2 *Chemical species and adsorption at substrate surface*

Behavior of chemical species at the substrate surface is noted briefly here. Above 850 or 873 K, no hydrogen atom is present at silicon (100) surface.[19-21] Oxygen atoms are removed rapidly from the substrate surface as SiO molecules above 1000 K.[22] The surface is terminated by Cl atoms as SiCl bonds during the low temperature molecular beam epitaxy (MBE),[23] but Cl atoms are desorbed above 623 K.[24] Hirva and Pakkanen[25] showed that $SiHCl_3$ molecules were chemisorbed at the silicon surface accompanying HCl formation. Photoemission measurements also show that most of

Cl adhering to silicon surfaces remain on the surface up to 873–1073 K. At higher temperature, they are desorbed as $SiCl_2$ molecules.[26] From this discussion, there is no hydrogen and oxygen atoms on the surface above 1000 K. However, Cl atoms and $SiCl_2$ molecules must be taken into account.

Adsorption is classified into physisorption and chemisorption. Physisorption is the weakest form of adsorption to a solid surface and is characterized by the lack of a true chemical bond between the adsorbate and the substrate.[27] Physisorbed species migrate toward reactive sites and react to be chemisorbed there.[28]

Whereas $SiHCl_3$ is valence saturated species which can only be physisorbed at the surface, $SiCl_2$ is valence unsaturated and can be chemisorbed at the surface.[29] The epitaxial growth on (100) surface has the predominant mechanism for stable dimer opening.[30] In the initial stage, the physisorbed species, $SiHCl_3$, migrates to the remaining dangling bonds of the dimer and decompose to $SiCl_x$ (x=1,2,3) which are chemisorbed.[31,32] This generates a Cl terminated surface, which reacts with H_2 molecules in the gas phase to desorb as HCl molecules.[30]

We assume that chemisorbed $SiCl_2$ ($^*SiCl_2$) is the dominant species for the epitaxial growth rate.

5.4.3 *Chemical reactions and rate process at the surface*

The purpose of this Chapter is to build a compact model for an epitaxial growth including both the transport phenomena and the surface processes, which is based on Eley and Rideal[33] and Langmuir.[34] To obtain the transport and epitaxy model, the followings are assumed.

(i) The substrate surface has a fixed number of reactive sites.

(ii) Each reactive site can hold one chemisorbed molecule.

(iii) The chemisorption is restricted to a monolayer.

(iv) At the epitaxial growth temperature and pressure, a fraction, Θ, of the reactive sites is occupied by chemisorbed molecules, and a fraction, 1-Θ, is not occupied.

(v) There is no interaction between chemisorbed molecules.

(vi) The heat due to the physisorption or chemisorption is ignored.

(vii) $SiHCl_3$ molecules do not decompose in the gas phase.

(viii) H_2 molecules are not adsorbed at the substrate surface.

By using equation (5-10), the overall rate constant k for the overall reaction of equation (5-9) is estimated. To discuss the surface reaction processes, the overall reaction of equation (5-9) is assumed to be decomposed of several elementary reactions.

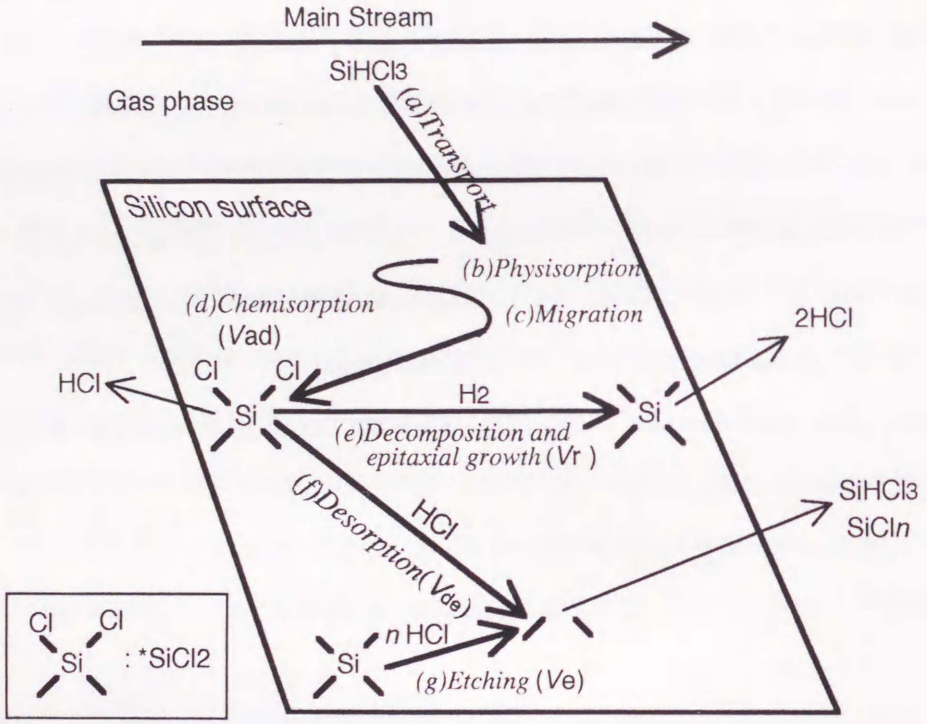

Fig.5-2 Transport and epitaxy processes during silicon epitaxial growth from chemical reactions of $SiHCl_3$, H_2 and HCl molecules at substrate surface.

The entire processes of the silicon epitaxial growth on a (100) silicon surface can be illustrated as Fig. 5-2. The reactant, an $SiHCl_3$ molecule, is transported from the gas phase to the vicinity of the substrate (process (a)) and is captured loosely at the substrate (process (b) : physisorption). Then, the reactant migrates or diffuses to an unoccupied reactive site (process (c)). At the unoccupied reactive

site, $SiHCl_3$ decomposes into $*SiCl_2$ and HCl. The substrate crystal of silicon has chemical bonds with the $*SiCl_2$ (process (d)), where Cl atoms are directed to the gas stream. Therefore this surface is regarded as a silicon crystal covered with Cl atoms. Such a chemisorbed surface reacts with H_2 molecules in the gas phase (process (e)) to produce silicon atoms releasing the by-product, HCl molecules. After these processes, the occupied reaction site returns to be an unoccupied site, and the surface undergoes the next growth process. At the same time, side reactions take place. Chemisorbed $*SiCl_2$ can react with HCl in the gas phase to produce $SiHCl_3$ which is desorbed from the substrate surface (process (f)). HCl molecules in the gas phase can attack the substrate surface to etch the surface and produce $SiCl_n$ which is transported away from the surface (process (g)).

Through these processes silicon epitaxial films are grown. The key processes in these are described by equations (5-14)–(5-17).

Chemisorption of $SiHCl_3$ (process (d)):

$$SiHCl_3 \rightarrow *SiCl_2 + HCl. \tag{5-14}$$

Desorption of $SiHCl_3$ (process (f)):

$$*SiCl_2 + HCl \rightarrow SiHCl_3. \tag{5-15}$$

Decomposition of $*SiCl_2$ (production of silicon film; process (e)):

$$*SiCl_2 + H_2 \rightarrow Si + 2HCl. \tag{5-16}$$

Etching (process (g)):

$$Si + nHCl \rightarrow SiCl_n + (n/2)\,H_2. \tag{5-17}$$

The rate of reactions (5-14)–(5-17) at the substrate surface are described according to the rate process theory as follows.

Rate of $SiHCl_3$ chemisorption:

$$V_{ad} = k'_{ad} a (1 - \Theta)[SiHCl_3] = k_{ad}(1 - \Theta)[SiHCl_3], \tag{5-18}$$

where V_{ad} denotes the chemisorption rate of $SiHCl_3$, k'_{ad} is the chemisorption rate constant for a reactive site, a is the density of reactive sites and k_{ad} is $k'_{ad} \times a$. $[SiHCl_3]$ is the mole concentration of $SiHCl_3$ at the substrate surface.

Rate of $SiHCl_3$ desorption:

$$V_{de} = k'_{de} a \Theta [HCl] = k_{de} \Theta [HCl], \tag{5-19}$$

where V_{de} denotes the desorption rate of $SiHCl_3$, k'_{de} is the desorption rate constant for a reactive site, k_{de} is $k'_{de} \times a$, and $[HCl]$ is the mole concentration of HCl at the substrate surface.

Rate of decomposition:

$$V_r = k'_r a \Theta [H_2] = k_r \Theta [H_2], \tag{5-20}$$

where V_r denotes the decomposition rate to produce Si, k'_r is the decomposition rate constant for a reactive site, and k_r is $k'_r \times a$. $[H_2]$ is the mole concentration of H_2 at the substrate surface.

Rate of etching:

$$V_e = k'_e a (1 - \Theta) [HCl]^n = k_e (1 - \Theta) [HCl]^n, \tag{5-21}$$

where V_e denotes the rate of etching the silicon surface, k'_e is the etching rate constant for a reactive site, n is the order of etching reaction and k_e is $k'_e \times a$.

Under the reaction condition for obtaining a very large growth rate, the rate of $SiHCl_3$ desorption should be much smaller than that of $SiHCl_3$ chemisorption.[35] The desorption of $SiHCl_3$ is hence ignored in this study.

The fraction of occupied reactive sites, Θ, is obtained at a steady state from equations (5-18) and (5-20).

$$\frac{\partial}{\partial t} a \Theta = V_{ad} - V_r = 0, \tag{5-22}$$

$$\Theta = \frac{k_{ad} [SiHCl_3]}{k_{ad} [SiHCl_3] + k_r [H_2]}. \tag{5-23}$$

The mole growth rate of silicon epitaxial film, V, is described using equations (5-20), (5-21) and (5-23).

$$V = V_{\mathrm{r}} - V_{\mathrm{e}}. \tag{5-24}$$

$$V = k_{\mathrm{r}}[\mathrm{SiHCl_3}][\mathrm{H_2}]\frac{k_{\mathrm{ad}} - k_{\mathrm{e}}[\mathrm{HCl}]^n/[\mathrm{SiHCl_3}]}{k_{\mathrm{ad}}[\mathrm{SiHCl_3}] + k_{\mathrm{r}}[\mathrm{H_2}]}. \tag{5-25}$$

As described in equation (5-12)

$$V = \frac{R_{\mathrm{Si}}}{M_{\mathrm{Si}}} = k[\mathrm{SiHCl_3}][\mathrm{H_2}]. \tag{5-26}$$

Equations (5-25) and (5-26) give

$$k = k_{\mathrm{r}}\frac{k_{\mathrm{ad}} - k_{\mathrm{e}}[\mathrm{HCl}]^n/[\mathrm{SiHCl_3}]}{k_{\mathrm{ad}}[\mathrm{SiHCl_3}] + k_{\mathrm{r}}[\mathrm{H_2}]}, \tag{5-27}$$

or

$$\frac{1}{k} = \frac{1}{k_{\mathrm{ad}} - k_{\mathrm{e}}[\mathrm{HCl}]^n/[\mathrm{SiHCl_3}]}\left(\frac{k_{\mathrm{ad}}[\mathrm{SiHCl_3}]}{k_{\mathrm{r}}} + [\mathrm{H_2}]\right). \tag{5-28}$$

For the epitaxial growth, H_2 molecules comprize generally more than 95% of the total gas molecules and thus the concentration is assumed as constant at each temperature.

$$[\mathrm{H_2}] = \text{constant}. \tag{5-29}$$

When the growth rate is very large, the contribution of etching process can be ignored in comparison with the contribution of silicon formation.

$$k_{\mathrm{ad}} - k_{\mathrm{e}}[\mathrm{HCl}]^n/[\mathrm{SiHCl_3}] \simeq k_{\mathrm{ad}}. \tag{5-30}$$

Finally, the following equation is obtained.

$$\frac{1}{k} \simeq \frac{[\mathrm{SiHCl_3}]}{k_{\mathrm{r}}} + \frac{[\mathrm{H_2}]}{k_{ad}}. \tag{5-31}$$

Equation (5-31) shows that $1/k$ and $[\mathrm{SiHCl_3}]$ have a linear relationship. Here, k_{r} and k_{ad} are obtained by the slope of $1/k$ with respect to $[\mathrm{SiHCl_3}]$ and the intercept to the $1/k$ axis, respectively. The growth rate is expressed using equations (5-26) and (5-31).

$$V = \frac{k_{\mathrm{r}}k_{\mathrm{ad}}}{k_{\mathrm{ad}}[\mathrm{SiHCl_3}] + k_{\mathrm{r}}[\mathrm{H_2}]}[\mathrm{SiHCl_3}][\mathrm{H_2}]. \tag{5-32}$$

When the concentration of $SiHCl_3$ at the substrate surface is very small, equation (5-32) is simplified to equation (5-33).

$$V = k_{ad}[SiHCl_3]. \tag{5-33}$$

Equation (5-33) gives the growth rate when the rate is limited by the chemisorption of $SiHCl_3$. On the contrary, in the case that the surface concentration of $SiHCl_3$ is very high, the growth rate is expressed as

$$V = k_r[H_2]. \tag{5-34}$$

Clearly, this film growth rate does not depend on the $SiHCl_3$ concentration. Equation (5-34) is, in other words, the growth rate when the rate is limited by the decomposition of $*SiCl_2$.

5.5 Results and discussion

In this section, the validity of the transport and epitaxy model proposed above is examined by analyzing measured growth rates.

5.5.1 *Silicon epitaxial growth rate and grown film quality*

The measured epitaxial growth rates are shown in Fig. 5-3. At every temperature, the growth rate increases with increasing the average molecular weight, MW, when MW is small. However, its slope decreases gradually, and finally the growth rate saturates with MW. This behavior is obvious at 1073 and 1223 K.

The quality of grown silicon films was evaluated prior to discussion of the growth rate and the surface phenomena. Over the entire temperature range, the grown films were characterized as single crystal by using the electron beam diffraction method. The gate oxide integrity (GOI)[36] was also evaluated throughout the surfaces of epitaxial wafers. According to the results of the GOI measurements, the epitaxial films were in the group of C mode failure. This evaluation shows that the film

prepared here with the $SiHCl_3$-H_2 system under atmospheric pressure has sufficient quality for fabricating microelectronic devices. This coincides with Sedgwick et al.,[37,38] who showed possibility of growing films of good quality under atmospheric pressure down to 873 K using an SiH_2Cl_2-H_2 system. Consequently, the growth rates obtained in this study are considered to be reliable for the analysis of the epitaxial growth.

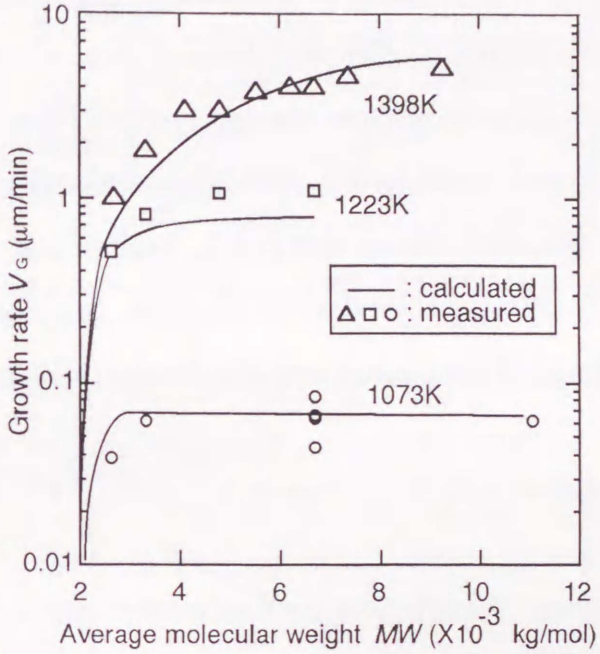

Fig.5-3 Epitaxial growth rates calculated (solid lines) and measured at 1073, 1223 and 1398 K (circles, squares and triangles, respectively).

5.5.2 *Transport phenomena in the single-wafer horizontal reactor*

Prior to discussing the surface processes, the transport of momentum, heat and chemical species in the single-wafer horizontal reactor incorporating chemical reactions at a substrate surface in a steady state are mentioned briefly since it is essentially the same as those in Chapter 3. which discussed the transport phenomena for the epitaxial silicon thin-film growth in detail.

Streamlines in the reactor were essentially the same over the temperature and $SiHCl_3$ concentration range of this study; the streamlines above the substrate were almost parallel to its surface, and flow induced by natural convection was not observed in the reactor. The gas temperature decreased almost linearly with the distance from the substrate due to a cold-wall environment. At 1398 K, $SiHCl_3$ concentration at the substrate surface were calculated to be much lower than that at the inlet of the reactor because of the consumption by the surface chemical reactions, the diffusion and the thermal diffusion as discussed in Chapter 3. This difference of $SiHCl_3$ concentration became smaller with decreasing the substrate temperature mainly due to depressing the the surface chemical reaction rates.

Over the epitaxial growth conditions in this Chapter, the gas flow, the temperature profile and the chemical species distribution kept similar patterns as those at 1423 K (Chapter 3) although the values of velocities, temperatures and species concentrations varied with the substrate temperature and MW.

5.5.3 *Surface rate process*

As mentioned, equations (5-1)–(5-13) are solved numerically to obtain the overall rate constant, k, and the surface mole concentration of $SiHCl_3$, $[SiHCl_3]$, so that the calculated growth rates agree with the measured growth rates. Figure 5-4 shows that $1/k$ changes linearly with $[SiHCl_3]$ as predicted by equation (5-31). A linear relationship between $[SiHCl_3]$ and $1/k$ holds over a wide temperature range. This relationship also clearly indicates that the species and the elemental processes of the epitaxial growth do not change in the wide temperature range.

The rate constants, k_r and k_{ad}, are obtained by the slope and the intercept respectively in Fig. 5-4 from equation (5-31). Figure 5-5 shows k_r and k_{ad} as a function of $1/T$. The rate constants, k_r and k_{ad}, obey the Arrhenius law and are described as follows:

$$k_{ad} = 2.72 \times 10^6 \exp(-1.72 \times 10^5 / RT), \tag{5-35}$$

$$k_r = 5.63 \times 10^3 \exp(-1.80 \times 10^5 / RT). \quad (5\text{-}36)$$

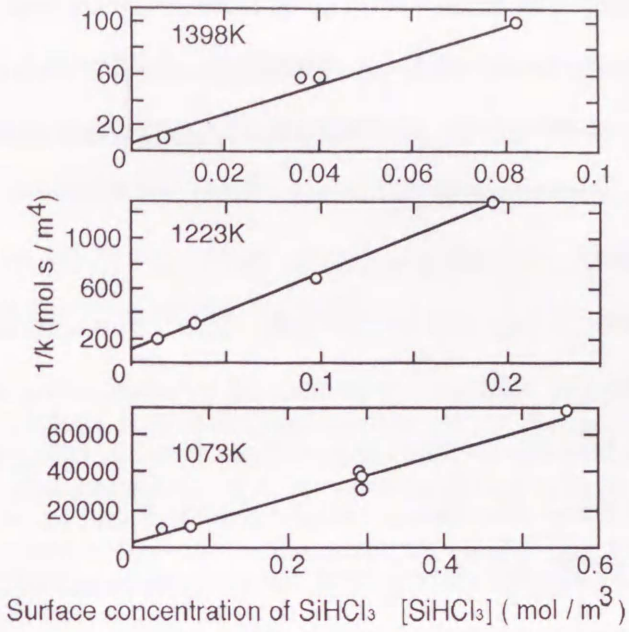

Fig.5-4 Change in $1/k$ with $SiHCl_3$ concentration at 1073, 1223 and 1398 K.

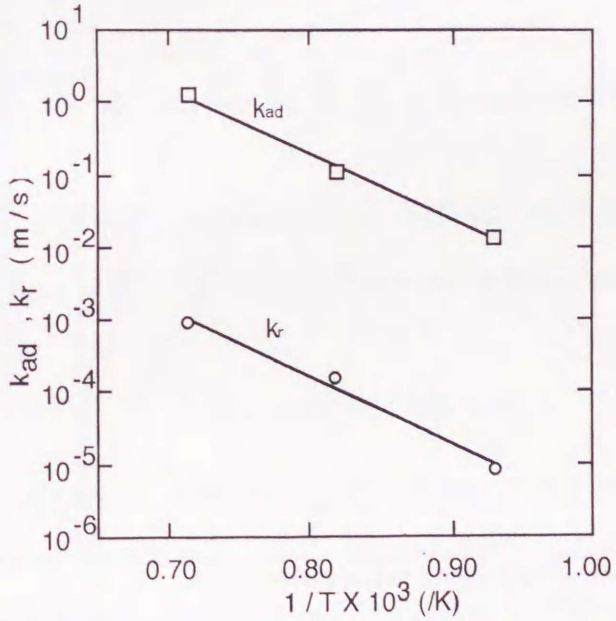

Fig.5-5 Rate constants of chemisorption, k_{ad}, and decomposition of $*SiCl_2$, k_r, as a function of reciprocal temperature.

As discussed in the previous section, the surface during the epitaxial growth is ter-

minated with chlorine atoms or bonded with $SiCl_2$ or SiCl.[39] The activation energy of the surface reaction leading to silicon formation is calculated to be 1.8×10^5 J/mol as shown in equation (5-36), which is close to 2.2×10^5 J/mol reported by Ohshita and Hosoi.[40] The desorption of $SiCl_2$ and HCl may take place simultaneously since the surface reactions in $SiHCl_3$-H_2 and SiH_2Cl_2-H_2 system are considered to be the same after the chemisorption of $SiCl_2$.

The calculated growth rates using equations (5-35) and (5-36) in two dimensional coordinates are shown in Fig. 5-3 by the solid lines. Furthermore, the three dimensional calculations are additionally performed by introducing the equations (5-32),(5-35) and (5-36) into the calculation model discussed in Chapter 4. The growth rates obtained by the three dimensional calculations are found to be overlapped with those measured and by the two dimensional calculations as shown in Fig. 5-3. The measured growth rates are explained well by the calculated growth rates. It follows that the transport and epitaxy model developed here can describe the surface reaction processes incorporating the transport phenomena in the reactor.

5.5.4 *Evaluation of HCl etching effect on silicon epitaxial growth rate*

The by-product produced by the decomposition of $SiHCl_3$ and $SiCl_2$, HCl molecules, can etch the silicon surface as[12]

$$Si + 2HCl \rightarrow SiCl_2 + H_2. \qquad (5\text{-}37)$$

In an $SiCl_4$-H_2 system, the epitaxial growth rate have its maximum with respect to temperature and $SiHCl_3$ concentration. This phenomenon is attributed to the etching reaction by the HCl by-product.[41] The $SiHCl_3$-H_2 system also has the maximum epitaxial growth rate[42,43] in a temperature range above 1493 K or 1500 K. This phenomena is thought to be caused by decrease in the total amount of chemisorbed $SiHCl_3$ at that temperature range.[43] These phenomena are found above 1473 K, but such a high temperature is not used in recent silicon epitaxial growth processes. Dis-

cussion in Chapter 3 showed that a growth rate calculation ignoring etching by HCl could reproduce the measured growth rate qualitatively. It has been clearly shown in Fig. 5-4 that there is a linear relationship between $1/k$ and [$SiHCl_3$], which means that equation (5-30) is sufficient to describe the growth in the $SiHCl_3$-H_2 system. The etching of silicon surface by HCl can therefore be ignored in the calculation of epitaxial growth rate under the conditions of this study.

5.5.5 *State of surface during epitaxial growth*

The state of the surface during the epitaxial growth is discussed further. The discussion in this Chapter has shown that the non-linear dependence of the growth rate on the reactant concentration can be described by considering both the chemisorption and decomposition.

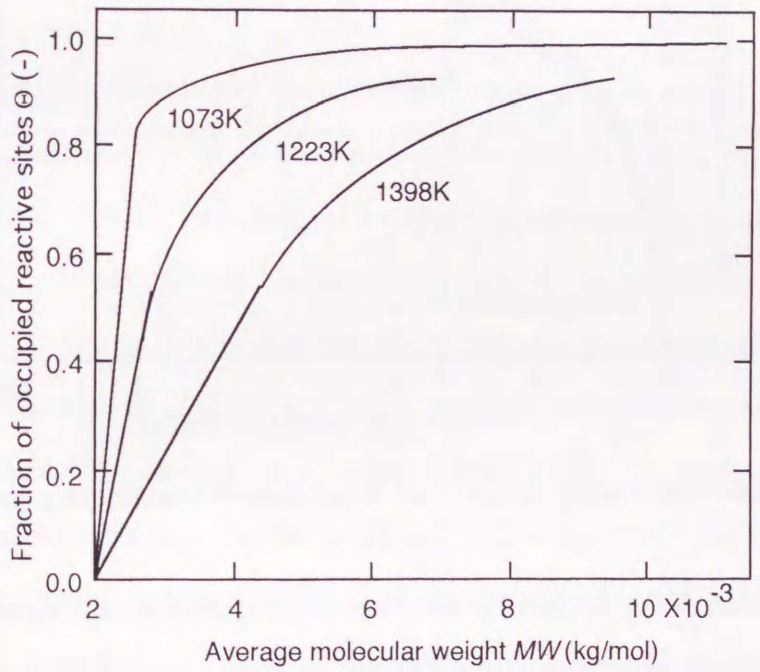

Fig.5-6 Fraction of occupied reaction sites, Θ, at substrate surface at 1073, 1223 and 1398 K.

The substrate surface is covered with the chemisorbed species, *$SiCl_2$. The fraction of occupied reactive sites, Θ, is obtained from equation (5-23) using equations (5-35) and (5-36). Figure 5-6 shows the state of the chemisorbed surface during the epitaxial growth. At 1073 K, nearly all reactive sites are occupied by *$SiCl_2$ even at a very low average molecular weight of mixed gases, MW. With increasing the growth temperature, Θ tends to decrease, but over 80% of the reactive sites at the substrate surface are covered with *$SiCl_2$ even at 1398 K and MW of 6.7. This means that large portion of the reactive sites is chemisorbed by *$SiCl_2$ under both the transport and reaction limited conditions used in industrial processes.

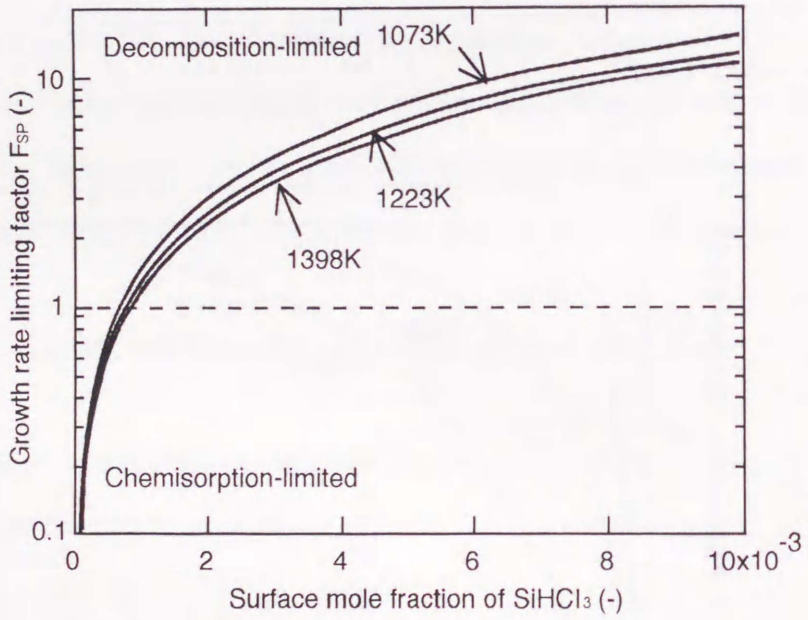

Fig.5-7 Growth rate limiting factor, F_{SP}, at substrate surface during epitaxial growth.

It is also interesting to identify the rate limiting process at the substrate surface. By considering a balance between the growth rates limited by the chemisorption (equation (5-33)) and the that by the decomposition (equation (5-34)), the surface process limiting factor, F_{SP}, is defined here as follows:

$$F_{SP} = \frac{k_{ad}[SiHCl_3]}{k_r[H_2]}. \tag{5-38}$$

F_{SP} is larger than one when the decomposition is the rate limiting process, while it is smaller than one when the chemisorption is the rate limiting process. Figure 5-7 shows the variation of the growth rate limiting factor, F_{SP}, as a function of the surface mole fraction of $SiHCl_3$. With increasing the growth temperature, F_{SP} tends to decrease, that is, the growth rate is limited more by the chemisorption.

Although the physisorption process does not appear in the description of the epitaxial growth rate, the physisorption is thought to be important for the quality of the film because physisorbed reactants migrate and diffuse on the substrate surface. Since the chemisorbed species can hardly migrate on the surface, the physisorbed reactant species should migrate to appropriate sites where silicon atoms should be incorporated. It is considered that this phenomenon makes it possible to obtain good quality films even under the reaction limited condition.

5.5.6 *Non-linear increase in epitaxial growth rate*

Here, it is again considered why the silicon epitaxial growth rate changes non-linearly with the increase in the MW. As mentioned in Chapter 3, the transport phenomena are important. Especially, all physical constants, for example, heat capacity, viscosity, diffusivity and thermal diffusivity, change with the temprature and the MW in gas phase. The reactor for silicon epitaxial growth usually employs temperature environment of *cold wall* where the substrate and the susceptor have the highest temperature, thus, the gas temperature decreases with the distance from the substrate and susceptor surface. As shown in Fig. 5-8, the increase in the MW causes the increase in heat capacity of gas mixture and thermal diffusivity. Since larger heat capacity requires more heat to raise the temperature of gases, the gas temperature decreases with increasing the MW. This leads to the increase in the temperatute gradient in gas phase, since the temperature of the substrate surface is controlled to keep constant by using the heating and the temperature-monitoring system of the epitaxial reactor. Furthermore, diffusivity and many other physical constants

of gas mixture dectrease due to low gas temperature. Although the decrease in the gas temperature lower the thermal difusivity, totally, the flux due to thermal diffusion increases. The changes in transport phenomena are a part of the non-linear change in the epitaxial growth rate, however, these are not sufficient as described in Chapter 3. The most important reason should be ascribed to the surface coverage by the source species at the substrate. When the substrate surface is covered completely by the source species as discussed in this Chapter, the reaction rate at the surface, that is, the epitaxial growth rate, saturates and cannnot increase any more. This behavior is observed especially at the low substrate temperature. As discussed above, the mechanism of the non-linear increase in the silicon epitaxial growth rate is composed of the change in transport phenomena and in surface chemical process. Here, the former is minor and the latter is major.

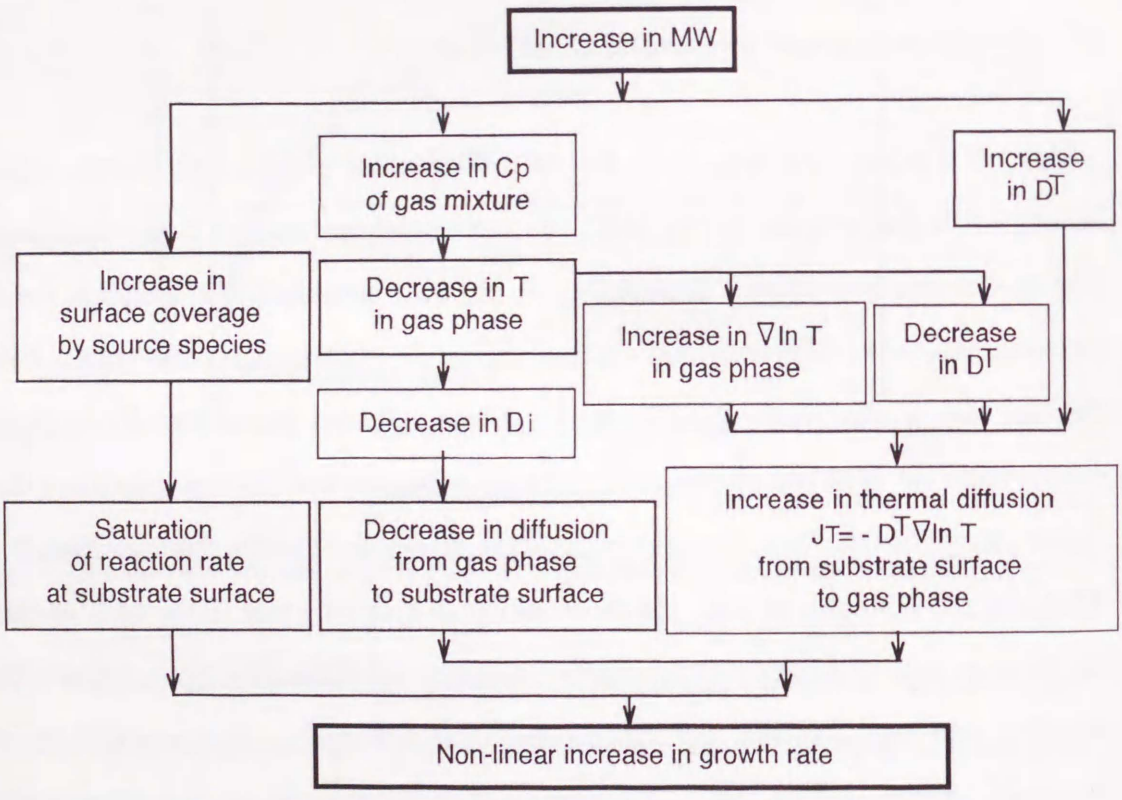

Fig.5-8 Mechanism for non-linear dependence of epitaxial growth rate on source species concentration in $SiHCl_3$-H_2 system.

5.6 Summary

The transport and epitaxy model in the $SiHCl_3$-H_2 system have been developed and evaluated experimentally and theoretically. The growth rate influenced by the transport phenomena in the reactor and chemical reactions at the surface has been described following the Eley-Rideal model. The entire processes of the silicon epitaxial growth in the $SiHCl_3$-H_2 system have been assumed to be composed of five processes in the model, that is, (a) transport, (b) physisorption, (c) migration or diffusion, (d) chemisorption, (e) decomposition of chemisorbed species and desorption of by-products. The surface reaction processes determining the growth rate consist of the chemisorption of $SiHCl_3$ and the decomposition of the chemisorbed species, $^*SiCl_2$, which reacts with H_2 in the gas phase to produce silicon atoms and HCl molecules. By using the rate process theory, the transport and epitaxy model has been verified to be an effective method which can estimate the rate constants of the chemisorption and decomposition accounting for the transport phenomena in the reactor. The physisorption is also important for the film quality because it enables $^*SiCl_2$ to migrate appropriately on the surface, which results in excellent epitaxial films under industrial epitaxial growth conditions. Since the epitaxial growth of silicon films are usually performed below 1473 K, the etching effect due to the by-product, HCl, on the growth rate can be neglected.

Nomenclature

a : density of reactive sites $(\mathrm{mol\,m^{-2}})$

C_p : heat capacity at constant pressure $(\mathrm{J\,kg^{-1}\,K^{-1}})$

D_i : binary diffusion coefficient of species i in H_2 $(\mathrm{m^2\,s^{-1}})$

D_i^T : thermal diffusion coefficient of species i in H_2 $(\mathrm{kg\,m^{-1}\,s^{-1}})$

F_SP : surface process limiting factor (-)

g : acceleration due to gravity $(\mathrm{m\,s^{-2}})$

h_s : distance from substrate surface (m)

$[i]$: mole concentration of species i at substrate surface $(\mathrm{mol\,m^{-3}})$

j_C : diffusion flux driven by concentration gradient $(\mathrm{kg\,m^{-2}\,s^{-1}})$

j_T : diffusion flux driven by temperature gradient $(\mathrm{kg\,m^{-2}\,s^{-1}})$

k : overall rate constant $(\mathrm{m^4\,mol^{-1}\,s^{-1}})$

k'_ad : chemisorption rate constant per unit mole concentration of reactive site $(\mathrm{m^3\,mol^{-1}\,s^{-1}})$

k_ad : $k'_\mathrm{ad} \times a$ $(\mathrm{m\,s^{-1}})$

k'_de : desorption rate constant per unit mole concentration of reactive site $(\mathrm{m^3\,mol^{-1}\,s^{-1}})$

k_de : $k'_\mathrm{de} \times a$ $(\mathrm{m\,s^{-1}})$

k'_e : etching rate constant per unit mole concentration of reactive site $(\mathrm{m^{3n}\,mol^{-n}\,s^{-1}})$

k_e : $k'_\mathrm{e} \times a$ $(\mathrm{m^{3n-2}\,mol^{1-n}\,s^{-1}})$

k'_r : reaction rate constant per unit mole concentration of reactive site $(\mathrm{m^3\,mol^{-1}\,s^{-1}})$

k_r : $k'_\mathrm{r} \times a$ $(\mathrm{m\,s^{-1}})$

M_av: average molecular weight of gas mixture $(\mathrm{kg\,mol^{-1}})$

M_Si: molecular weight of Si $(\mathrm{kg\,mol^{-1}})$

M_i: molecular weight of species i $(\mathrm{kg\,mol^{-1}})$

MW: average molecular weight of gas mixture at reactor inlet $(\mathrm{kg\,mol^{-1}})$

n : an order of etching reaction (-)

p : pressure (Pa)

R : gas constant $(\mathrm{J\,mol^{-1}\,K^{-1}})$

R_i : mass rate of change in species i by chemical reaction $(\mathrm{kg\,m^{-2}\,s^{-1}})$

R_{Si} : mass rate of change in Si by chemical reaction $(\mathrm{kg\,m^{-2}\,s^{-1}})$

T : temperature (K)

u : fluid velocity in x-direction $(\mathrm{m\,s^{-1}})$

v : fluid velocity in y-direction $(\mathrm{m\,s^{-1}})$

V : growth rate $(\mathrm{mol\,m^{-2}\,s^{-1}})$

V_{ad} : chemisorption rate of $SiHCl_3$ $(\mathrm{mol\,m^{-2}\,s^{-1}})$

V_{de} : desorption rate of $SiHCl_3$ $(\mathrm{mol\,m^{-2}\,s^{-1}})$

V_{e} : etching rate of Si surface $(\mathrm{mol\,m^{-2}\,s^{-1}})$

V_{G} : growth rate $(\mu\mathrm{m\,min^{-1}})$

V_{r} : decomposition rate to produce Si $(\mathrm{mol\,m^{-2}\,s^{-1}})$

x : coordinate in horizontal direction (m)

x_i : mole fraction of species i (-)

y : coordinate in vertical direction (m)

α_i : thermal diffusion factor of species i (-)

λ : thermal conductivity of gas mixture $(\mathrm{W\,m^{-1}\,K^{-1}})$

μ : viscosity of gas mixture (Pa·s)

ν_i : molar stoichiometry coefficient for species i in chemical reaction (-)

Θ : fraction of reaction sites by adsorbed molecules (-)

ρ : density of gas mixture $(\mathrm{kg\,m^{-3}})$

ρ_{Si} : density of Si $(\mathrm{kg\,m^{-3}})$

ω_i : mass fraction of species i (-)

$*$: chemisorbed state.

References

[1] *FLUENT User's Manual, Ver. 3.0* (Fluent Inc., Hanover, 1990).

[2] *Kagaku Binran* (Handbook of Chemistry) (Iwanami, Tokyo, 1984) 3rd ed., Chap. 6, p. II-39 [in Japanese].

[3] *Kagaku Binran* (Handbook of Chemistry) (Iwanami, Tokyo, 1984) 3rd ed., Chap. 6, p. II-71 [in Japanese].

[4] *Kagaku Binran* (Handbook of Chemistry) (Iwanami, Tokyo, 1984) 3rd ed., Chap. 9, p. II-239 [in Japanese].

[5] P. Pollard and J. Newman: *J. Electrochem. Soc.*, **127**, 744 (1980).

[6] R.C.Reid, J.M.Prausnitz and B.E.Poling: *The Properties of Gases and Liquids* (McGraw-Hill, New York, 1987) 4th ed.

[7] W. L. Holstein: *J. Electrochem. Soc.*, **135**, 1788 (1988).

[8] T. Aoyama, Y. Inoue and T. Suzuki, *J. Electrochem. Soc.*, **130**, 2103 (1983).

[9] J. Nishizawa and H. Nihira, *J. Crystal Growth*, **45**, 82 (1978).

[10] A. A. Chernov and M. P. Rusaikin, *J. Cryst. Growth*, **45**, 73 (1978).

[11] E. Sirtl, L. P. Hunt and D. H. Sawyer, *J. Electrochem. Soc.*, **121**, 919 (1974).

[12] P. van der Putte, L. J. Giling and J. Bloem, *J. Cryst. Growth*, **41**, 133 (1977).

[13] R. F. Lever, *IBM J. Res. Dev.*, **8**, 460 (1964).

[14] M. Nakagawa, *Kogyo Kagaku Zasshi*, **62**, 177 (1959).

[15] J. Nishizawa and M. Saito, *J. Cryst. Growth*, **52**, 213 (1981).

[16] V. S. Ban and S. L. Gilbert, *J. Electrochem. Soc.*, **122**, 1382 (1975).

[17] V. S. Ban, *J. Electrochem. Soc.*, **122**, 1389 (1975).

[18] Y. Sato, T. Tamura and T. Ohmine: *Extended Abstracts 1992 Int. Conf. Solid State Devices and Materials*, 20 (1992).

[19] M. Copel and R. M. Tromp, *Phys. Rev. Lett.*, **72**, 1236 (1994).

[20] Y. J. Chabal and K. Raghavchari, *Phys. Rev. Lett.*, **53**, 282 (1984).

[21] F.Hirose, M.Suemitsu and N.Miyamoto, *Jpn. J. Appl. Phys.*, **29**, L1881 (1990).

[22] M. P. D'evelyn, M. M. Nelson and T. Engel, *Surf. Sci.*, **186**, 75 (1987).

[23] T. Urisu, J. Takahashi, Y. Utsumi, T. Akutsu and K. Kuchitsu, *J. Electrochem. Soc.*, **141**, 1562 (1994).

[24] Y. Takahashi and T. Urisu, *Jpn. J. Appl. Phys.*, **30**, L209 (1991).

[25] P. Hirva and T. A. Pakkanen, *Surf. Sci.*, **220**, 137 (1989).

[26] L. J. Whitman, S. A. Joyce, J. A. Yarmoff, F. R. McFreely, and L. J. Terminello, *Surf. Sci.*, **232**, 297 (1990).

[27] A. Zangwill, *Physics at Surfaces* (Cambridge Univ. Press, Cambridge, 1988) Chap.8, p188.

[28] A. Sasaki, *J. Jpn. Assoc. Cryst. Growth*, **20**, 321 (1993).

[29] W. A. Tiller, *The Science of Crystallization:Microscopic interfacial phenomena* (Cambridge University Press, Cambridge, 1991) Chap.5, p209.

[30] W. A. Tiller, *The Science of Crystallization:Microscopic interfacial phenomena* (Cambridge University Press, Cambridge, 1991) Chap.5, p191.

[31] Q. Gao, Z. Dohnalek, C. C. Cheng, W. J. Choyke and J. T. Yates, Jr., *Surf. Sci.*, **302**, 1 (1994).

[32] A. C. Dillon, M. L. Wise, M. B. Robinson and S. M. George, *J. Vac. Sci. Technol.*, **A 13**, 1 (1995).

[33] D. D. Eley and E. K. Rideal, *Proc. Roy. Soc. (London)*, **A178**, 429 (1941).

[34] I. Langmuir, *Trans. Faraday Soc.*, **17**, 621 (1921).

[35] M. Kato, J. Murota and S. Ono, *J. Crystal Growth*, **115**, 117 (1991).

[36] K.Yamabe and K.Taniguchi, *IEEE Trans.Electron Devices*, **ED-32**, 423 (1985).

[37] T.O.Sedgwick, M.Berkenblit and T.S.Kuan, *Appl. Phys. Lett.*, **54**, 2689 (1989).

[38] T. O. Sedgwick, P. D. Agnello, M. Berkenlit and T. S. Kuan, *J. Electrochem. Soc.*, **138**, 3042 (1991).

[39] Y. Ohshita, A. Ishitani and T. Takada, *J. Crystal Growth*, **108**, 499 (1991).

[40] Y. Ohshita and N. Hosoi, *J. Cryst. Growth*, **131**, 495 (1993).

[41] W. A. Tiller, *The Science of Crystallization:Microscopic interfacial phenomena* (Cambridge University Press, Cambridge, 1991) Chap.5, p202.

[42] S. E. Bradshaw, *Int. J. Electronics*, **21**, 205 (1966).

[43] J. M. Charig and B. A. Joyce, *J. Electrochem. Soc.*, **109**, 957 (1962).

Chapter 6

Effect of Transport Phenomena on Boron Concentration Profiles in Silicon Epitaxial Wafers

6.1 Introduction

In this chapter, the boron concentration profile in silicon epitaxial wafers grown under atmospheric pressure in a single-wafer horizontal reactor and a pancake reactor is studied, since boron is the most important dopant for MOS devices. From the discussion of solid-state diffusion and the relationship between autodoping and main gas stream in the reactor, it is shown that the large recirculation of gas in the epitaxial reactor greatly enhances autodoping.

6.2 Basic equations for solid-state diffusion

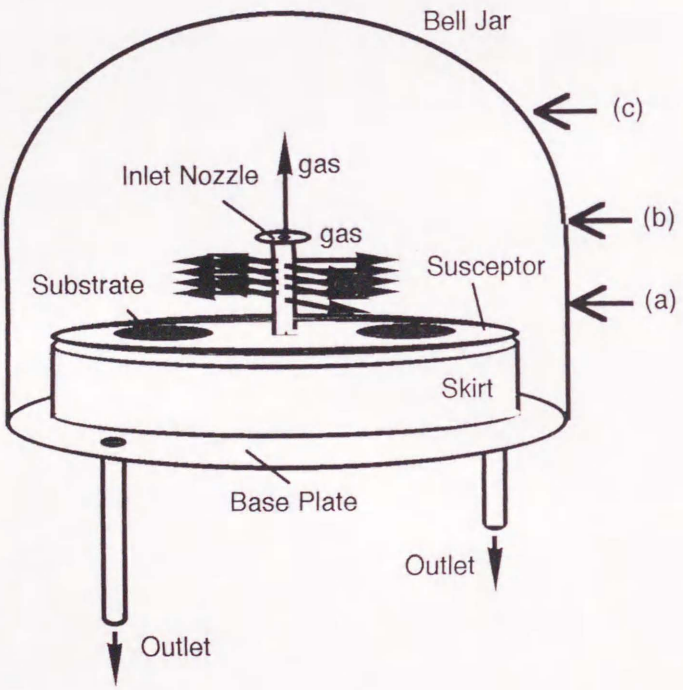

Fig.6-1 Pancake reactor for preparation of silicon film. (a), (b) and (c) show the heights of horizontal planes of 20, 70 and 130 mm, respectively, from the susceptor and the substrates, where gas flow motion is visualized under a sheet of laser light from the near to the far side of the reactor chamber.

To improve the accuracy of evaluation of solid-state diffusion in an epitaxial wafer,

the diffusivity of boron atoms in p-type (100) silicon single crystals is evaluated from boron concentration profiles formed due to out-diffusion through heating in a hydrogen ambient at 1173, 1273 or 1373 K for 60 min in the pancake reactor shown in Fig. 6-1. Using the boron diffusivity obtained, the boron concentration profiles in the epitaxial wafers are calculated.

Equation and boundary conditions used for calculations of solid-state diffusion are shown schematically in Fig. 6-2. Conservation of boron atoms is described by the following equation:

$$\frac{\partial C}{\partial t} = \frac{\partial}{\partial x}\left(D\frac{\partial C}{\partial x}\right), \tag{6-1}$$

where C is boron concentration (m^{-3}) and D is the diffusivity (m^2/s) of boron atoms in a silicon crystal. In the calculation of out-diffused boron concentration profile, the following boundary conditions are imposed on the substrate surface using an evaporation coefficient h (m/s) as shown in Fig. 6-2 (a),

$$D\left(\frac{\partial C}{\partial x}\right)_{\text{surface}} = h(C_{\text{s}} - C_{\text{g}}), \tag{6-2}$$

where C_{s} and C_{g} are the concentrations of boron atoms (m^{-3}) on the substrate surface and in the gas phase, respectively. Additionally, a boundary condition is imposed wherein the boron concentration at an infinite depth from the surface at time t, $C_{\infty,t=t}$, keeps its initial value.

$$C_{\infty,t=t} = C_{\infty,t=0} \tag{6-3}$$

For the calculation of boron concentration in the epitaxial wafer, the boron concentration at a position in the epitaxial film sufficiently far from the interface between the epitaxial film and the substrate at time t, $C_{-\infty,t=t}$, is fixed to the value measured by secondary ion mass spectrometry (SIMS), C_{obs}, as shown in Fig. 6-2 (b).

$$C_{-\infty,t=t} = C_{\text{obs}} \tag{6-4}$$

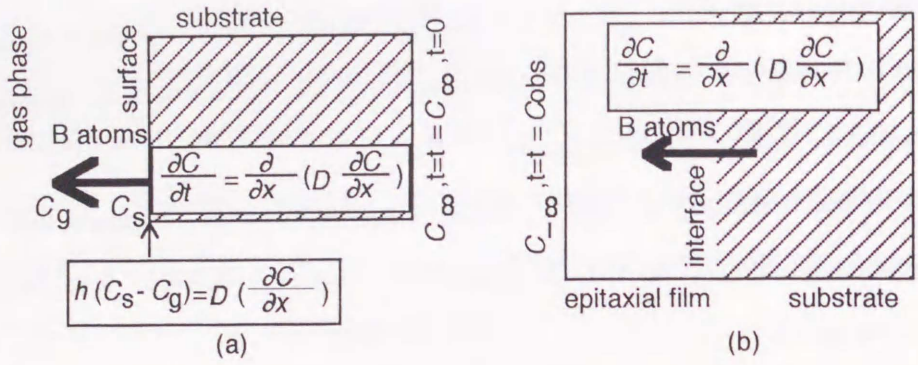

Fig.6-2 Equation and boundary conditions for calculations of solid-state diffusion. (a) is for a heat treatment and a prebaking process; (b) is for an epitaxial growth process.

Although equation (6-1) can be analytically solved for evaporation and diffusion from the substrate to the epitaxial layer individually, the epitaxial growth must be performed immediately after the prebaking process in which remove a native oxide film of the substrate surface. Since boron atoms are evaporated during the prebaking process, the initial boron concentration profile for the epitaxial growth shows rather a gradual shape. Diffusion equation with such an initial condition can be solved only numericaly, therefore, equation (6-1) is discretized into finite difference formulae. The calculation domain is divided into 300 nonuniform meshes for the evaluation of diffusivity and 500 nonuniform meshes for the calculation of boron concentration profile in the epitaxial wafers. The mesh widths are less than 1×10^{-8} m.

The diffusivity of boron in a silicon wafer is assumed to be independent of boron concentration since the diffusivity is essentially constant at low boron concentrations ($<10^{25}\,\mathrm{m}^{-3}$).[1] The diffusivity of boron, D, and the evaporation coefficient, h, are determined so that the calculated boron concentration profiles agree with the measured ones.

6.3 Preparation of epitaxial silicon thin-film

To compare the effects of various transport phenomena in an epitaxial reactor on the dopant profiles, two kinds of epitaxial reactors were used to prepare epitaxial silicon thin-films.

Epitaxial silicon thin-films were grown in the single-wafer horizontal reactor shown in Fig. 6-3, which transport phenomena and reaction chemistry were discussed in Chapter 3 and Chapter 5. This reactor has streamlines that are parallel to the substrate without formation of a vortex above the substrate. A mixture of $SiHCl_3$ and H_2 is introduced into the reactor for reaction at the surface of a boron-doped (100) 8-inch-diameter substrate held horizontally in the reactor at 1073, 1273 or 1373 K for 120–1200 s after prebaked in a hydrogen ambient at 1463 K for 90 s for removing a native oxide film of the substrate surface.

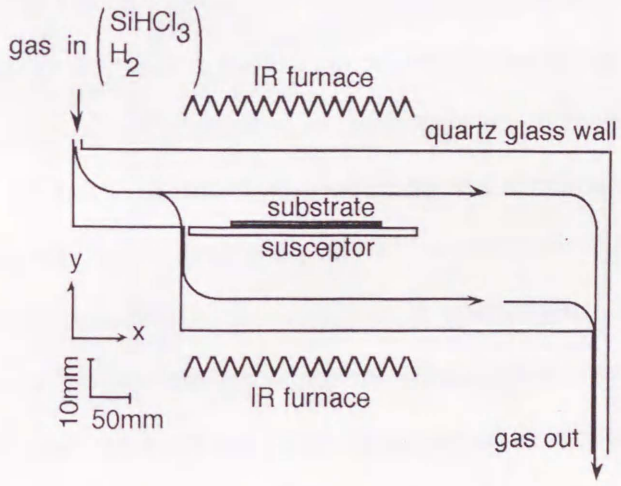

Fig.6-3 Single-wafer horizontal reactor for preparation of silicon film and for numerical calculations of transport phenomena.

Using the pancake reactor in Fig. 6-1, epitaxial silicon thin-films were also grown on boron-doped (100) 4-inch-diameter substrates. The epitaxial films were grown at 1273 and 1398 K for 300–480 s after prebaked in a hydrogen ambient at 1273 K for 240 s and 1398 K for 60 s, respectively.

A mixture of $SiHCl_3$ and H_2 was introduced from the inlet nozzle located at the center of the susceptor to four horizontal directions of the reactor chamber.

Boron concentration in the substrates was $4\text{–}6\times10^{24}\,m^{-3}$, and their back surfaces were covered with 500 nm-thick SiO_2 film since this effectively suppresses autodoping.[2-4] Thicknesses of the epitaxially grown films were measured using interference fringes in Fourier-transform infrared spectra. The concentration profiles of boron atoms were measured by SIMS using CAMECA model IMS-4f. The influence of autodoping was evaluated from the difference between the boron concentration profiles measured by SIMS and those calculated by equations (6-1),(6-3) and (6-4) of the solid-state diffusion.

6.4 Analysis of gas flow

To study the transport phenomena, the gas flow patterns in the single-wafer horizontal reactor in Fig. 6-3 and the pancake reactor in Fig. 6-1 were analyzed. Since the quartz chamber of the single-wafer horizontal reactor is completely surrounded by a heating lamp module, no visualization technique[5] could be applied. Therefore, the gas flow pattern analysis was performed by calculating transport equations with appropriate boundary conditions. In the pancake reactor, the numerical calculation required much computation time due to the three-dimensional nature of the transport phenomena. Fortunately the reactor chamber of the pancake reactor is equipped with a window at its side wall, thus the gas flow visualization technique[6] could be applied in this case. Therefore, gas flow at room temperature was visualized using small NH_4Cl particles which trace the motion of gas mixtures of $SiHCl_3$-H_2 at epitaxial growth temperatures. Motion of the tracer particles was illuminated under a horizontally spread sheet of Ar^+ (4 W) laser light in the horizontal planes at distances of (a) 20, (b) 70 and (c) 130 mm from the susceptor shown in Fig.6-1.

6.5 Results and discussion

6.5.1 *Boron Diffusivity*

Figure 6-4 shows boron concentration profiles measured by SIMS as a function of depth from the surface after heating in a hydrogen ambient for 60 min. Triangles, squares and circles denote the measured profiles at temperatures of 1173, 1273 and 1373 K, respectively. Although boron atom concentrations do not change at infinite depths, they exponentially decrease with decreasing depth from the substrate surface. The boron atom concentration near the surface decreases with increasing temperature.

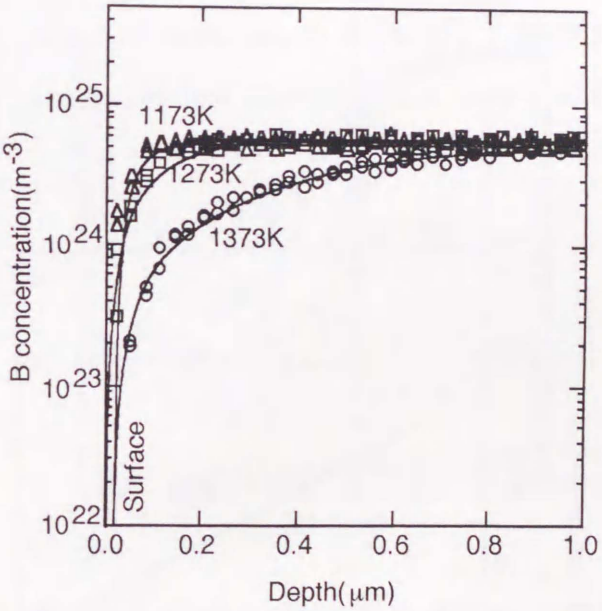

Fig.6-4 Boron concentration profiles after heating in a hydrogen ambient for 60 min. Triangles, squares and circles denote measured profiles at temperatures of 1173, 1273 and 1373 K, respectively. Solid lines represent calculated boron concentrations under the same conditions of temperature.

To evaluate boron diffusivity, equation (6-1) is solved numerically using the boundary conditions of equations (6-2) and (6-3). The diffusivity is determined so that

the calculated boron concentration profile near the substrate surface agrees with the measured one. The solid lines in Fig. 6-4 show the calculated boron concentration profiles which agree well with the measured profiles. From these calculations, boron diffusivity in a p-type silicon single crystal is

$$D = 1.22 \times 10^{-5} \exp \frac{-3.65 \times 10^4}{T} \ \mathrm{m^2/s}, \tag{6-5}$$

as shown in Fig. 6-5 as a function of reciprocal temperature (solid line). The diffusivity from equation (6-5) agrees well with the boron intrinsic diffusivity.[1,7-10] This also indicates that the anomalous diffusion[11] due to crystal imperfection can be ignored in the substrates used in this study. The evaporation coefficient, h, affected the boron concentration profile slightly only at positions near the surface; thus, for every temperature h was assumed to be 0.1 m/s, which was comparable to 0.3 m/s obtained by Grove et al.[12] The effect of gas phase turbulence on the evaporation coefficent can be ignored since the gas flows in both reactors are laminar as discussed later.

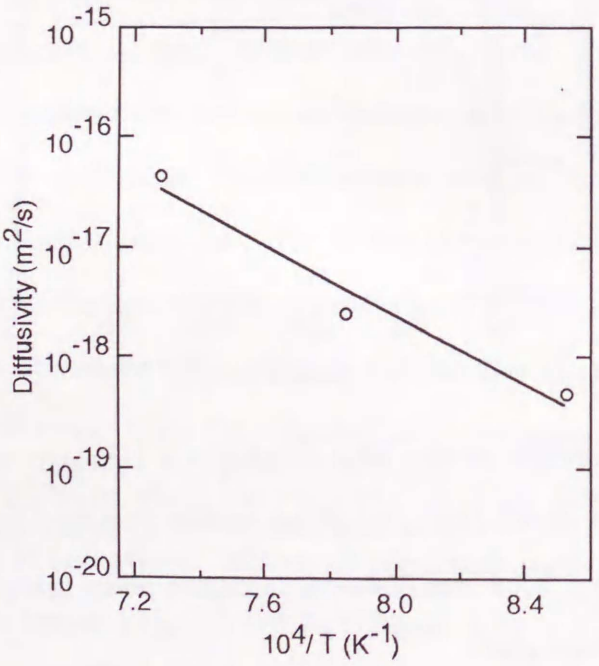

Fig.6-5 Boron diffusivity in p-type silicon single crystal as a function of reciprocal temperature.

Although the calculated profiles are slightly different from the measured ones near the substrate surface, the depths of boron diffusion under the heating temperatures are obtained accurately.

6.5.2 *Boron concentration profiles in epitaxial wafers*

Boron concentration profiles are calculated using equations (6-1)-(6-3) for the prebaking process and using equations (6-1), (6-3) and (6-4) for the epitaxial growth process. The evaporation of boron atoms at the substrate surface, equation (6-2), is ignored since the epitaxial growth is much faster than the diffusion of boron in silicon.

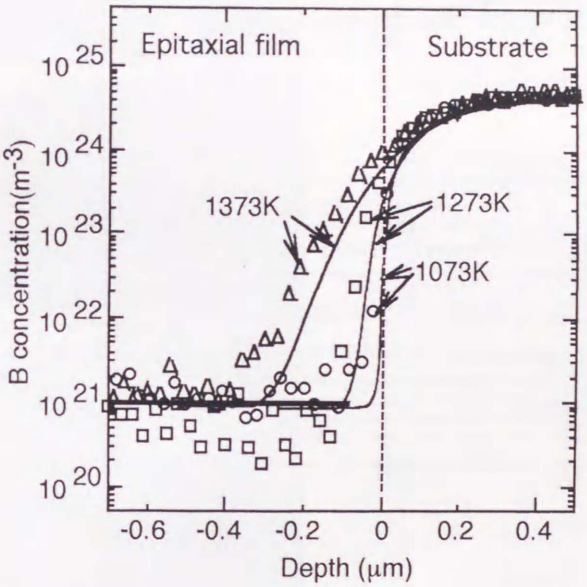

Fig.6-6 Measured and calculated boron concentration profiles around the interface between the substrate and the epitaxial film. Epitaxial films were grown in the single-wafer horizontal reactor at 1073 K for 1200 s, and at 1273 and 1373 K for 120 s.

Figure 6-6 shows boron concentration profiles around the interface between the substrate and epitaxial films which were grown in the single-wafer horizontal reactor at 1073 K for 1200 s, and at 1273 and 1373 K for 120 s. The change in boron concentration is gradual with increasing epitaxial growth temperature. Although

the boron concentration profile changes at depths of -0.4 to 0 μm at the growth temperature of 1373 K, those grown at 1273 and 1073 K change at depth of -0.1 to 0 μm.

The solid lines in Fig. 6-6 are calculated boron concentration profiles based on the solid-state diffusion of equation (6-1) using the boundary conditions of equations (6-3) and (6-4) and the diffusivity of equation (6-5), and show minimum change in the boron concentration profile due to the epitaxial growth process. The calculated profile for growth at 1373 K has a slight difference from the measured profile, which is ascribed to autodoping. For growth at 1273 and 1073 K, the calculated boron concentration profiles agree well with the measured ones. For epitaxial wafers grown in the single-wafer horizontal reactor at temperatures lower than 1273 K, the boron concentration profile is concluded to be due entirely to solid-state diffusion, and autodoping is negligible.

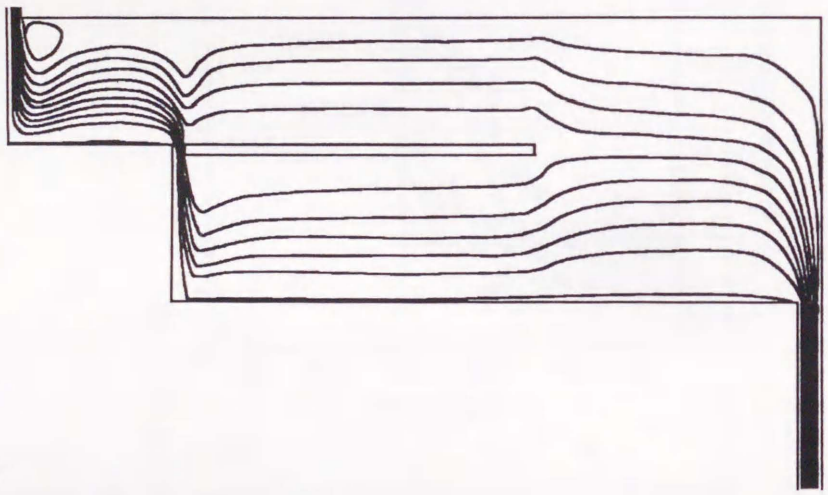

Fig.6-7 Calculated streamlines at 1373 K in the single-wafer horizontal reactor.

An analysis of the transport phenomena in the single-wafer horizontal reactor discussed in Chapter 3 shows that the laminar streamlines near and above the substrate are parallel to the substrate and show no vortex, as depicted in Fig. 6-7. In this figure, the calculated streamlines at 1373 K using the transport equations were the same as those calculated at 1273 and 1073 K. This gas stream transports boron

atoms vaporized from the substrate to the outlet. In this environment, the number of autodoped boron atoms in the epitaxial film is negligible. Since vaporization of boron atoms from the substrate is suppressed with decreasing epitaxial growth temperature, autodoping shows a negligible effect on the boron concentration profile at temperatures lower than 1273 K in the single-wafer horizontal reactor.

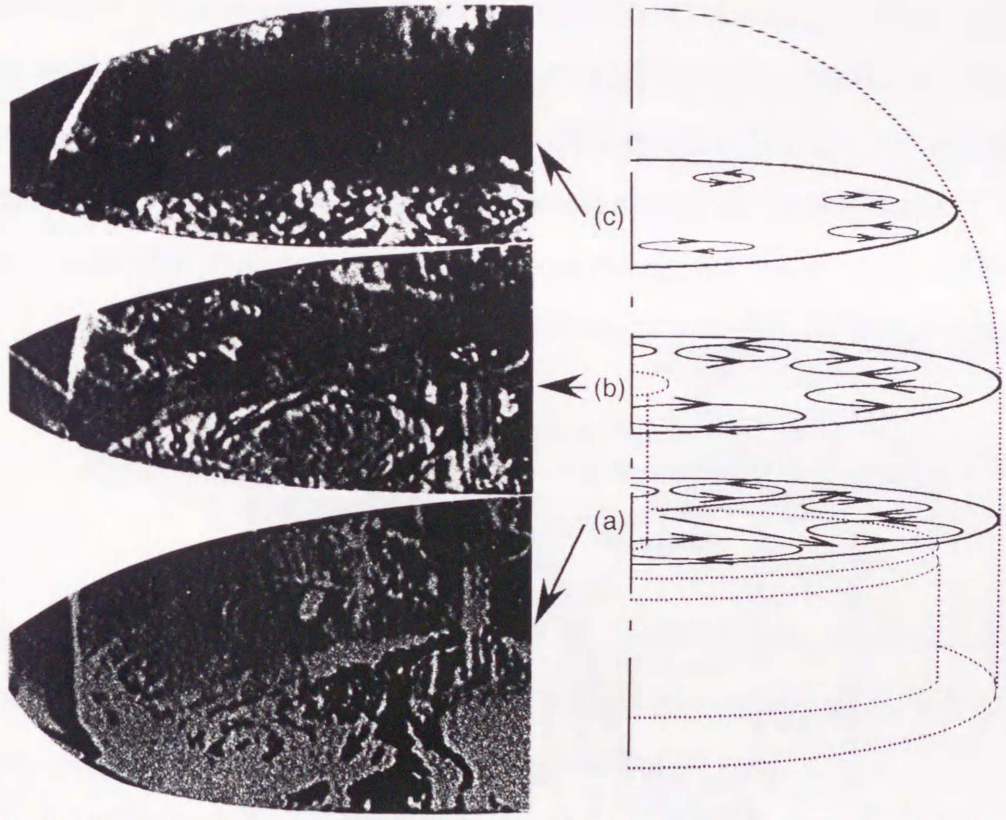

Fig.6-8 Visualized gas stream coming out of the inlet in the pancake reactor at room temperature in the horizontal plane at (a) 20, (b) 70 and (c) 130 mm from the substrate. Left half is a photograph of visualized gas flow and right half depicts gas motion using arrows. Dotted lines show the configuration of the pancake reactor.

To discuss the relationship between the boron concentration profile and the transport phenomena, the gas flow visualization technique[6] was applied to the pancake reactor in Fig. 6-1, by which epitaxial films were also grown. Figure 6-8 shows the

gas stream out of the inlet in the pancake reactor at room temperature. Gas motion is observed in the horizontal cross-sectional images at heights of 20, 70 and 130 mm from the substrates. The left half of Fig.6-8 is a photograph taken from the visualization and the right half depicts the gas flow patterns using arrows. Although gas motion at 130 mm is not clear, those at 20 and 70 mm show recirculating flows. Gases coming out of the small holes of the inlet tube flow directly to the chamber wall and return to the inlet at the center of the reactor to form the recirculating flows. These gas motions are not turbulent and are the same as those in a small pancake reactor observed by Suzuki et al.[13] Since the forced recirculations are dominant, it can be assumed that the gas flow pattern at the epitaxial growth temperatures is essentially the same as that at room temperature. Although the recirculating gas motion at the near side of the reactor is easily recognized as shown in Fig.6-8, the motions of the far side are not clearly shown because of the laser light intensity being weakened due to scattering by the tracer particles in the reactor.

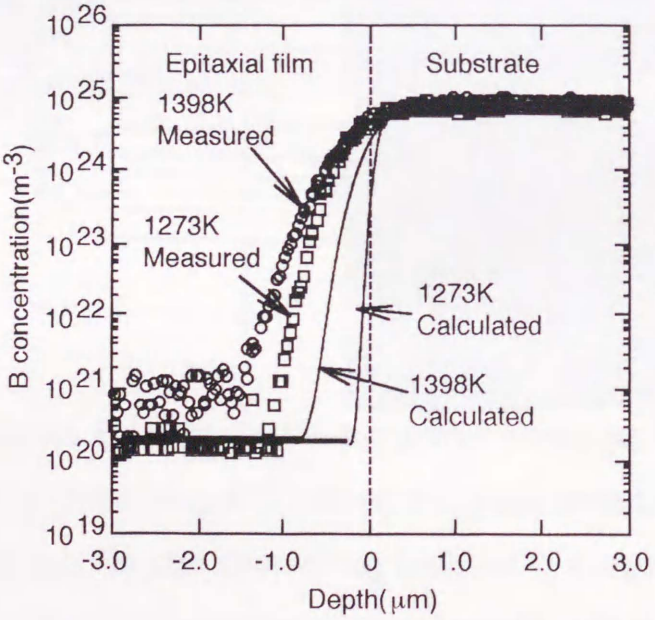

Fig.6-9 Measured and calculated boron concentration profiles around the interface between the substrate and the epitaxial film. Epitaxial films were grown in the pancake epitaxial reactor. Circles: prebaked at 1398 K for 60 s and grown at 1398 K for 300 s; squares: prebaked at 1273 K for 240 s and grown at 1273 K for 480 s.

The large amount of recirculation above the substrates transports both $SiHCl_3$ molecules and the vaporized boron dopant to the substrate surface. The difference in the gas stream between the two types of epitaxial reactors is considered to affect the boron concentration profiles in the epitaxial wafers. The epitaxial films were grown in the pancake reactor at 1273 or 1398 K, and the boron concentration profiles around the interface of the substrate and the epitaxial film were measured by SIMS and are represented by squares (1273 K) and circles (1398 K) in Fig. 6-9. The solid lines are the boron concentration profiles at 1273 and 1398 K obtained by the numerical calculations of the solid-state diffusion. Although the difference between the measured and the calculated boron concentration profiles obtained at 1273 K in the single-wafer horizontal reactor is very small, that at the same temperature in the pancake reactor is very large and can be ascribed to autodoping.

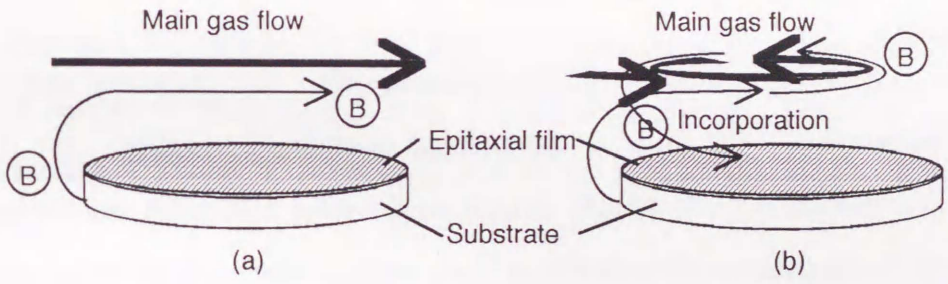

Fig.6-10 Schematinc view of the transport of boron atoms in gas phase. (a) is for the single-wafer horizontal epitaxial reactor without recirculation; (b) is for the pancake epitaxial reactor having large amounts of recirculation of gas.

A large amount of boron atoms is vaporized from the substrate at temperatures above 1273 K, the majority of which possibly come from the back surface of the substrate through the silicon oxide film. Although the vaporized boron atoms are transported from the substrate to the outlet in the single-wafer horizontal reactor, they are transported back to the substrate via the recirculating gas stream in the pancake reactor, as schematically shown in Fig. 6-10. An abrupt boron concentration profile can be formed in the epitaxial growth environment without the large

recirculating flows near and above the substrate because of the short gas residence time.[14, 15] The numerical calculation of the relationship between autodoping and the recirculation of gas is believed to be theoretically possible, where the calculation must be performed three-dimensionally in non-steady-state. Since such a calculation requires enormously long calculation time, the boron concentration profile due to autodoping is not calculated in this study.

In the single-wafer horizontal reactor, the substrate is usually rotated to obtain an uniform epitaxial film thickness; however, the rotation rate is usually less than 50 rpm and is considered to induce recirculating flow which is limited to the area in close proximity to the substrate. Therefore, the effect of autodoping is still minor in the single-wafer horizontal reactor using substrate rotation.

6.6 Conclusions

Boron concentration profiles in silicon epitaxial wafers were measured and studied with consideration of the transport phenomena in epitaxial reactors.

Epitaxial growth at 1073–1273 K using a single-wafer horizontal reactor leads to an abrupt boron concentration profile at the interface between the epitaxial film and the substrate, the back of which is covered with an SiO_2 film. In the single-wafer horizontal reactor, the boron concentration profile is formed predominantly by solid-state diffusion at temperatures lower than 1273 K even under atmospheric pressure because of negligible autodoping due to little or no recirculation of gas flow near and above the substrate. In a pancake reactor which has very large recirculating flows in its chamber, a gradual change in the boron concentration profile is observed due to autodoping. To obtain an abrupt boron concentration profile, large amounts of recirculation of gas in the epitaxial reactor should be avoided.

References

[1] R. B. Fair, *J. Electrochem. Soc.*, **122**, 800 (1975).

[2] B.A.Joyce, J.C.Weaver and D.J.Maule, *J.Electrochem.Soc.*, **112**, 1100 (1965).

[3] G. Skelley and A. C. Adams, *J. Electrochem. Soc.*, **120**, 116 (1973).

[4] W. H. Shepherd, *J. Electrochem. Soc.*, **115**, 652 (1968).

[5] W. J. Yang, *Handbook of Flow Visualization* (Hemisphere, New York, 1989).

[6] Chapter 2 in this thesis.

[7] *Rika Nenpyo (Chronological Scientific Tables)*, National Astronomical Observatory (ed.), Maruzen Co., Ltd., Tokyo, (1995) p. 450.

[8] K. Osada, Y. Zaitsu, S Matsumoto, M. Yoshida, E. Arai and T. Abe, *J. Electrochem. Soc.*, **142**, 202 (1995).

[9] A. D. Kurtz and R. Yee, *J. Appl. Phys.*, **31**, 303 (1960).

[10] C. S. Fuller and J. A. Ditzenberger, *J. Appl. Phys.*, **27**, 544 (1956).

[11] D.Kahng, C.O.Thomas and R.C.Manz, *J.Electrochem.Soc.*, **109**, 1106 (1962).

[12] A. S. Grove, A. Roder and T. Sah, *J. Appl. Phys.*, **36**, 802 (1965).

[13] T. Suzuki, Y. Inoue, T. Aoyama and M. Maki, *J. Electrochem. Soc.*, **132**, 1480 (1985).

[14] C. A. Wang, S. H. Groves, S. C. Palmateer, D. W. Weyburne and R. A. Brown, *J. Crystal Growth*, **77**, 136 (1986).

[15] D.I.Fotiadis, A.M.Kremer, D.R.McKenna and K.F.Jensen, *J. Crystal Growth*, **85**, 154 (1987).

Chapter 7

Roughness of Silicon Surface Heated in Hydrogen Ambient

7.1 Introduction

Native oxide film at the silicon substrate surface must be removed without surface roughening before the epitaxial growth process, which is usually performed at high temperatures in an hydrogen ambient. To realize a desirable heat treatment process, roughening of the silicon surface during the removal of the native oxide film at the temperatures lower than 1000 °C should be studied. Moreover, surface roughening under atmospheric pressure must be investigated because atmospheric-pressure epitaxy can be applied to improve cost performance in microelectric device fabrication. In spite of the importance of such research, the mechanism of surface roughening is still unfortunately unknown.

In this chapter, surface roughness under atmospheric pressure is discussed from the viewpoint of the etch rates of silicon and silicon dioxide by hydrogen gas, for the first time. It is shown that the competitive etching reactions of silicon and silicon dioxide with hydrogen gas play key roles in the formation of the pits on the silicon surface.

7.2 Experimental

Samples used were mainly 100-mm-diameter polished silicon wafers of *p*-type 0.01–0.02 Ωcm (100) which were cleaned by the RCA process.[1] Thickness of the native oxide films on the polished wafer surfaces was measured to be 1.0–1.5 nm using an ellipsometer (L115 B, Gaertner Scientific Corp.). To avoid incorporation of trace impurities of water or oxygen during heat treatment, a pancake-type epitaxial reactor (AEC-1620, Shimada Rika) and hydrogen gas with less than 1 ppm water content under atmospheric pressure were used because this combination can produce epitaxial wafers of excellent quality. The three heat treatment processes shown in Fig. 7-1 were adopted. In process (a), the wafers were heated at 900, 1000 and 1100 °C for 1–100 min. In process (b), the wafers were exposed to air for 24 h after the growth

of a 10μm silicon epitaxial film at 1125 °C, and were finally heated at 900, 1000 and 1100 °C for 30 min. In process (c), the wafers were heated at 1100 °C for 10 min and were additionally heated at 900 °C for 30 min without exposure to any ambient other than hydrogen. After these heat treatment processes, all wafers were cooled to below 350 °C in hydrogen ambient to obtain a silicon surface terminated by hydrogen atoms.[2] Thickness of the native oxide film was measured with the ellipsometer to estimate the removal of the native oxide films. Employing the same process, the etch rate of silicon dioxide film was estimated using native oxide films and thermal oxide films of about 30 nm thick. Roughness of each wafer surface was evaluated by a light scattering method (LS-6030, Hitachi Electronic Engineering). Surfaces of some wafers were further evaluated by atomic force microscopy (AFM) (Nanoscope II, Digital Instruments) to identify the surface roughness morphology.

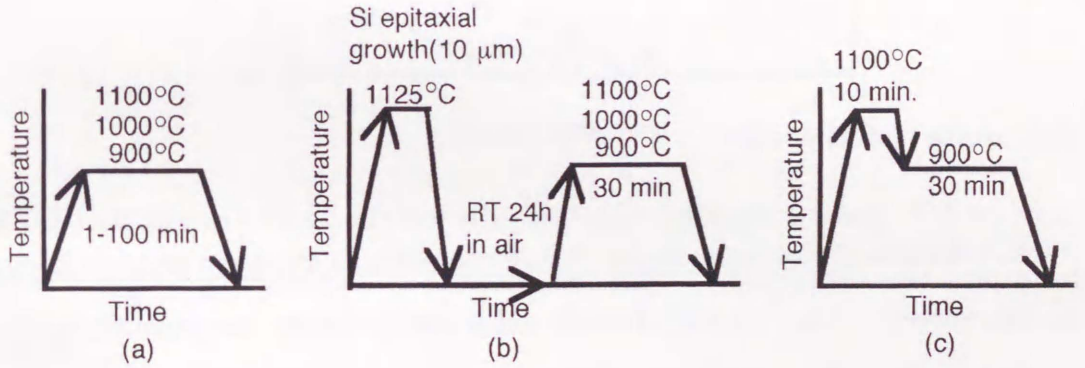

Fig.7-1 Heat treatment of silicon wafer in hydrogen ambient: (a) heated at 900, 1000 and 1100 °C for 1–100 min, (b) kept in air for 24 h after 10 μm silicon epitaxial film growth, and heated at 900 °C, 1000 °C and 1100 °C for 30 min, (c) heated at 1100 °C for 10 min and 900 °C for 30 min.

The etch rates of silicon surfaces due to their chemical reaction with hydrogen gas were estimated using the process shown in Fig. 7-2. Silicon wafer surfaces were oxidized in oxygen ambient containing water vapor at 1100 °C to produce silicon dioxide films of 500 nm thick. Some portion of the silicon dioxide film on the

wafer was removed using the patterning process.[3] Next, these wafers were heated in hydrogen ambient for 60 min. After these heat treatment processes, the silicon dioxide films were removed using HF aqueous solution, and finally a step appeared at the boundary between the area etched by hydrogen gas and that covered with silicon dioxide film. The step height was measured mechanically (α-step, TENCOR Instruments).

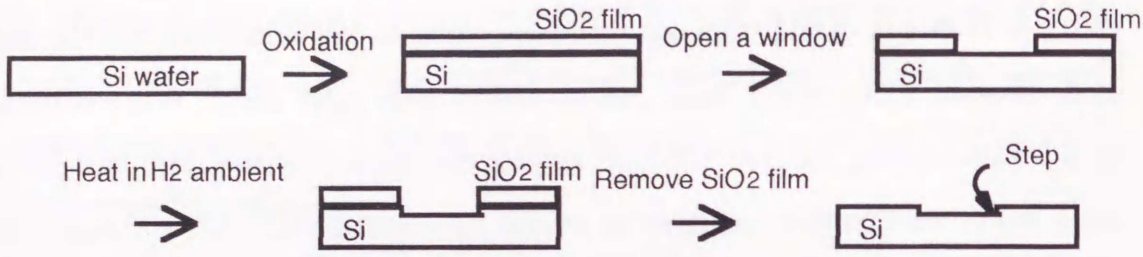

Fig.7-2 Process to estimate the etch rates of silicon surface by hydrogen gas.

7.3 Results and discussion

First, thickness of the native oxide film after heating in hydrogen ambient is measured as shown in Fig. 7-3, as a function of heating time to recognize the surface situation quickly. The conditions of the heating time at 1000 and 1100 °C in Fig. 7-3 were chosen empirically considering the minimum prebaking time to obtain good surfaces of epitaxial films in the epitaxial growth process. At 1100 °C, the native oxide film was easily removed within 1 min. At lower temperatures, removal of the native oxide film became more difficult; they were removed within 4 min at 1000 °C, but removal took more than 10 min at 900 °C. The measured oxide thickness in Fig. 7-3 not being reduced to zero after heating long time is attributable to a measurement error.

After heat treatment in hydrogen ambient, the native oxide films recovered their original thickness when left to stand in air for about 2 weeks.

Some of the wafer surfaces show an intense haze after heating in hydrogen ambient. Figure 7-4 shows haze intensity of the silicon surface as a function of heating temperature in hydrogen ambient, the values of which were measured at a photomultiple threshold voltage (PMTHV) of 450 V. Haze of the silicon surfaces heated for 60 min intensifies with decreasing heating temperature, as shown by the triangles in Fig. 7-4(a). To confirm this trend, haze intensity after heated at 800 °C for 30 min was additionally observed to be near 200 bit.

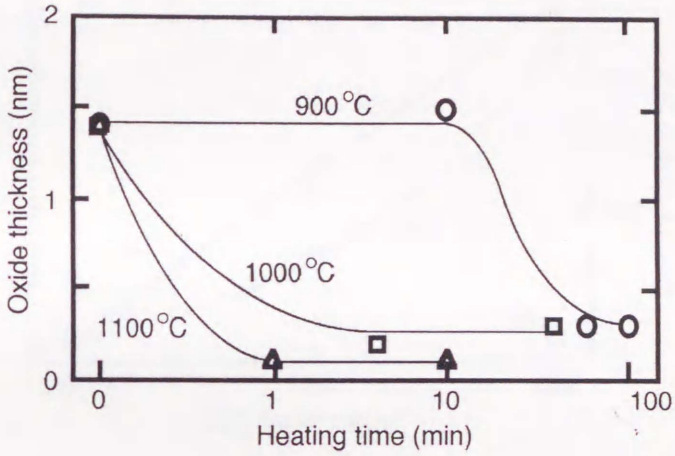

Fig.7-3 Thickness of native oxide film after heating in hydrogen ambient. The wafers are heated at 900 °C (circles), 1000 °C (squares) and 1100 °C (triangles) under atmospheric pressure.

The relationship between haze generation and oxygen atoms incorporated in the silicon crystal[4] is examined experimentally using process (b) in Fig. 7-1. The circles in Fig. 7-4(b) show haze intensity behavior of the epitaxial silicon film surface. Haze of the epitaxial films also intensifies with decreasing heating temperature, the same as in the samples grown by the Czochralski (CZ) method in Fig. 7-4(a). This result clearly shows that this haze intensity behavior does not depend on the oxygen atoms incorporated in the silicon crystal, because the epitaxial film has a markedly lower oxygen content compared to CZ crystal. The haze intensity behavior is assumed to be due to native oxide film of even as thin as 0.4 nm which is expected to be formed

on the hydrogen-terminated silicon surface after a 24-h exposure to air.[5,6] To verify this assumption, the haze intensity of the silicon surface obtained using process (c) in Fig. 7-1 is measured, where the native oxide film is completely removed after heating at 1100 °C for 10 min prior to the heat process at 900 °C. The haze intensity after process (c) is very low as shown by the square in Fig. 7-4. Hence it is concluded that the native oxide film, even though quite thin, plays a key role in increasing surface roughness during the heat treatment process in hydrogen ambient.

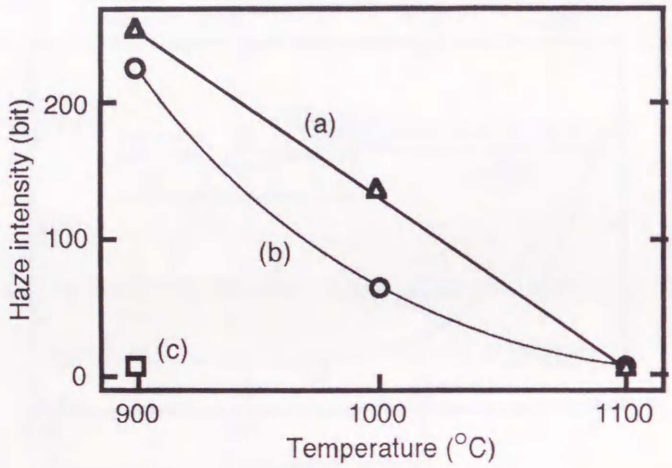

Fig.7-4 Haze intensity of the silicon surface measured by the light scattering method after heating in hydrogen ambient under atmospheric pressure: (a) polished wafer heated at 900–1100 °C for 60 min (triangles), (b) epitaxial wafer kept in air for 24 h and heated at 900–1100 °C for 60 min (circles), (c) polished wafer heated at 1100 °C for 10 min and 900 °C for 30 min (square).

To investigate the behavior of surface roughening, surfaces heated in hydrogen ambient are observed using AFM since the relationship between the haze and the surface roughness measured by AFM have been well discussed experimentally[7] and theoretically.[8] Figure 7-5 shows AFM images of the (100) silicon surface after heat treatment in hydrogen ambient at (a) 1000 °C for 4 min and (b) 1100 °C for 1 min. A nonheated polished wafer is shown in (c) as a reference. Although the AFM image in Fig. 7-5 (b) shows a surface as smooth as that in Fig. 7-5 (c), that in

Fig. 7-5 (a) has slightly steeper hills and valleys than those in Figs. 7-5 (b) and (c). The morphology shown in Fig. 7-5 agrees with the haze intensity behavior in Fig. 7-4. Figure 7-6 also shows AFM images of the (100) silicon surfaces after heat treatment in hydrogen ambient at 900 °C for (a) 3 min, (b) 10 min and (c) 30 min under atmospheric pressure. As shown in Fig. 7-6 (a), many small pits are formed even after 3 min of heat treatment. As the heating time is increased, the pit size becomes larger, as shown in Figs. 7-6 (b) and (c). However, both peak-to-valley ($P-V$) and root-mean-square (RMS) pit depths determined by AFM remain nearly constant after 10 min as a major behavior, as shown in Fig. 7-7.

— MEMO —

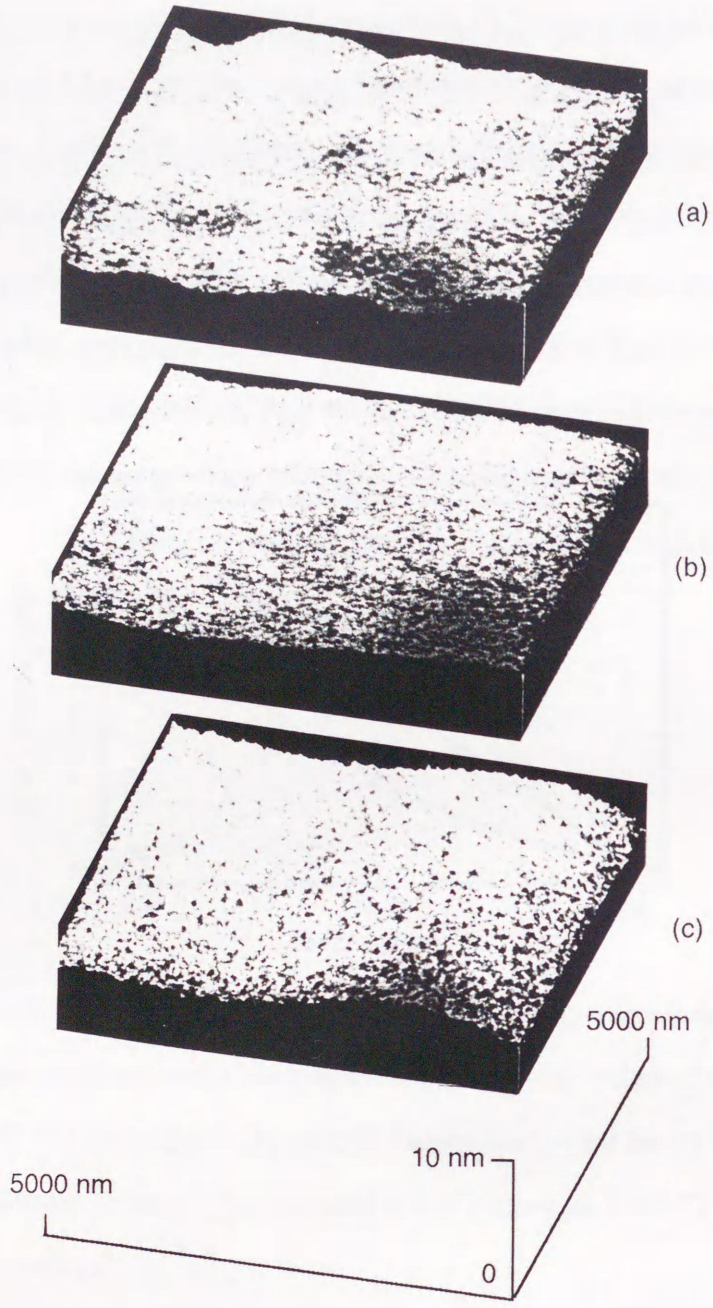

Fig.7-5 The (100) silicon surface observed by AFM after heat treatment in hydrogen ambient at (a) 1000 °C for 4 min and (b) 1100 °C for 1 min under atmospheric pressure. Polished wafer without any heat treatment is shown in (c) as a reference.

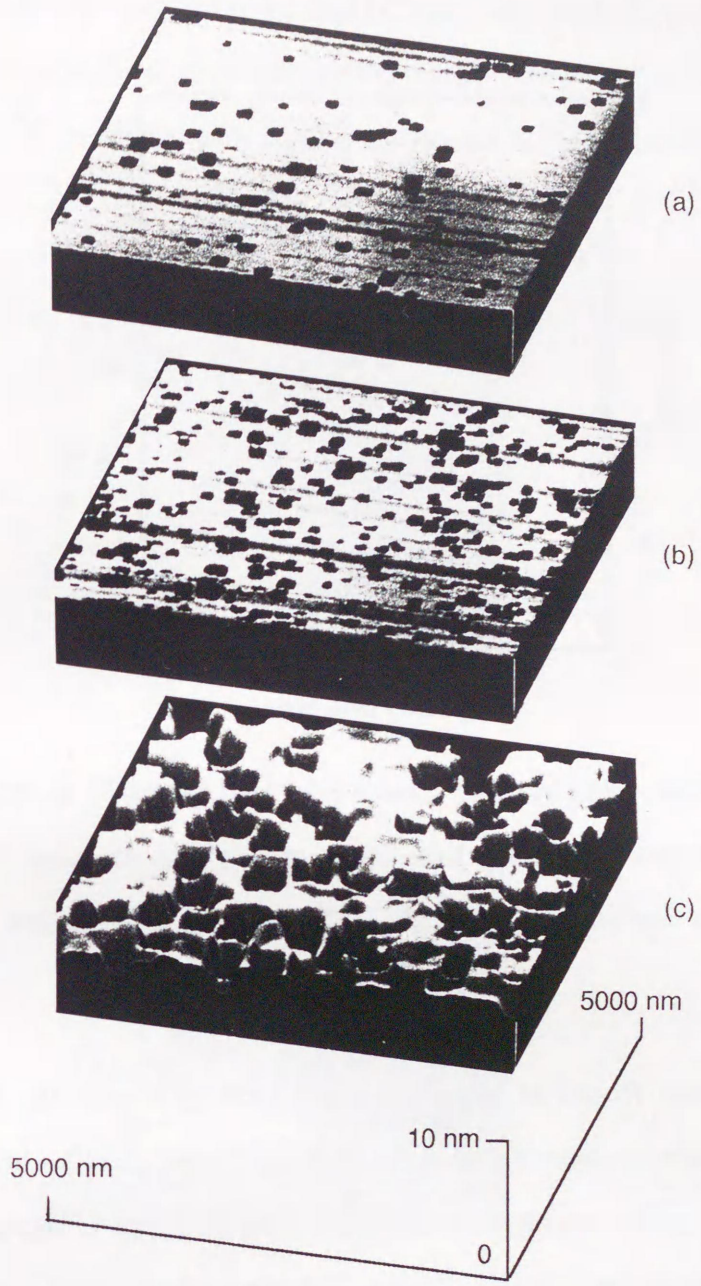

Fig.7-6 The (100) silicon surface observed by AFM after heat treatment in hydrogen ambient at 900 °C for (a) 3 min, (b) 10 min, (c) 30 min under atmospheric pressure.

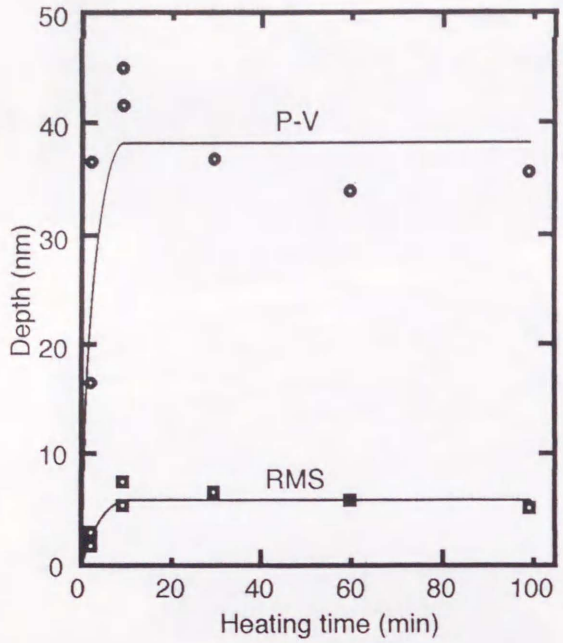

Fig.7-7 Measured pit depth at (100) surface after heat treatment at 900 °C in hydrogen ambient as a function of heating time under atmospheric pressure. The circles and the squares show the peak-to-valley ($P-V$) and root-mean-square (RMS) values, respectively.

Figure 7-8 shows the AFM images of the silicon surface of the (a) (100) plane and (b) (111) plane having small pits due to heat treatment in hydrogen ambient at 900 °C for 3 min under atmospheric pressure. The pit shape is square for the (100) plane and triangular for the (111) plane. This dependence of the pit shape on the crystal plane is the same as in various other surface etching methods.[9]

These results from AFM show that the formation of small pits is responsible for haze on the surface, and that the pits are formed by some etch reactions on the surface, where the native oxide film, the silicon surface and hydrogen gas play key roles.

The most probable mechanism is the etching of silicon or native oxide by hydrogen. The measured etch rates of silicon and silicon dioxide film by hydrogen gas after the

heat treatment process in Figs. 7-1 (a) and 7-2 under atmospheric pressure are shown in Fig. 7-9. The etch rate of silicon by hydrogen gas is slower than that obtained by Gallois et al.[10], but is comparable to that by Langer and Goldstein.[11]

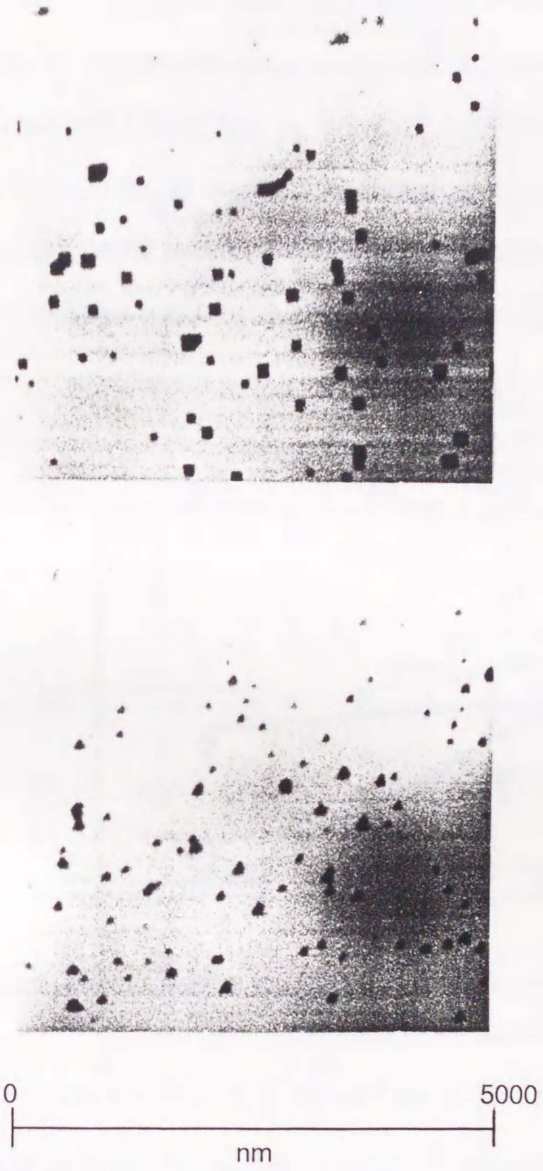

Fig.7-8 Silicon surface of (a) (100) plane and (b) (111) plane observed by AFM after 3 min of heat treatment in hydrogen ambient at 900 °C under atmospheric pressure.

The etch rate of silicon shown in Fig. 7-9 should be considered as the minimum estimation, because the step height measurement in this study detects the depth or height at only the highest hill in contact with the probe, diameter of 5 μm. The

etch rate of silicon by hydrogen gas changes gradually throughout the measured temperature range of 900–1100 °C, as shown in Fig. 7-9. Since the etching reaction is a heterogeneous one, the etch rate of silicon by hydrogen gas is governed by transport phenomena of reactants and products as discussed in this thesis; therefore it is governed by the reactor configuration, the desorption of silicon hydrides,[10] and the temperature field, such as hot wall or cold wall. The weak dependence of the etch rate of silicon on heating temperature may be attributed to the transport phenomena in the reactor. Additionally, silicon redeposition from silicon hydrides produced during the etching reaction may occur simultaneously.

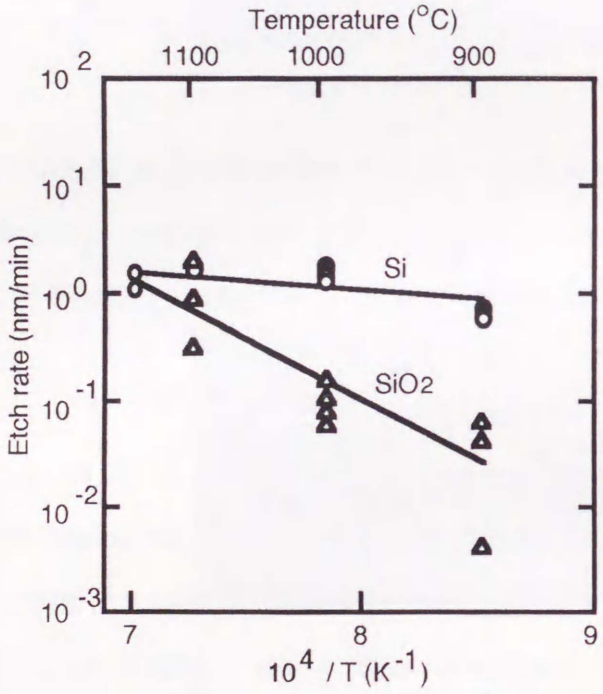

Fig.7-9 Etch rates of silicon (circles) and silicon dioxide (triangles) by hydrogen gas under atmospheric pressure as a function of reciprocal temperature.

Unlike the case of silicon, the etch rate of the native oxide film decreases significantly with decreasing the temperature, as shown in Fig.7-9.

At a higher temperature of 1100 °C, the native oxide film is quickly and completely removed, thus etching by hydrogen gas begins at approximately the same time over

an entire silicon surface, shown on the left side of Fig. 7-10. Here the silicon surface etched by hydrogen gas is very smooth.

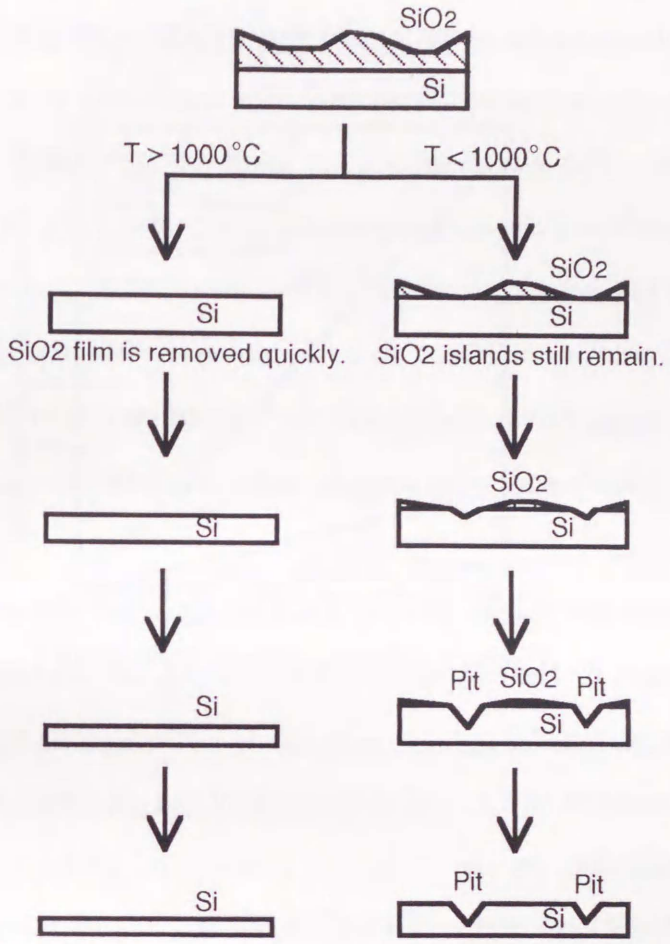

Fig.7-10 The pit formation model at the silicon surface heated in hydrogen ambient.

At a lower temperature of 900 °C, because the etch rate of the native oxide film is much slower than that of the silicon surface, the removal of the native oxide film is expected to be very slow and incomplete. This relationship leads to the model of small pit formation shown on the right side of Fig. 7-10. At small areas where the native oxide is removed earlier than the rest of the wafer, the bare silicon surfaces are etched faster by hydrogen gas than the remaining native oxide film; thus many pits are ultimately formed.

The native oxide film appears as continuing hills and valleys, because the silicon

surface is oxidized nonuniformly and the native oxide film appears as islands shapes.[12-14] The oxide islands are 30–70 nm in diameter[14] which corresponds to 1×10^{11} – $2\times10^{10}\,cm^{-2}$ of the density of the islands or valleys. Furthermore, it has been reported[15-20] that decomposition due to chemical reaction between silicon dioxide and silicon leads to evaporation of silicon monoxide and finally to void formation in the native oxide film. The void density is on the order of $10^9\,cm^{-2}$.[17] Densities of the native oxide islands and the voids are comparable to $3–4\times10^8\,cm^{-2}$ in this study and $4\times10^9\,cm^{-2}$ of Yanase et al.,[21] which are less than that of the oxide islands and valleys. At the valleys, the voids tend to be formed easily because the void density increases with decreasing native oxide thickness.[16] Based on this finding, the density of the native oxide islands and valleys can be assumed to be the maximum density of the surface pits.

It is considered that the valleys and the voids do not affect the native oxide film thickness measurement by the ellipsometer, for example, the thickness after heated at 900 °C for 10 min in Fig. 7-3.

This pit formation model in Fig. 7-10 indicates that the pit depth does not change after the native oxide film on the surface is removed completely. This behavior agrees with both $P-V$ and RMS shown in Fig. 7-7.

The pit depth is calculated following the pit formation model in Fig. 7-10. Since the bare silicon surface begins to react with hydrogen gas after the removal of the native oxide from it, the time at which silicon etching begins at each site depends on the local thickness of the native oxide film. Therefore, the pit depth can be calculated from the time required to remove the native oxide of thickness Δ which is the $P-V$ of native oxide film.

$$Pit\ depth\ (\mathrm{nm}) = \frac{\Delta}{Etch\ rate\ of\ SiO_2} \times Etch\ rate\ of\ Si \qquad (7\text{-}1)$$

Figure 7-11 shows the calculated pit depths at 900, 1000 and 1100 °C as a function of Δ using the etch rates in Fig. 7-9. The calculated pit depth increases with decreasing heating temperature, consistent with the experimental results of this

study. Considering that Δ is less than the thickness of the native oxide film, 1.0–1.5 nm, and that the etch rate of silicon by hydrogen gas in Fig. 7-9 is a minimum estimation, $P - V$ in Fig. 7-7 is consistently larger than the pit depth estimated using the etch rate in Fig. 7-9 and that calculated in Fig. 7-11.

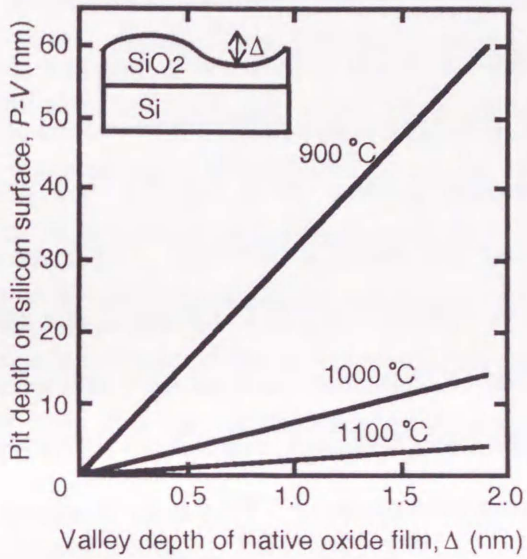

Fig.7-11 Calculated pit depth, $P - V$, on silicon surface at 900, 1000 and 1100 °C as a function of valley depth of native oxide film.

The chemical reactions for hydrogen-silicon[10] and hydrogen-silicon dioxide[22] can be assumed as

$$\mathrm{Si} + 2\mathrm{H_2} \rightarrow \mathrm{SiH_4} \uparrow, \tag{7-2}$$

$$\mathrm{Si} + \mathrm{H_2} \rightarrow \mathrm{SiH_2} \uparrow, \tag{7-3}$$

$$\mathrm{SiO_2} + \mathrm{H_2} \rightarrow \mathrm{SiO} \uparrow + \mathrm{H_2O} \uparrow, \tag{7-4}$$

where $\mathrm{SiH_4}$, $\mathrm{SiH_2}$ and SiO are considered to be the volatile products of the etching reactions.

The etch rates of silicon and silicon dioxide are estimated as

$$\textit{Etch rate of } \mathrm{Si} = k_1[\mathrm{H_2}]^2 + k_2[\mathrm{H_2}], \tag{7-5}$$

$$\textit{Etch rate of } \mathrm{SiO_2} = k_3[\mathrm{H_2}], \tag{7-6}$$

where $[H_2]$ denotes the molar concentration of hydrogen in gas phase, and k_1, k_2 and k_3 are the etch rate constants of equations (7-2), (7-3) and (7-4), respectively. Using equations (7-1), (7-5) and (7-6), the pit depth is obtained from equation (7-7).

$$Pit\ depth\ (\mathrm{nm}) = \Delta \times \frac{k_1[H_2] + k_2}{k_3} \tag{7-7}$$

According to this model, the pit depth from equation (7-7) is reduced with decreasing hydrogen pressure. To examine this model qualitatively, silicon wafers covered with native oxide films were heated in hydrogen ambient under reduced pressure of 90 torr at 900, 1000 and 1100 °C following process (a) in Fig. 7-1. At 900 °C, more than 30 min was necessary to remove the native oxide film. The haze intensity of the silicon surface was measured at PMTHV of 700 V to detect the difference in haze intensity more sensitively. When the heating temperature was lowered from 1100 °C to 900 °C, the increment of the haze intensity was within 10 bit which was much smaller than that under atmospheric pressure. This haze intensity behavior with hydrogen pressure agrees with results of Ohkura et al.[23]

From the discussion in this Chapter, the validity of the pit formation model is clear. The slightly steeper hills and valleys at 900 °C in Fig. 7-5 (a) can be also considered to be due to an uneven oxide thickness and voids formation. Additionally, the minor behavior of $P-V$ and RMS reaching their peaks at 10 min in Fig. 7-7 can be considered that the pits having initially very sharp edge shape are rounded due to the etching by hydrogen gas. It is noted here that the result for surface roughness at 800 °C does not agree with that reported by Yanase et al.[21] who showed no surface roughening. The reason for this discrepancy is believed to be that their heat treatment of 10 min is too short to generate surface pits, since the etch rate of silicon dioxide by hydrogen gas at 800 °C is expected to be extremely slow compared to that at 900 °C. In some other cases, it may be possible that the etch rate of silicon is enhanced by thermal etching[24] or the effects of moisture and oxygen[25] which are not dominant in this study.

7.4 Conclusion

The change of the surface roughness of silicon wafer after heating in hydrogen ambient at 800–1100 °C under atmospheric pressure was studied. The AFM images show that the rough surface after heating at 900 °C consists of small pits whose shape depends on the crystal plane. These pits are formed primarily due to the chemical reaction of silicon with hydrogen gas, since the bare silicon surface is etched faster than the native oxide islands. The pit depth on the silicon surface after heating in hydrogen ambient is described as a function of $P - V$ depth of native oxide film. The competitive etch reactions of silicon and native oxide with hydrogen gas are the driving force in the formation of the many small pits on the silicon surface heated at low temperature, with the help of the incomplete removal of the native oxide films and the void formation.

References

[1] W. Kern and D. A. Puotinen, *RCA Rev.*, **31**, 187 (1970).

[2] Y. J. Chabal and K. Raghavachari, *Phys. Rev. Lett.*, **53**, 282 (1984).

[3] D.C.Gupta ed., *Silicon Processing* (Am.Soc.Test.Mater., Philadelphia, 1983).

[4] F. Shimura, *Semiconductor Silicon Crystal Technology* (Academic Press, San Diego, 1989) Chap.5, p.161.

[5] M. Hirose, M. Takakura, T. Yasaka and S. Miyazaki, *Hyomenkagaku*, **13**, 324 (1992).

[6] M.Morita, T.Ohmi, E.Hasegawa, M.Kawakami and M.Ohwada, *J.Appl.Phys.*, **68**, 1272 (1990).

[7] W. M. Bullis, *SEMICONDUCTOR* Si/*1994 7th INT. SYMP. on* Si/ *Materials Science and Technology*, Huff, Bergholtz, Sumino(Eds), Electrochemical Society, 1994, p.1156.

[8] I.J.Malik, K.Vepa, S.Pirooz, A.C.Martin and L.W.Shive, *SEMICONDUCTOR* Si/*1994 7th INT. SYMP. on* Si/ *Materials Science and Technology*, Huff, Bergholtz, Sumino(Eds), Electrochemical Society, 1994, p.1182.

[9] F. Shimura, *Semiconductor Silicon Crystal Technology* (Academic Press, San Diego, 1989) Chap.3, p.49.

[10] B.M.Gallois, T.M.Besmann and M.W.Stott, *J.Am.Ceram.Soc.*, **77**, 2949 (1994).

[11] P. H. Langer and J. I. Goldstein, *J. Electrochem. Soc.*, **124**, 591 (1977).

[12] T.O.Sedgwick, P.D.Agnello and D.A.Grützmacher, *J.Electrochem.Soc.*, **140**, 3684 (1993).

[13] Y.Tamura, K.Ohishi, H.Nohira and T.Hattori, *Extended Abstracts of the 1992 Int. Conf. Solid State Devices and Materials*, 1992, Tsukuba, p.111.

[14] T. Aoyama, T. Yamazaki and T. Ito, *Appl. Phys. Lett.*, **61**, 102 (1992).

[15] Y. Kobayashi, Y. Shinoda and K. Sugii, *Jpn. J. Appl. Phys.*, **29**, 1004 (1990).

[16] S. I. Raider, *The Physics and Chemistry of SiO_2 and the Si-SiO_2 Interface*, C. R. Helms and B. E. Deal ed., p. 35, Plenum Press, New York, (1988).

[17] Y. Kobayashi and K. Sugii, *J. Vac. Sci. Technol.*, **B9**, 748 (1991).

[18] Y. Kobayashi and K. Sugii, *J. Vac. Sci. Technol.*,**A10**, 2308 (1992).

[19] R. Tromp, G. W. Rubloff, P. Balk and F. K. LeGoues, *Phys. Rev. Lett.*, **55**, 2332 (1985).

[20] M. Liehr, J. E. Lewis and G. W. Rubloff, *J. Vac. Sci. Technol.*, **A5**, 1559 (1987).

[21] Y.Yanase, H.Horie, Y.Oka, M.Sano, S.Sumita and T.Shigematsu, *J.Electrochem. Soc.*, **141**,3259 (1994).

[22] E.G.Alexander and R.R.Runyan, *Trans. Metall. Soc., AIME*, **236**, 284 (1966).

[23] A.Ohkura, H.Oku, K.Matsumoto and T.Ohmi, *Extended Abstracts of the 1991 Int. Conf. Solid State Devices and Materials*, Yokohama, 1991, p.559.

[24] M. Futagami and M. Hamazaki, *Jpn. J. Appl. Phys.*, **21**, 1782 (1982).

[25] J. A. Friedrich and G. W. Neudeck, *Appl. Phys. Lett.*, **53**, 2543 (1988).

Summary and Conclusions

The transport phenomena in epitaxial reactors for preparation of epitaxial silicon thin-films have been discussed experimentally and theoretically. Additionally, some qualities of a silicon epitaxial wafer affected by the growth condition have been discussed in this thesis.

The gases near the substrate and the susceptor flow horizontally in both the pancake reactor and the single-wafer horizontal reactor, at the epitaxial growth temperatures under atmospheric pressure. These motions are consistent with those indicated by the growth rate profile.

For preparation of silicon thin-films in a $SiHCl_3$-H_2 system, the nonlinear dependence of growth rate on the concentration of $SiHCl_3$ was partly attributed to the change in the gas flow and temperature fields in the reactor with the $SiHCl_3$ concentration. The effect of thermal diffusion in the present system was found to result in a reduced growth rate. A substrate rotation in a single-wafer horizontal reactor causes averaging effect of the nonuniform growth rate along concentric circles on the substrate surface to achieve the good uniformity in film thickness. Although nearly uniform film thickness is achieved by the rotating substrate, the concentration of $SiHCl_3$ itself is not uniform on the substrate even at very high rotation rates. From the view point of the rate theory, the entire processes of the silicon epitaxial growth in the $SiHCl_3$-H_2 system have been assumed to be mainly composed of chemisorption and decomposition of chemisorbed species which rate constants can be estimate accounting for the transport phenomena in the reactor. The chemical reactions at the surface following the Eley-Rideal model can describe the nonlinear behavior of the epitaxial growth rate.

As a quality of silicon epitaxial wafer, boron concentration profiles in silicon epitaxial wafers by two types of the epitaxial reactors are studied with consideration of the transport phenomena in epitaxial reactors. Large amounts of recirculation of gas in the epitaxial reactor should be avoided for obtaining a sharp dopant concentration

profile.

The change of the surface roughness of silicon wafer after heating in hydrogen ambient at 800–1100 °C under atmospheric pressure is observed. Small pits are formed primarily at low temperatures due to the competitive etch reactions of silicon and native oxide with hydrogen gas with the help of the incomplete removal of the native oxide films and the void formation.

論　文　目　録

氏名　羽深　等

第2章　H. Habuka, M. Mayusumi, N. Tate and M. Katayama, "Gas Flow and Heat Transfer in a Pancake Chemical Vapor Deposition Reactor", *J. Cryst. Growth*, **151**, 375 (1995). 1995年6月発行

第3章　H. Habuka, M. Katayama, M. Shimada and K. Okuyama, "Numerical Evaluation of Silicon-Thin Film Growth from $SiHCl_3$-H_2 Gas Mixture in a Horizontal Chemical Vapor Deposition Reactor", *Jpn. J. Appl. Phys.*, **33**, 1977 (1994). 1994年4月発行

第4章　H. Habuka, T. Nagoya, M. Katayama, M. Shimada and K. Okuyama, "Modeling of Epitaxial Silicon Thin-Film Growth on a Rotating Substrate in a Horizontal Single-Wafer Reactor", *J. Electrochem. Soc.*, **142**, 4272 (1995). 1995年12月発行

第5章　H. Habuka, T. Nagoya, M. Mayusumi, M. Katayama, M. Shimada and K. Okuyama, "Model on Transport Phenomena and Epitaxial Growth of Silicon Thin Film in $SiHCl_3$-H_2 System under Atmospheric Pressure", *J. Crystal Growth* (印刷中). 1996年発行予定

第5章　羽深 等, 片山 正健, 島田 学, 奥山 喜久夫, "輸送現象と表面反応を考慮した$SiHCl_3$-H_2系Siエピタキシャル成長の三次元数値解析", 日本結晶成長学会誌, **23**(1), 2 (1996). 1996年3月発行

第6章　H. Habuka, M. Mayusumi, H. Tsunoda and M. Katayama, "Effect of Transport Phenomena on Boron Concentration Profiles in Silicon Epitaxial Wafers", *J. Electrochem. Soc.*, **143**, 677 (1996). 1996年2月発行

第7章　H. Habuka, H. Tsunoda, M. Mayusumi, N. Tate and M. Katayama, "Roughness of Silicon Surface Heated in Hydrogen Ambient", *J. Electrochem. Soc.*, **142**, 3092 (1995). 1995年9月発行